AD_____

Award Number: W81XWH-06-1-0329

TITLE: Detection and Evaluation of Early Breast Cancer via Magnetic Resonance Imaging: Studies of Mouse Models and Clinical Implementation

PRINCIPAL INVESTIGATOR: Sanaz A. Jansen

CONTRACTING ORGANIZATION: University of Chicago
Chicago, IL 60637

REPORT DATE: March 2008

TYPE OF REPORT: Annual Summary

PREPARED FOR: U.S. Army Medical Research and Materiel Command
Fort Detrick, Maryland 21702-5012

DISTRIBUTION STATEMENT: Approved for Public Release;
Distribution Unlimited

The views, opinions and/or findings contained in this report are those of the author(s) and should not be construed as an official Department of the Army position, policy or decision unless so designated by other documentation.

REPORT DOCUMENTATION PAGE

Form Approved
OMB No. 0704-0188

Public reporting burden for this collection of information is estimated to average 1 hour per response, including the time for reviewing instructions, searching existing data sources, gathering and maintaining the data needed, and completing and reviewing this collection of information. Send comments regarding this burden estimate or any other aspect of this collection of information, including suggestions for reducing this burden to Department of Defense, Washington Headquarters Services, Directorate for Information Operations and Reports (0704-0188), 1215 Jefferson Davis Highway, Suite 1204, Arlington, VA 22202-4302. Respondents should be aware that notwithstanding any other provision of law, no person shall be subject to any penalty for failing to comply with a collection of information if it does not display a currently valid OMB control number. **PLEASE DO NOT RETURN YOUR FORM TO THE ABOVE ADDRESS.**

1. REPORT DATE *(DD-MM-YYYY)*	**2. REPORT TYPE**	**3. DATES COVERED** *(From - To)*
01-03-2008	Annual Summary	06 FEB 2007 - 05 Feb 2008

4. TITLE AND SUBTITLE

Detection and Evaluation of Early Breast Cancer via Magnetic Resonance Imaging: Studies of Mouse Models and Clinical Implementation

5a. CONTRACT NUMBER

5b. GRANT NUMBER
W81XWH-06-1-0329

5c. PROGRAM ELEMENT NUMBER

6. AUTHOR(S)
Sanaz A. Jansen

E-Mail: sarkani@uchicago.edu

5d. PROJECT NUMBER

5e. TASK NUMBER

5f. WORK UNIT NUMBER

7. PERFORMING ORGANIZATION NAME(S) AND ADDRESS(ES)

University of Chicago
Chicago, IL 60637

8. PERFORMING ORGANIZATION REPORT NUMBER

9. SPONSORING / MONITORING AGENCY NAME(S) AND ADDRESS(ES)
U.S. Army Medical Research and Materiel Command
Fort Detrick, Maryland 21702-5012

10. SPONSOR/MONITOR'S ACRONYM(S)

11. SPONSOR/MONITOR'S REPORT NUMBER(S)

12. DISTRIBUTION / AVAILABILITY STATEMENT
Approved for Public Release; Distribution Unlimited

13. SUPPLEMENTARY NOTES

14. ABSTRACT
The general goals of this research are to (i) improve the specificity of MRI to early cancer, particularly ductal carcinoma in situ (DCIS), by studying the MR presentation of early cancers compared with other malignant and benign lesions in women, (ii) to develop techniques for imaging DCIS and early invasive cancer in mice via MR imaging, and (iii) to use these techniques to study the progression of murine mammary cancer. The pre-clinical animal research proposed here can directly lead to clinical improvements in both early breast cancer detection, as well as effective breast cancer therapy. To date, we have performed a comprehensive evaluation of the MR kinetic and morphologic characteristics of DCIS and early invasive cancers compared with other lesions. We have also developed techniques to image early murine mammary cancer, including DCIS, using in vivo MRI. To our knowledge, this is the first report of the in vivo detection of murine DCIS with histopathologic correlation. We have also performed a longitudinal imaging experiment in 12 transgenic mice, following the development and progression of murine DCIS into invasive carcinoma. In this study we have found that some DCIS lesions have remained stable and did not progress to invasive cancer during the study window. These represent the first steps towards probing in vivo the radiologic and biologic changes that occur during the transition from in situ to invasive cancer.

15. SUBJECT TERMS
Early detection, MRI, mouse models, DCIS

16. SECURITY CLASSIFICATION OF:			**17. LIMITATION OF ABSTRACT**	**18. NUMBER OF PAGES**	**19a. NAME OF RESPONSIBLE PERSON**
a. REPORT	**b. ABSTRACT**	**c. THIS PAGE**			USAMRMC
U	U	U	UU	119	**19b. TELEPHONE NUMBER** *(include area code)*

Table of Contents

	Page
Introduction……..…….	**4**
Body…….	**5**
Key Research Accomplishments…….…….	**16**
Reportable Outcomes……	**17**
Conclusion……	**19**
References……	**20**
Appendices……	**21**

INTRODUCTION

The early detection of breast cancer is a major prognostic factor in the management of the disease. In particular, detecting breast cancer in its pre-invasive form as ductal carcinoma *in situ* (DCIS) improves prognosis greatly compared with invasive tumors. Although dynamic contrast enhanced MR imaging (DCEMRI) of the breast has demonstrated high sensitivity to invasive breast cancer, there is room for improving the diagnostic accuracy of DCEMRI to DCIS. However, there is another competing clinical concern; DCIS is being overdiagnosed and overtreated, as there is evidence to suggest that not all DCIS lesions will progress into invasive cancers. The goals of this project are to improve sensitivity and specificity of DCEMRI to DCIS by comparing its kinetic and morphologic features with other types of breast lesions, and to use mouse models to probe the progression of DCIS into invasive cancer. The specific aims are to: (1) characterize the MR kinetic and morphologic findings of DCIS in women and compare with benign lesions and other malignant cancers, (2) develop techniques to detect early mammary cancer in mice, and (3) study the development and progression of early mammary cancer in mice by performing longitudinal MRI studies of development of DCIS and transition to invasive cancer.

BODY

During the second year of funding of this award, we have continued to work on accomplishing many of the aims of the approved Statement of Work.

Task 1. To evaluate the development of ductal carcinoma *in situ* (DCIS) in mammary glands of a transgenic mouse model via MRI.

a. *Develop in vivo high resolution imaging of mouse mammary glands.*
b. *Perform detailed correlation of MRI with histology to improve understanding of features on MR images.*
c. *Perform serial MRI studies to follow mice while DCIS develops and continue to follow the transition to invasive cancer.*

Task 1a and 1b: Last year, we reported that we had developed techniques to image early cancer, including DCIS, in the Sv40 TAg transgenic mouse model of breast cancer and had performed a sensitivity and specificity study by making correlations with histology. This year, we have improved the analysis of this *in vivo* data by performing quantitative analysis of image properties, such as signal-to-noise ratio and contrast-to-noise ratio [see page 94, Table 1 in *Detection of in situ mammary cancer in a transgenic mouse model: in vitro and in vivo MRI studies demonstrate histopathologic correlation,* Appendix**]**. We have also assessed murine lesion morphology and found that there were many similarities between human and murine cancers: DCIS lesions presented as nonmass lesions in a ductal shape, while early invasive tumors appeared as round masses [see page 89 in *Detection of in situ mammary cancer in a transgenic mouse model: in vitro and in vivo MRI studies demonstrate histopathologic correlation,* Appendix**]**. In addition, we also expanded our analysis to include data in vitro studies, where we again demonstrated that in vitro MRI could reliably detect early murine mammary cancer in over 40 specimens [see page 97, Figure 1 in *Detection of in situ mammary cancer in a transgenic mouse model: in vitro and in vivo MRI studies demonstrate histopathologic correlation,* Appendix**].**

From March to September 2007 a new 9.4 T Bruker magnet was installed in what is now the Florsheim Magnetic Resonance Imaging and Spectroscopy facility at the University of Chicago. This new magnet has replaced the 4.7 T magnet on which our prior data had been acquired. During the past year we have optimized imaging parameters and techniques for detecting early murine mammary cancer on the new 9.4 T scanner, including gradient echo (GE) and spin echo (SE) pulse sequences. In addition, we have recently installed a 12 cm gradient set that enables us to obtain images at higher spatial resolution. Figure 1 is an example of a DCIS lesion at 68-micron spatial resolution, which is nearly double the spatial resolution that we have obtained in our earlier results (117 microns).

Figure 1: Example of DCIS lesion (thin arrow) and lymph node (thick arrow) obtained with 68 micron in plane resolution. Imaging parameters: FLASH GE TR/TE: 1000/5, FOV=3.0 x 1.5 cm, slice thickness=0.5mm.

Task 1c: After optimizing the imaging parameters and techniques on the new 9.4T magnet, we began in October 2007 to perform a serial imaging experiment following the progression of DCIS into invasive cancer. To date, such studies have not been performed. Our recent techniques developed in Task 1a and 1b have demonstrated that MR imaging of early murine mammary cancer, including DCIS, is feasible. The purpose of this study was to use MR imaging to follow the progression of early murine mammary cancer *in vivo*. In particular, we are interested in measuring certain timescales of progression: the growth rate of DCIS, the growth rate of small invasive tumors and the timescale of progression of DCIS to invasive tumors.

METHODS

Animals

Twelve C3(1) SV40 large T antigen mice were selected for MR imaging. This mouse model targets expression of large T antigen to the mammary gland in females via the C3 promoter. Female mice develop mammary cancer that resembles human ductal carcinoma, including progression through atypical ductal hyperplasia (~8 weeks), DCIS (~12 weeks), and IDC (~16 weeks)(20). 4/12 mice were selected for serial imaging every two weeks from ages 10-20 weeks. 6/12 were selected for 4 imaging sessions (every 3 weeks and from 12-20 weeks of age) and 2/12 were serial imaged twice (once at 13 weeks and once at 16 weeks). During the experiment, four mice died prematurely. All procedures were carried out in accordance with our institution's Animal Care and Use Committee approval. Animals were anesthetized prior to imaging experiments, and anesthesia was maintained during imaging at 1.5% isoflorane. Body temperature was maintained with a warm air blower. The temperature, heart rate and respiration rate were monitored with data taken every minute. The respiration rate was used to obtain gated images.

MRI Experiments

Imaging was performed with a Bruker 9.4 Tesla magnet equipped with a self-shielded gradient set that delivers maximum gradient strength of 20 gauss/cm. A homebuilt 8-leg low pass half-open birdcage coil (3 cm length x 3 cm width x 2 cm height) that produced high flux density in the mammary gland was used for *in vivo* imaging. Gradient echo (GE) images with fat suppression (FLASH, TR/TE: 675/7 ms, FOV=3.0 × 3.0 cm, NEX=2, slice thickness=0.5mm, in-plane resolution=117 microns and flip angle=30°) and spin echo (SE) images with fat suppression (RARE, TR/TE: 3000/29 ms, RARE acceleration factor = 4, FOV=3.0 × 3.0 cm, NEX=2, slice thickness=0.5mm and in-plane resolution=117) across the entire sensitive volume of the coil were obtained.

The inguinal mammary glands on the left side of each mouse were selected for longitudinal *in vivo* imaging. To facilitate spatial correlations between subsequent MR images, a fine polyethylene mesh ~ 3.0 cm x 2.0 cm in size with 3.0 mm spacing was embedded in partially deuterated agar and wrapped around each mouse. This agar grid produced a pattern on MRI that was used for registration of serial MRI images. It also served to eliminate the air tissue interface near the mammary gland, which is expected to reduce susceptibility artifacts.

Image Analysis

For each mouse, the images were reviewed beginning at the earliest age. At each time point, the number and locations of DCIS lesions and invasive tumors were determined, and the lesion volumes were measured. In addition, the signal-to-noise ratio of each lesion was calculated, as well as the contrast-to-noise ratio relative to muscle and lymph nodes.

Lesion Morphology: The morphology of the lesions and lymph nodes detected by *in vivo* MRI were analyzed in the same way as lesions found in clinical breast MRI of women. For clinical examinations, the Breast Imaging- Reporting and Data System (BI-RADS) lexicon classifies the type, shape, margins and enhancement pattern of the lesion (ACR, 2003). In our study, the morphology of the lesions was classified based on a simplified version of the BI-RADS lexicon as follows: type (mass or non-mass), shape/distribution (for mass lesions: round, oval, lobular or irregular; for non-mass lesions: linear, ductal or segmental), margins (for mass lesions only: smooth or irregular) and pattern (for mass lesions: homogeneous or heterogeneous; for non-mass lesions: homogeneous, stippled or clumped).

Timescales of Progression: For each lesion, the time at initial development of DCIS ($\mathbf{T_{DCIS}}$) or the time at initial development of invasive tumors ($\mathbf{T_{tumor}}$) was determined. The growth rate of DCIS and invasive tumors were calculated according to the following equation:

$$V=V_0\exp(\alpha t)$$

Finally, for DCIS lesions in which progression to invasive tumors can be identified the progression time $\mathbf{T_{prog}}$ was measured.

RESULTS

In total, 16 invasive tumors and 21 DCIS lesions developed in the mice and these lesions were followed. Due to the multiple imaging sessions many of these lesions were imaged more than once, in a total 43 DCIS lesions imaged, and 28 invasive tumors imaged. The average SNR and CNR calculated from FLASH GE images are shown in Table 1. The SNR of DCIS was comparable to muscle, but less than lymph nodes on average. Conversely, invasive tumors demonstrated a higher CNR compared with muscle and lymph nodes. The distribution of morphology characteristics for DCIS lesions and early invasive tumors are shown in Table 2. DCIS lesions typically presented as nonmass lesions, in a segmental shape with a homogeneous pattern. Conversely, early invasive tumors presented predominantly as round masses with smooth margins.

Timescales of Progression: DCIS initially developed at age $\mathbf{T_{DCIS}}$ =12.7 weeks on average, with an initial volume of 0.3399±0.2161 mm^3. Invasive tumors developed at $\mathbf{T_{tumor}}$ =16 weeks on average, with and average initial volume of 17.13±61 mm^3. This average initial volume is skewed by one tumor that was first detected at over 200 mm^3. Removing this outlier yields an average initial invasive tumor size of 1.7 mm^3. Figures 2 and 3 show distributions of initial age at development of DCIS lesions and invasive cancers, respectively.

For lesions where the volume was measured at least twice, the growth rate was calculated. The average growth rate for DCIS lesions was α_{DCIS}= 0.0817±0.2289 $week^{-1}$, and for invasive tumors was α_{tumor}= 0.5466±0.3516 $week^{-1}$. Figure 4 shows a plot of α_{tumor} and α_{DCIS}. The growth rate of DCIS lesions is significantly smaller than invasive tumors (p=0.0012 by t-test). This suggests that DCIS lesions grow rather slowly, however once these lesions have transitioned into small invasive cancers the growth rate increases. The progression from DCIS to IDC could be determined for 12 lesions. The average progression time $\mathbf{T_{prog}}$=3.75 weeks, and the distribution of progression times is shown in Figure 5. Eight DCIS did not progress within the study window, and three of these were stable for 10 weeks. This indicates that the rates of progression of DCIS are variable in this model, and some DCIS may even be stable. Thus, even in a transgenic mouse model with a genetic predisposition to developing carcinoma, some DCIS lesions may progress slowly if at all. Figures 6 shows several examples of lesion progression.

Table 1: The average signal-to-noise ratio (SNR) of DCIS lesions and invasive tumors calculated from FLASH gradient echo (GE) images. The contrast-to-noise ratio of DCIS and tumors compared with muscle and lymph nodes are also shown.

	SNR	CNR (muscle)	CNR (Lymph node)
DCIS	26.4±10.2	1.2± 10.3	-3.8 ± 9.5
Invasive Tumor	30.9±11.2	8.9± 10.9	5.5 ± 8.9

Table 2: Distribution of morphology attributes of DCIS lesions and early invasive tumors according to a modified version of the BI-RADS lexicon.

	Invasive Tumor N=28	DCIS N=43
Type		
Mass	28	0
Nonmass	0	43
Shape		
Ductal	0	16
Segmental	0	26
Linear	0	1
Irregular	6	0
Round	17	0
Oval	0	0
Lobular	5	0
Margins		
NA	0	43
Smooth	21	0
Irregular	7	0
Pattern		
Clumped	0	8
Homogeneous	22	26
Stippled	0	9
Heterogeneous	6	0

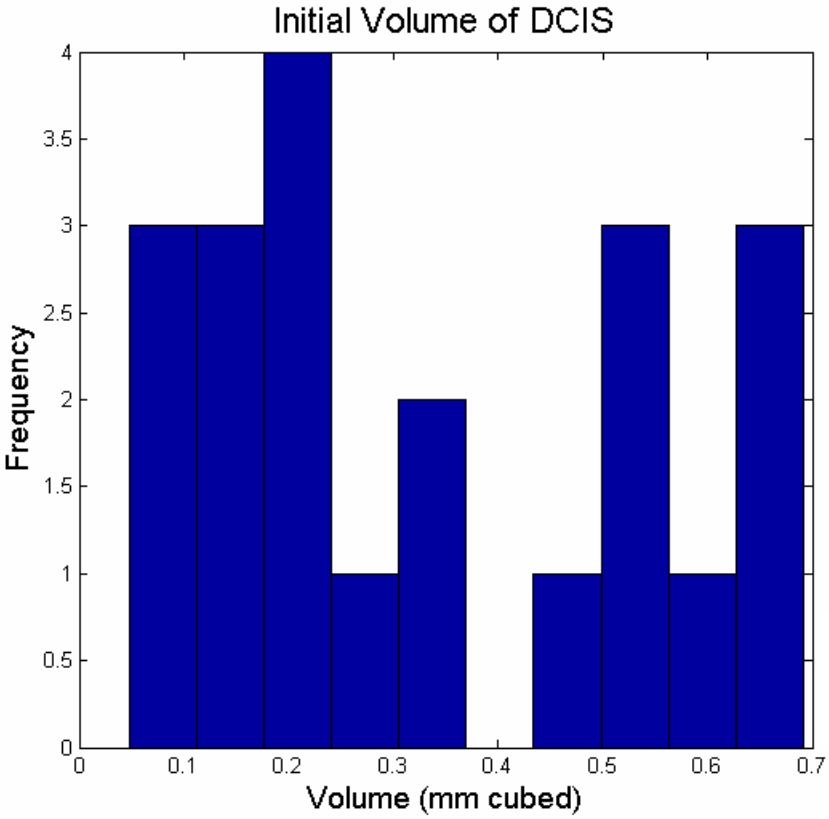

Figure 2: Distribution of DCIS volume at initial detection.

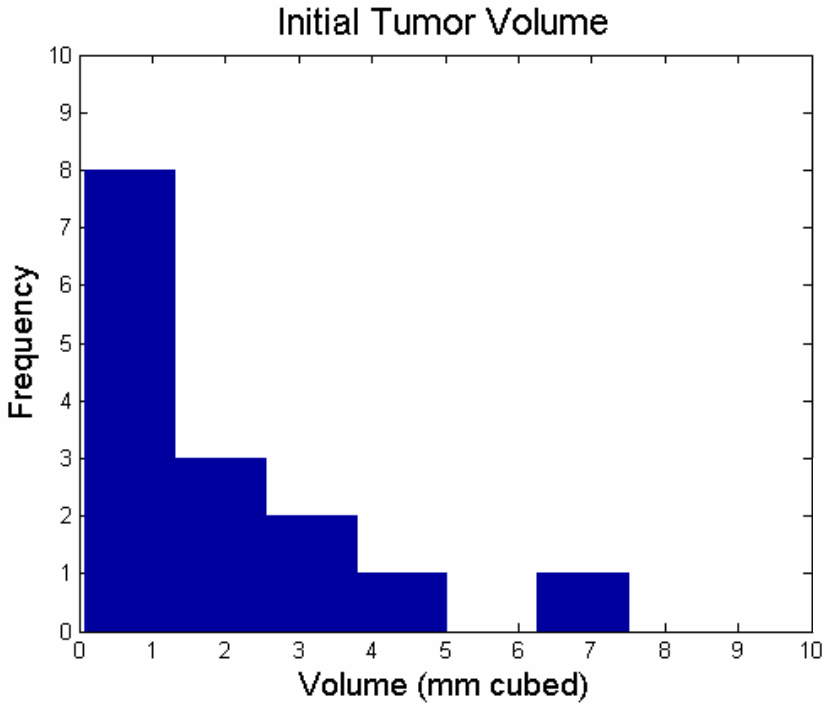

Figure 3: Distribution of invasive tumor volume at initial detection. This histogram does not include an outlier at 250 mm^3.

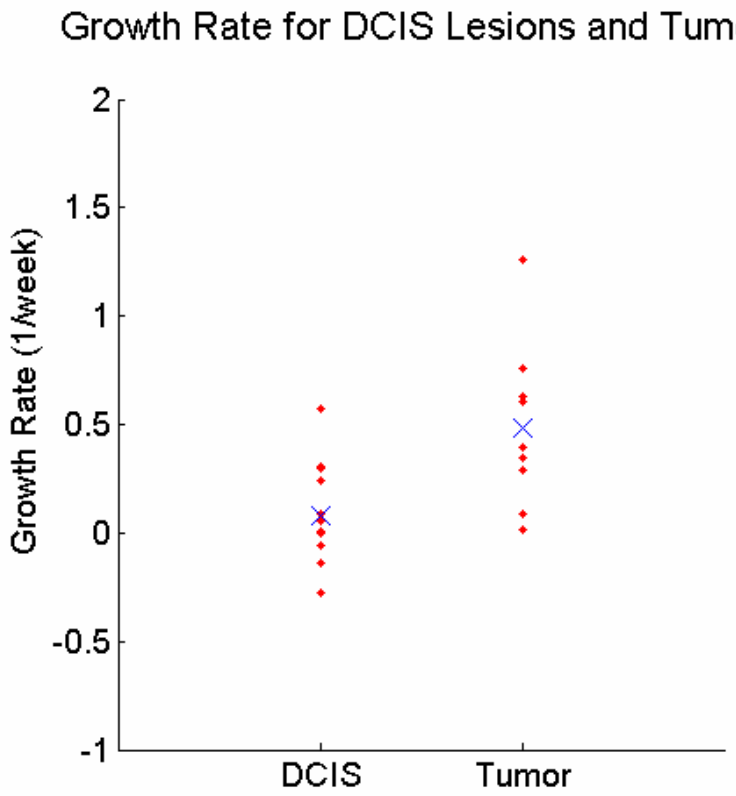

Figure 4: The growth rates α_{tumor} and α_{DCIS} for invasive tumors and DCIS lesions, respectively. The blue x marks the average value.

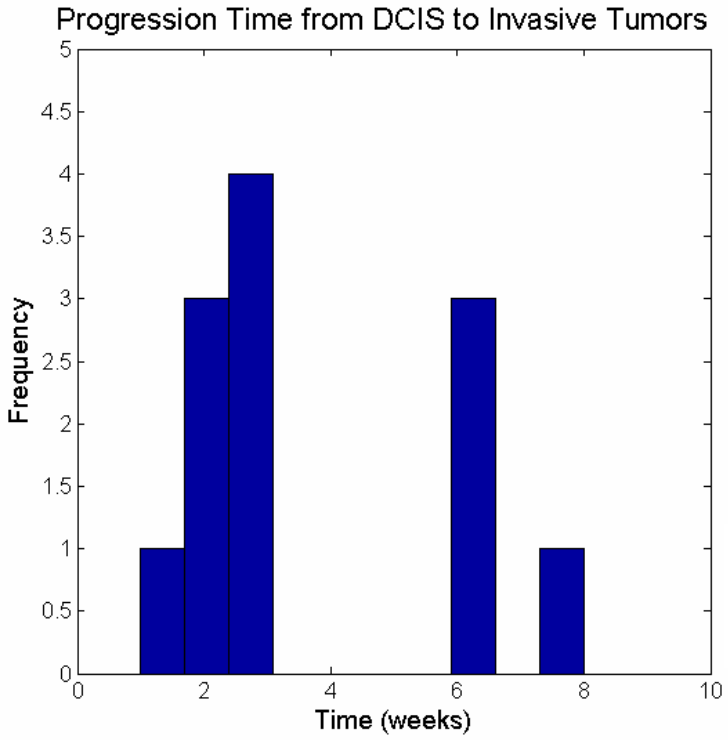

Figure 5: Distribution of progression time $\mathbf{T}_{prog}$ from DCIS to invasive tumor.

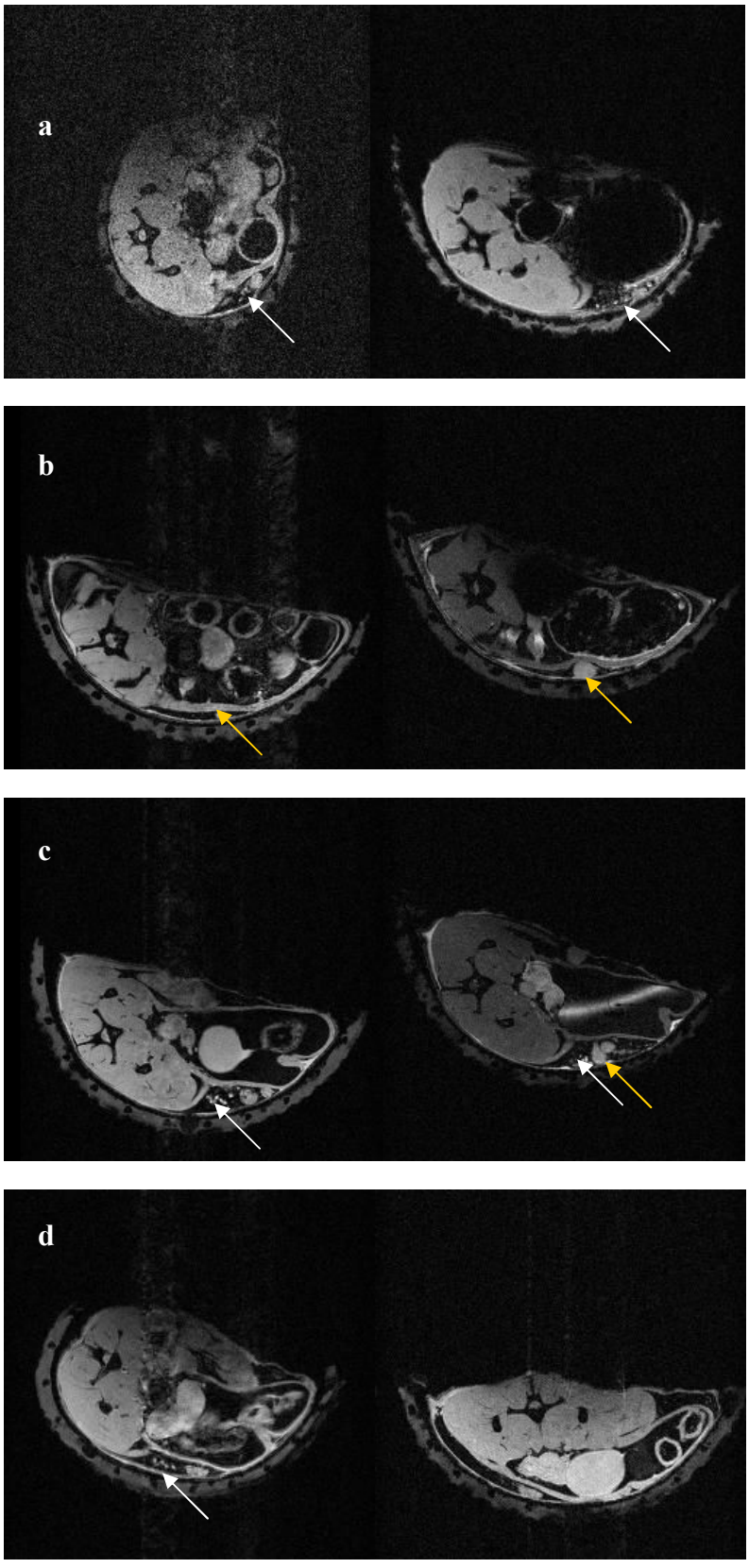

Figure 6: Examples of lesion progression.
a) *Stable DCIS*. On the left is an image of DCIS (white arrow) in a mouse at 10 weeks of age. On the right in the same area DCIS is re-demonstrated, and no invasive tumors have developed.
b) *Tumor growth*. On the left is a tumor (yellow arrow) at 12 weeks of age, and on the right at 15 weeks.
c) *DCIS progression*. On the left is DCIS (white arrow) at 12 weeks, and on the right the DCIS has progressed to invasive cancer (yellow arrow), and some residual DCIS remains (white arrow).
d) *DCIS regression*. On the left DCIS (white arrow) is demonstrated at 12 weeks. At 15 weeks, no DCIS is detected,

Task 2. To perform quantitative and qualitative analysis of clinical breast dynamic contrast enhanced magnetic resonance images (DCEMRI).

a. *Maintain research database.*
b. *Quantitative assessment and mathematical modeling of enhancement patterns in lesions of many pathology subtypes.*
c. *Quantitative assessment of parenchymal enhancement patterns in the normal breast.*
d. *Use recently developed imaging methods and develop novel imaging acquisitions*.

Task 2a: We have continued to maintain the research database. It now contains approximately 3400 records, with ~ 1000 histologically proven malignant lesions and ~300 histologically proven benign lesions.

Task 2b: We have also continued to perform quantitative analysis of the contrast enhancement kinetics in several groups of lesions. In one study, we compared the efficacy of kinetic analysis in non-mass vs. mass lesions. Analyzing lesion presentation on DCEMRI involves an assessment of contrast media uptake and washout kinetics, as well as classification of lesion morphology as mass-like or nonmass-like enhancement. In our first pilot study, we found that kinetic parameters derived from an empirical mathematical model (EMM—the same EMM used in last years report and description of Task 2b) capturing the initial, peak and washout phase of the curve could distinguish benign and malignant mass lesions. However, no EMM kinetic parameters were useful in discriminating non-mass-like benign from malignant lesions [see page 80, Figure 3 in *DCEMRI of breast lesions: Is Kinetic analysis equally effective for both mass and non-mass-like enhancement?,* Appendix**].** In a second study with more lesions but less sophisticated mathematical analysis, we again found that found that kinetic parameters capturing both the initial and washout phase of the curve could distinguish benign and malignant mass lesions, but only one parameter related to washout was useful in discriminating non-mass-like benign from malignant lesions [see page 108, *Non-mass vs. mass-like enhancement: Which kinetic parameters distinguish benign and malignant breast lesions?,* Appendix]. This suggests that to maximize diagnostic utility, the first step before kinetic analysis should be to classify lesion morphology as mass or non-mass-like enhancement. Furthermore, better understanding of the physiology of non-mass lesions may lead to new, diagnostically useful kinetic parameters. This work is strongly related to some of the data presented in last years report, particularly on the kinetic parameters of pure DCIS lesions. We showed that DCIS lesions most often presents as non-mass-like enhancement, with a variable kinetic pattern. It is likely that the physiological basis of enhancement of non-mass lesions is different than mass lesions, and that new image acquisitions or analysis will need to be developed to distinguish benign and malignant non-mass lesions.

In last years annual report we studied how kinetic parameters of enhancement are related to prognostic markers such as estrogen receptor status, progesterone receptor status and Her2/Neu amplification. This year we continued along this path, this time restricting our analysis to only small lesions. The motivation for this is that tumor size is strongly correlated with prognosis in breast cancer—the larger and more advanced a tumor, the worse the prognosis. Other prognostic indicators are in turn correlated with tumor size: advanced tumors frequently

exhibit positive nodes, ER negativity and poorer differentiation. Since kinetics of contrast media uptake and washout measured by MRI are related to the underlying physiology and biology of lesions, it is possible that kinetic parameters could be used as surrogates for prognostic indicators. Our prior study found that lesions with poorer prognosis have more suspicious enhancement kinetics, but these studies have included large tumors; it could be that the kinetic patterns they have found are simply a reflection of the tumor size, rather than being correlated to specific markers. The purpose of this study was to separate the effect of lesion size from the assessment of the relationship between MR parameters and certain prognostic indicators. We evaluated the morphologic and kinetic characteristics of 71 small T1 (< 2.0 cm) invasive ductal carcinoma (IDC) lesions, and classified these findings by ER status, nuclear grade and node invasion. We found that enhancement kinetics in < 2.0cm cancers were associated with ER status and grade, but did not depend on whether the cancer had spread to lymph nodes. Compared with ER positive and grade I and II lesions, ER negative and poorly differentiated tumors showed stronger washout [see page 107, *Are Kinetic Parameters Related to Prognostic Indicators in <2.0 cm Invasive Ductal Carcinomas?,* Appendix]

We also performed another study, looking at the MR kinetic characteristics of MR-only lesions. DCEMRI of the breast is a promising tool for improving the detection of breast cancer due to its higher sensitivity to breast cancer compared with x-ray mammography. Some have suggested that the benefit of DCEMRI of the breast is not clear; perhaps lesions detected only on MRI may not develop into life-threatening cancers. In our study, we found that among similar subtypes of cancer (i.e., invasive ductal carcinoma), the kinetic characteristics of x-ray mammographically occult cancers were similar to that of mammographically visible cancers. If these results could be verified in a larger study, it would suggest that the 'extra' cancers detect by DCEMRI and incorporated into patient management may yield future survival benefits. [see page 109, *The kinetic and morphologic characteristics of mammographically occult, MR visible breast cancers: How different are the extra cancers found at MR imaging?*, Appendix].

We were also interested in the effect of race on the MR characteristics of lesions. Disparities in breast cancer mortality and stage at diagnosis between African American and Caucasian women has been a topic of recent interest, with evidence to suggest earlier onset of more aggressive cancer in African American women. In our study, we were interested in comparing the MR morphologic and kinetic presentation of malignant breast lesions in African American and Caucasian women. We found no difference in the lesion size, MR morphologic or kinetic presentation of malignant lesions between African American and Caucasian women [see page 112, *Are the MRI characteristics of malignant breast lesions different for African American women?*, Appendix].

Finally, we also investigated how patient weight may affect contrast enhancement when patients are injected with a fixed volume of contrast. We found that malignant lesions in obese women exhibited lower contrast uptake compared with malignant lesions in normal weight women [see page 114 *DCEMRI of Malignant Breast Lesions: Should a Fixed Volume of Contrast be Injected, or a Fixed Dose,* Appendix].

Task 2d. As mentioned earlier in the discussion of Task 2b, kinetic analysis is not very effective in non-mass lesions, most of which are DCIS. This leads to the question: what the physiological basis of enhancement is in DCIS? Perhaps if we can better understand why and how DCIS lesions enhance, we can design novel imaging acquisition and analysis techniques that target DCIS, which is the subject of Task 2d.

This past year, we have begun to investigate this question using the SV40 mouse model. We injected several mice with Gd-DTPA, an MR contrast agent, and used x-ray fluorescence microscopy to image the spatial distribution of Gd in murine DCIS [see page 104, *Why do Ductal Carcinoma in situ Lesions Enhance on Dynamic Contrast Enhance MRI of the Breast? Using X-Ray Fluorescence and MRI to Track the Spatial Distribution of Gd-DTPA in Murine DCIS,* Appendix]. We found that Gd was present in mouse mammary ducts distended with DCIS. This is an important new insight into the mechanism of contrast enhancement in DCIS. We can use this insight to design novel image analysis methods to model contrast uptake and washout in DCIS. In particular, this observation implies that the traditional two compartment mathematical models of contrast uptake and washout most often used in breast imaging, may not be applicable to DCIS. Rather, a 3 compartment model may be more appropriate since Gd entering ducts may be evidence of a 3rd compartment as shown in Figure 7. Perhaps by using new more accurate mathematical models we can be in a better position to detect DCIS lesions and to distinguish DCIS from benign lesions of similar morphology.

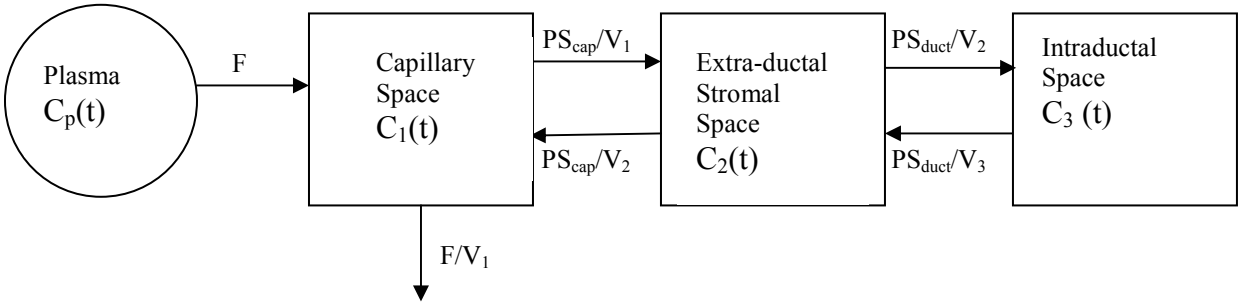

Figure 7: Three compartment model of contrast enhancement in DCIS. PS_{cap} and PS_{duct} are the permeability surface area products for the capillary and basement membrane of the duct, respectively. V_i are the fractional volumes of the spatial compartments, Ci(t) the concentration in each compartment, and F is the blood flow. This is similar to three compartment models used in PET imaging (J Nucl Med. 1997 Apr;38(4):660-7).

KEY RESEARCH ACCOMPLISHMENTS: Feb 2007-Feb 2008

- We have performed a longitudinal imaging experiment tracking the development and progression of murine DCIS in transgenic mice. To our knowledge, this the first time the progression of murine DCIS has been measured *in vivo*. We found that there was a wide range of progression rates, and that some DCIS lesions remained stable within the study window [see page 105, *Do all in situ cancers progress to invasive disease? A first look at progression of mammary cancer from in situ to invasive carcinoma in vivo*, Appendix].
- We have used mouse models to provide a new insight into the mechanism of contrast enhancement in DCIS: that Gd enters mouse mammary ducts distended with DCIS. This indicates that it may be more accurate to model the contrast enhancement kinetics of DCIS lesions using a 3 compartment model, rather than a 2 compartment model. [see page 104, *Why do Ductal Carcinoma in situ Lesions Enhance on Dynamic Contrast Enhance MRI of the Breast? Using X-Ray Fluorescence and MRI to Track the Spatial Distribution of Gd-DTPA in Murine DCIS*, Appendix]
- We have also continued to maintain the research database, which now contains over 3400 records with ~900 malignant lesions and ~300 benign lesions
- We have performed a study comparing the efficacy of kinetic analysis in non-mass vs. mass lesions. We found that kinetic parameters work well to distinguish benign and malignant mass lesions, but not non-mass benign and malignant lesions. This suggests that the first step before kinetic analysis should be to classify the lesion morphology as mass or non-mass. [see page 58, *DCEMRI of breast lesions: Is Kinetic analysis equally effective for both mass and non-mass-like enhancement?* and page 108 *Non-mass vs. mass-like enhancement: Which kinetic parameters distinguish benign and malignant breast lesions?* Appendix]
- We have demonstrated that to achieve similar levels of contrast enhancement in normal weight vs. obese women, contrast media should be administered at a fixed dose rather than a fixed volume of contrast. This result is pertinent because several institutions continue to administer fixed volume of contrast. [see page 114, *DCEMRI of Malignant Breast Lesions: Should a Fixed Volume of Contrast be Injected, or a Fixed Dose,* Appendix].

REPORTABLE OUTCOMES: Feb 2007-Feb 2008

Manuscripts:

1. **MR Imaging of Pure Ductal Carcinoma *in situ*: Kinetics, Morphology and Correlation with Mammographic Presentation and Nuclear Grade**. Radiology. 2007 Dec;245(3):684-91.
2. **Differentiation between benign and malignant breast lesions detected by bilateral dynamic contrast enhanced MRI: A sensitivity and specificity study.** Magnetic Resonance in Medicine (in press).

Abstracts and Presentation: Full versions of these abstracts can be found in the Appendix.

1. Sanaz A. Jansen, Tatjana Paunesku, GayleWoloschak, Stefan Vogt, Suzanne Conzen, Gillian M. Newstead and Gregory S. Karczmar. *Why do Ductal Carcinoma in situ Lesions Enhance on Dynamic Contrast Enhance MRI of the Breast? Using X-Ray Fluorescence and MRI to Track the Spatial Distribution of Gd-DTPA in Murine DCIS.* in 16th Annual Meeting of the Society for Magnetic Resonance in Medicine, May 2008.

2. Sanaz A. Jansen, Gillian Newstead, Suzanne D. Conzen, Marta Zamora, Thomas Krausz and Gregory Karczmar. *Do all in situ cancers progress to invasive disease? A first look at progression of mammary cancer from in situ to invasive carcinoma in vivo*. in 16th Annual Meeting of the Society for Magnetic Resonance in Medicine, May 2008.

3. Sanaz A. Jansen, Xiaobing Fan, Gregory Karczmar, Maryellen Giger, Hiroyuki Abe and Gillian M. Newstead. *Are Kinetic Parameters Diagnostically Useful for Breast Lesions Exhibiting Nonmass-like- Enhancement?* in 16th Annual Meeting of the Society for Magnetic Resonance in Medicine, May 2008.

4. Sanaz A. Jansen, Gregory Karczmar, Akiko Shimauchi, Hiroyuki Abe and Gillian M. Newstead. *Are Kinetic Parameters Related to Prognostic Indicators in <2.0 cm Invasive Ductal Carcinomas?* in 16th Annual Meeting of the Society for Magnetic Resonance in Medicine, May 2008.

5. Sanaz A. Jansen, Xiaobing Fan, Gregory S. Karczmar, Hiroyuki Abe, Akiko Shimauchi and Gillian M Newstead. *Non-mass vs. mass-like enhancement: Which kinetic parameters distinguish benign and malignant breast lesions?* in108th Annual Meeting of the American Roentgen Ray Society, April 2008.

6. Sanaz A. Jansen, Akiko Shimauchi, Hiroyuki Abe, Gregory S. Karczmar and Gillian M Newstead. *The kinetic and morphologic characteristics of mammographically occult, MR visible breast cancers: How different are the extra cancers found at MR imaging?* in 108th Annual Meeting of the American Roentgen Ray Society, April 2008.

7. Sanaz A Jansen, Suzanne Conzen, Marta Zamora, Thomas Krausz, Gillian M Newstead and Gregory S Karczmar. *A new approach to studying the progression of breast cancer in mice: High resolution MRI of early cancer and DCIS.* in 30th Annual San Antonio Breast Cancer Symposium, December 2007.

8. Sanaz A Jansen, Hiroyuki Abe, Akiko Shimauchi, Gregory S Karczmar and Gillian M Newstead. *How does ER/PR and Her2/Neu status affect the MR characteristics of invasive ductal carcinoma?* in 30th Annual San Antonio Breast Cancer Symposium, December 2007.

9. Sanaz A Jansen, Hiroyuki Abe, Akiko Shimauchi, Gregory S Karczmar, Olufunmilayo Olopade, Lindsay Zak and Gillian M Newstead. *Are the MRI characteristics of malignant breast lesions different for African American women?* in 30th Annual San Antonio Breast Cancer Symposium, December 2007.

10. Sanaz A. Jansen, Xiaobing *Fan, Gregory Karczmar, Hiroyuki Abe, Robert A. Schmidt and Gillian M. Newstead. DCEMRI of Breast Lesions: Is Kinetic Analysis Equally Effective for Both Mass and Nonmass- like Enhancement?* in 93rd Scientific Assembly and Annual Meeting of the Radiological Society of North America, November 2007.

11. Sanaz A. Jansen, Cheng Yang, Hiroyuki Abe, Akiko Shimauchi, Gregory Karczmar and Gillian M. Newstead. *DCEMRI of Malignant Breast Lesions: Should a Fixed Volume of Contrast be Injected, or a Fixed Dose* in 93rd Scientific Assembly and Annual Meeting of the Radiological Society of North America, November 2007.

Informatics: The database (Task 2a) currently contains approximately 1000 histologically proven malignant lesions, 300 histologically proven benign lesions and over 1300 normal MR exams. For each lesion, the MR kinetic and morphologic data acquired as outlined above, is recorded. Then, the subsequent final pathology of the lesion, if available, is also noted. This database is a useful resource that has been used by several collaborators in the departments of Radiology, Hematology/Oncology and Radiation Oncology. In addition, Philips Medical Systems has licensed use of the database for testing of CAD algorithms, as well as other product development.

Funding Applied for based on work supported by this award:

1. We have received pilot funding from the University of Chicago Cancer Resource Center in Fall 2007.
2. We are currently in the process of modifying an RO1.

CONCLUSIONS

In our second year of funding we have 1) performed a serial imaging experiment of the development and progression of DCIS, 2) continued to perform detailed quantitative and qualitative analysis of the MR features of malignant and benign lesions, and 3) used x-ray fluorescence microscopy to show that Gd-DTPA enters ducts distended with DCIS, which is a new insight into the mechanism of contrast enhancsement of these lesions. The overall goal of this project is to improve the understanding and detection of early cancer via MRI. On the clinical side, we have continued to use our large database of lesions to compile a rich source of data regarding the enhancement patterns in many groups of patients and lesion subtypes. On the animal side, we have performed the first experiments monitoring the development and progression of murine DCIS. In the next year, we hope to analyze in greater detail these serial imaging results. In addition, we hope to apply 3 compartment modeling techniques to kinetic data of DCIS lesions.

So what? There are a number of potential implications of this work:

- To our knowledge, ours is the first report using MR imaging to probe the development and progression of early murine mammary cancer. This represents the first steps towards probing *in vivo* the biological and radiologic changes that occur during the development and progression of DCIS into invasive cancer. Potential radiologic markers that identify aggressive DCIS lesions could be evaluated. This work may also yield future improvements of the effective treatment of early cancers. To date, most longitudinal pre-clinical studies of the efficacy of cancer therapies have focused on tumors that are large enough to be palpable. Relative to DCIS and early invasive cancers, which represent the majority of newly diagnosed breast cancers in women, these more advanced tumors are not realistic models. By using the techniques developed in Task 1, we can evaluate the efficacy of therapies on more realistic tumors.
- We found that kinetic parameters work well to distinguish benign and malignant mass lesions, but not non-mass benign and malignant lesions. This suggests that the first step before kinetic analysis should be to classify the lesion morphology as mass or non-mass. For mass lesions, kinetic curves can be used diagnostically. For non-mass lesions, kinetic curves may not be helpful. This result can help improve the radiologists interpretation of breast DCEMRI exams.
- We used x-ray fluorescence microscopy to demonstrate that MR contrast (Gd-DTPA) was present in mouse mammary ducts distended with DCIS. This new insight can improve mathematical models used to analyze contrast uptake and washout in DCIS, towards ultimately improving its reliable detection.
- We found that in order to obtain comparable enhancement in patients of different weights, contrast media should be injected at a fixed dose rather than a fixed volume. Recent studies have demonstrated that patients with kidney failure may develop Nephrogenic Systemic Fibrosis, and because of this some patients with compromised kidney function receive half-dose of contrast. Our study implies that changing the dose of contrast administered may affect how lesions will be appreciated.

REFERENCES: The references are included in each manuscript (see Appendix).

APPENDIX

Manuscripts:

MR Imaging of Pure Ductal Carcinoma *in situ*:
Kinetics, Morphology and Correlation with Mammographic
Presentation and Nuclear Grade.
Radiology. 2007 Dec;245(3):684-91. ……..23

Differentiation between benign and malignant breast
lesions detected by bilateral dynamic contrast enhanced
MRI: A sensitivity and specificity study.
Magnetic Resonance in Medicine (in press). ……..31

DCEMRI of breast lesions: Is Kinetic analysis equally
effective for both mass and non-mass-like enhancement?
Medical Physics
(provisional acceptance pending revisions) ……..58

Detection of in situ mammary cancer in a transgenic mouse
model: in vitro and in vivo MRI studies demonstrate histopathologic
correlation.
Physics in Medicine and Biology
(provisional acceptance pending revisions) ……..81

Abstracts and Presentation:

Why do Ductal Carcinoma in situ Lesions Enhance on Dynamic
Contrast Enhance MRI of the Breast? Using X-Ray Fluorescence
and MRI to Track the Spatial Distribution of Gd-DTPA in
Murine DCIS. ……104

Do all in situ cancers progress to invasive disease? A first look at
progression of mammary cancer from in situ to invasive
carcinoma in vivo. ……..105

Are Kinetic Parameters Diagnostically Useful for Breast Lesions
Exhibiting Nonmass-like- Enhancement? ……..106

Are Kinetic Parameters Related to Prognostic Indicators in <2.0 cm
Invasive Ductal Carcinomas? ……..107

Non-mass vs. mass-like enhancement: Which kinetic parameters distinguish benign and malignant breast lesions? ……..108

The kinetic and morphologic characteristics of mammographically occult, MR visible breast cancers: How different are the extra cancers found at MR imaging? ……..109

A new approach to studying the progression of breast cancer in mice: High resolution MRI of early cancer and DCIS. ……..110

How does ER/PR and Her2/Neu status affect the MR characteristics of invasive ductal carcinoma? ……..111

Are the MRI characteristics of malignant breast lesions different for African American women? ……..112

DCEMRI of Breast Lesions: Is Kinetic Analysis Equally Effective for Both Mass and Nonmass- like Enhancement? ……..113

DCEMRI of Malignant Breast Lesions: Should a Fixed Volume of Contrast be Injected, or a Fixed Dose. ……..114

CV ……..115

Note: This copy is for your personal, non-commercial use only. To order presentation-ready copies for distribution to your colleagues or clients, use the *Radiology* Reprints form at the end of this article.

Pure Ductal Carcinoma in Situ: Kinetic and Morphologic MR Characteristics Compared with Mammographic Appearance and Nuclear Grade[1]

Sanaz A. Jansen, MSc
Gillian M. Newstead, MD
Hiroyuki Abe, MD, PhD
Akiko Shimauchi, MD
Robert A. Schmidt, MD
Gregory S. Karczmar, PhD

Purpose: To retrospectively compare the kinetic and morphologic characteristics of pure ductal carcinoma in situ (DCIS) lesions depicted on dynamic contrast material–enhanced magnetic resonance (MR) images with the nuclear grade and conventional mammographic appearance of these lesions.

Materials and Methods: This HIPAA-compliant retrospective study was institutional review board approved, and informed patient consent was waived. Seventy-eight patients with 79 histologically proved pure DCIS lesions were selected. There were 17 low-nuclear-grade, 26 intermediate-nuclear-grade, 30 high-nuclear-grade, and six unclassified lesions. Sixty-five lesions were classified as fine pleomorphic, fine linear, or fine linear-branching calcifications ($n = 31$); amorphous or indistinct calcifications ($n = 18$); noncalcified mass ($n = 10$); or occult ($n = 6$) at conventional (x-ray) mammography. One experienced radiologist analyzed lesion morphology and kinetic curve shape according to the Breast Imaging Reporting and Data System lexicon. Initial enhancement percentage, time to peak enhancement (T_{peak}), and signal enhancement ratio (a measure of washout) were calculated for each lesion.

Results: Of the 79 pure DCIS lesions, 20 (25%) exhibited enhancement plateau curves and 35 (44%) exhibited washout curves. The lesions with a masslike appearance on mammograms exhibited more suspicious kinetic characteristics (mean $T_{peak} \sim 2$ minutes) than did the lesions with amorphous or indistinct calcifications (mean $T_{peak} = 4.4$ minutes). There was no significant difference in enhancement kinetic properties across the nuclear grades. Lesion morphology was predominantly nonmass, with clumped or heterogeneous enhancement in a segmental or linear distribution.

Conclusion: The pure DCIS lesions exhibited washout, plateau, and persistent enhancement curves. Enhancement kinetic characteristics varied with mammographic appearance but not with nuclear grade.

© RSNA, 2007

Supplemental material: *http://radiology.rsnajnls.org/cgi/content/full/245/3/684/DC1*

[1] From the Department of Radiology, University of Chicago, 5841 S Maryland Ave, MC 2026, Chicago, IL 60637. Received December 4, 2006; revision requested January 29, 2007; revision received March 1; accepted April 11; final version accepted June 1. Supported by the Segal Foundation, Biological Sciences Division at the University of Chicago, Department of Defense grant W81XWH-06-1-0329, and National Institutes of Health grants R21 CA104774-01A2 and 2 R01 CA078803-05A2.
Address correspondence to G.M.N. (e-mail: *gnewstead@radiology.bsd.uchicago.edu*).

© RSNA, 2007

Ductal carcinoma in situ (DCIS) comprises a heterogeneous group of lesions with variable genetic, biologic, and histologic features. DCIS is generally considered a nonobligate precursor of invasive cancer; evidence suggests that in about 30%–50% of cases, the lesion will progress to become invasive (1). DCIS is typically depicted at conventional (x-ray) mammography as calcifications, although it may also appear masslike in its noncalcified form (2–5). Accurate depiction of the extent of DCIS is essential for successful breast conservation treatment.

Dynamic contrast material–enhanced magnetic resonance (MR) imaging (hereafter referred to as dynamic MR imaging) of the breast is being used with other conventional diagnostic techniques for several clinical purposes, including preoperative evaluation of the extent and multifocality of malignancy (6) and posttreatment follow-up (7). One advantage of dynamic MR imaging is high sensitivity (6,8,9). The contrast medium uptake (ie, kinetic) properties of invasive lesions typically involve a rapid increase and a washout over time, while benign lesions tend to enhance more slowly and persistently take up contrast medium over time (10,11).

There are relatively few prior reports of the appearance of pure DCIS at MR imaging, and the kinetic and morphologic properties of DCIS without evidence of microinvasion have not yet been well characterized (12–14). The reported sensitivity of MR imaging for detection of DCIS is 77%–96% (12,15–20). Pure DCIS lesions most often appear as nonmass clumped enhancement in a segmental or linear distribution (13,16), with mainly plateau or washout enhancement curves (12,13,16,17,21). These lesions are therefore thought to have less suspicious kinetic findings compared with invasive cancers (16,22). Various reports have indicated that the kinetic characteristics of low-grade pure DCIS lesions are different from those of intermediate- and high-grade lesions (13,22,23), whereas other studies have revealed no difference (15). The numbers of patients examined in these prior reports have been relatively small (n = 15–50), and these studies have mostly focused on morphologic and qualitative kinetic analyses. Thus, the purpose of our study was to retrospectively compare the kinetic and morphologic characteristics of pure DCIS lesions depicted on dynamic MR images with the nuclear grade and conventional mammographic appearance of these lesions.

Advances in Knowledge

- Qualitative and quantitative evaluations of the morphologic and kinetic features of 79 pure ductal carcinoma in situ (DCIS) lesions at dynamic contrast-enhanced MR imaging revealed that these lesions display a variety of enhancement kinetic curve types (persistent, plateau, and washout). Contradictory to published data on invasive cancers, DCIS lesions enhance less and attain peak enhancement at a later time.
- Enhancement kinetics varied significantly ($P < .05$) according to mammographic appearance but not according to nuclear grade. Lesions with fine pleomorphic, fine linear, or fine linear-branching calcifications, as well as those that appear as masses on conventional mammograms, have stronger washout curves than do lesions with amorphous or indistinct calcifications.
- The MR morphology of pure DCIS lesions was predominantly nonmass, clumped or heterogeneous enhancement in a segmental or linear distribution. MR lesion morphology did not vary significantly with either nuclear grade ($P > .24$) or mammographic appearance ($P > .14$).

Implication for Patient Care

- Recognition and understanding of the unique morphologic and kinetic characteristics of pure DCIS at MR imaging might improve the detection of early-stage breast cancer.

Materials and Methods

Patients

At our institution, it is a routine protocol to perform breast MR examinations for diagnostic imaging, evaluation of disease extent, posttreatment evaluation, and screening for high cancer risk. We maintain a clinical database that includes the MR morphologic and kinetic data for all lesions found. The final diagnosis of the lesions is also entered into the database. The MR imaging and histologic findings for all patients are reviewed at a weekly interdisciplinary breast conference that includes radiologists, pathologists, and surgeons. The institutional review board of the University of Chicago approved our Health Insurance Portability and Accountability Act–compliant retrospective study, with waived informed patient consent. A review of 1770 records (for January 2002 through August 2005) revealed 78 women with 79 histologically proved pure DCIS lesions. The average patient age was 56 years (range, 31–86 years).

MR Imaging Analysis

Dynamic MR imaging protocol.—MR imaging was performed with a 1.5-T GE Signa unit (GE Healthcare, Milwaukee, Wis) by using a dedicated four-channel

Published online
10.1148/radiol.2453062061

Radiology 2007; 245:684–691

Abbreviations:
BI-RADS = Breast Imaging Reporting and Data System
DCIS = ductal carcinoma in situ
E_1 = initial enhancement percentage
E_{peak} = peak enhancement percentage
SER = signal enhancement ratio
T_{peak} = time to peak enhancement

Author contributions:
Guarantors of integrity of entire study, S.A.J., G.M.N.; study concepts/study design or data acquisition or data analysis/interpretation, all authors; manuscript drafting or manuscript revision for important intellectual content, all authors; manuscript final version approval, all authors; literature research, S.A.J., G.M.N.; clinical studies, S.A.J., G.M.N., H.A., A.S., R.A.S.; statistical analysis, S.A.J., G.S.K.; and manuscript editing, S.A.J., G.M.N., G.S.K.

Authors stated no financial relationship to disclose.

breast coil (Invivo, Orlando, Fla) with the patient in the prone position. Two protocols were used: In the first protocol, one precontrast image and five postcontrast images were acquired in the coronal plane by using a T1-weighted three-dimensional spoiled gradient-recalled acquisition in the steady state sequence (7.7/4.2 [repetition time msec/echo time msec], 30° flip angle, 3-mm section thickness, 1.4-mm in-plane spatial resolution) with no fat saturation. Acquisition of the first postcontrast image was started 20 seconds after the contrast medium injection, and the remaining images were acquired every 68 seconds thereafter. In the second dynamic protocol, there were four postcontrast acquisitions. The first, second, and fourth acquisitions were performed as described for the first protocol, and the third was a high-spatial-resolution coronal acquisition for 128 seconds. Gadodiamide (Omniscan; Nycomed-Amersham, Princeton, NJ) was injected intravenously at a dose of 0.1 mmol per kilogram of body weight and at a rate of 2.0 mL/sec and was followed by a 20-mL saline flush administered at the same rate. The following MR analyses were performed by using subtraction images, which were viewed at a workstation:

Morphologic MR analysis.—One radiologist (G.M.N.) with 14 years breast MR experience retrospectively reviewed the images and classified the lesion morphology. This analysis was not performed with the radiologist blinded to patient information and clinical history; rather, it was performed without knowledge of the lesion's nuclear grade and mammographic classification (discussed later in the text). Lesion morphology was classified by viewing coronal, sagittal, and transverse reconstructed MR images. The type, shape, distribution, margins, and internal enhancement pattern of the lesions were assessed according to the Breast Imaging Reporting and Data System (BI-RADS) lexicon. In addition, the maximal extent of the lesion in the sagittal plane was measured (Fig 1).

Enhancement kinetics MR analysis.—After classifying the lesion morphology, the same radiologist performed a retrospective kinetic analysis. By using institutional software, the radiologist generated enhancement kinetic curves by manually tracing a region of interest around the most enhancing part of the lesion as it appeared on the first postcontrast MR image in the coronal plane. The average region-of-interest size was 6.3 pixels. The radiologist performed a qualitative analysis of the enhancement curve shape according to the BI-RADS lexicon by assessing the initial contrast medium uptake (rapid, medium, or slow) and delayed-phase enhancement (persistent, plateau, or washout) characteristics of the curve. Quantitative kinetic parameters were also derived from the curves. For each curve, the initial enhancement percentage (E_1), peak enhancement percentage (E_{peak}), and time to peak enhancement (T_{peak}) were measured, as described by Szabo et al (24). The signal enhancement ratio (SER) was calculated as a measure of washout, as was done by Esserman et al (25) (Appendix E1, *http://radiology.rsnajnls.org/cgi/content/full/245/3/684/DC1*).

Histologic Classification

The histologic diagnosis of pure DCIS was based on the initial review of the lumpectomy or mastectomy specimens and was determined by means of consensus between two pathologists with 9 and 20 years of experience. There was no evidence of microinvasion, and no axillary involvement was found in this specimen population. Histologic classification of the nuclear grade was possible for 73 of the 79 lesions: 17 were low-grade, 26 were intermediate-grade, and 30 were high-grade pure DCIS lesions. Six lesions were unclassified.

Mammographic Classification

At our institution, conventional (x-ray) mammograms of 65 lesions were available and were retrospectively assessed by the same experienced radiologist (G.M.N.), who viewed the diagnostic mammograms on film approximately 4 months after performing the MR morphologic and kinetic analyses. For mammographic analysis, the radiologist was not blinded to the patient information and was aware of the diagnosis of pure DCIS but not the nuclear grade. In 49 of 65 lesions, calcifications were found and the morphology was classified according to the BI-RADS lexicon as fine pleomorphic, fine linear, fine linear branching, amorphous, or indistinct (Figs 2, 3). The mammographic findings were divided accordingly into four groups: *(a)* fine pleomorphic, fine linear, or fine linear-branching calcifications ($n = 31$); *(b)* amorphous or

Figure 1

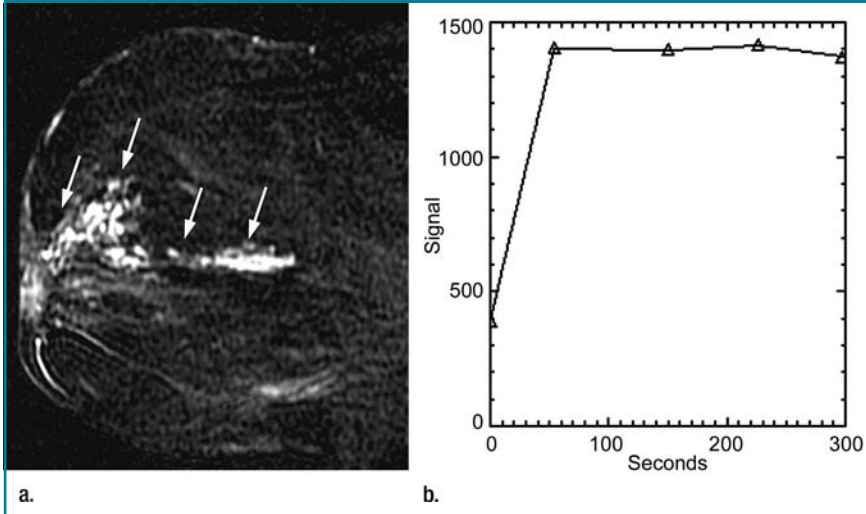

Figure 1: **(a)** Sagittal T1-weighted three-dimensional spoiled gradient-recalled acquisition in the steady state subtraction MR image (7.7/4.2, 30° flip angle) of pure DCIS (arrows). **(b)** Corresponding enhancement kinetic curve generated by using in-house software.

Figure 2

Figure 2: Digital mammogram of right breast (mediolateral view with spot magnification) shows faint indistinct calcifications near clip.

Figure 3

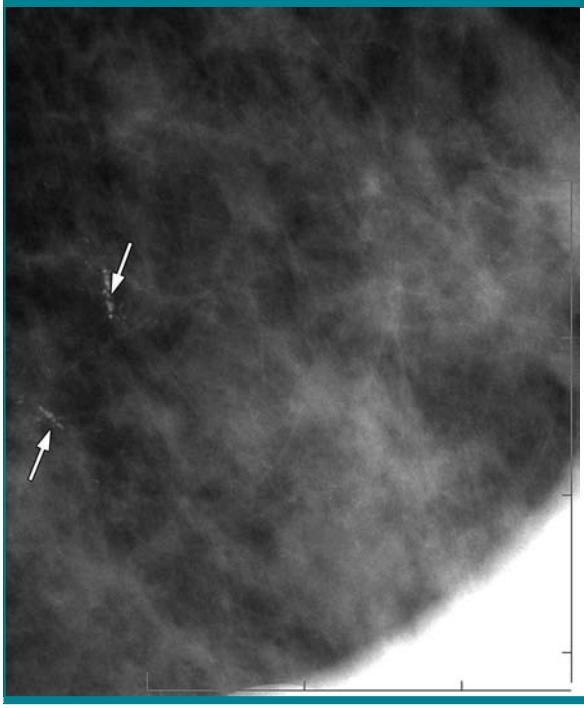

Figure 3: Digital mammogram of left breast (mediolateral view with spot magnification) shows linear-branching calcifications (arrows).

indistinct calcifications ($n = 18$); *(c)* noncalcified mass ($n = 10$); and *(d)* occult lesion ($n = 6$).

Statistical Analyses

The 73 lesions for which histologic classification was possible were classified according to nuclear grade (low, intermediate, or high), and the 65 lesions for which mammographic data were available were classified (fine pleomorphic, fine linear, or fine linear-branching calcifications; amorphous or indistinct calcifications; noncalcified mass; or occult lesion). The number of lesions with each kinetic and morphologic classification was determined for all 79 lesions and for each subpopulation. We compared the proportions of washout, plateau, and persistent (or rapid, medium, or slow) enhancement curves between lesions stratified according to either nuclear grade or mammographic appearance, and to test for significance, we used the pairwise Pearson χ^2 test, with $P < .05$ indicating significance. We performed a similar analysis of the qualitative morphologic variables—for example, we compared the proportions of mass, nonmass, and focus-type enhancement between lesions stratified by either nuclear grade or mammographic appearance.

The mean values (with standard deviations) for each quantitative kinetic parameter (E_1, E_{peak}, SER, and T_{peak}) were calculated for all 79 lesions and for the nuclear grade– and mammographic classification–based subpopulations. We performed a pairwise comparison of the mean kinetic parameter values in each of these subpopulations by using the independent samples t test, with $P < .05$ indicating significance.

We also determined the discrepancies in the SER-based versus BI-RADS–based assessment of washout as follows: For an SER higher than 1.1, any enhancement curves classified as plateau or persistent were counted as inconsistent, and for an SER of between 0.9 and 1.1, any curves classified as persistent were counted as inconsistent (Appendix E1, *http://radiology.rsnajnls.org/cgi/content/full/245/3/684/DC1*).

Table 1

Morphologic Distribution of Pure DCIS Lesions according to BI-RADS Lexicon

Morphologic Classification	No. of Lesions (n = 79)*
Lesion type	
Mass	14 (18)
Nonmass	64 (81)
Focus	1 (1)
Mass lesions	
Shape	
Round	2 (3)
Oval	1 (1)
Lobular	0
Irregular	11 (14)
Margin	
Smooth	3 (4)
Irregular	11 (14)
Spiculated	0
Internal enhancement pattern	
Homogeneous	7 (9)
Heterogeneous	7 (9)
Rim	0
Dark internal septa	0
Enhancing internal septa	0
Central	0
Nonmass lesions	
Distribution	
Focal	13 (16)
Linear	19 (24)
Ductal	0
Segmental	26 (33)
Regional	5 (6)
Multiple regions	0
Diffuse	1 (1)
Internal enhancement pattern	
Homogeneous	13 (16)
Heterogeneous	13 (16)
Stippled, punctate	6 (8)
Clumped	32 (41)
Reticular, dendritic	0
Sagittal-view lesion size†	
<20 mm	30 (38)
20–40 mm	28 (35)
>40 mm	21 (27)

* Numbers in parentheses are percentages.

† Maximal extent of lesion in sagittal view. Mean sagittal-view lesion size was 29 mm ± 18 (standard deviation).

Figure 4

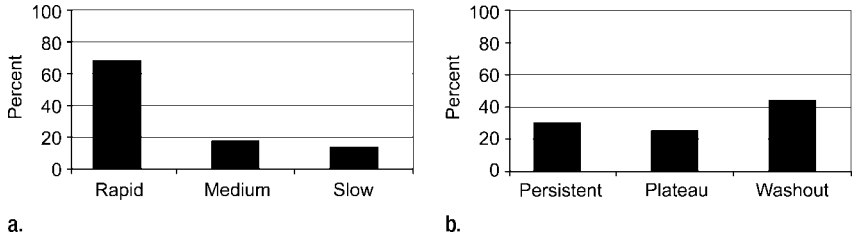

Figure 4: Graphs illustrate distribution of qualitative BI-RADS–based **(a)** initial contrast medium uptake and **(b)** delayed-phase enhancement characteristics of 79 pure DCIS lesions.

Results

MR Findings

The dominant MR features of pure DCIS lesions were nonmass and clumped, heterogeneous, or homogeneous enhancement in a segmental or linear distribution (Table 1). Fifty-four (68%) of the 79 pure DCIS lesions showed rapid enhancement. The distribution of delayed-phase enhancement characteristics was more uniform, with 35 (44%) lesions showing washout-type curves (Fig 4).

Mean kinetic parameter values were as follows: 188% ± 15 for E_1, 242% ± 16 for E_{peak}, 212 seconds ± 13 for T_{peak}, and 0.93 ± 0.04 for SER. On the basis of these quantitative measures of washout, the kinetic curves for pure DCIS lesions exhibited, on average, a plateau relative to the first postcontrast point. Overall, the quantitative and qualitative measures of washout were largely consistent. Of the 24 lesions with an SER higher than 1.1, one was classified as having a persistent enhancement curve and one was classified as having a plateau enhancement curve. Of the 17 lesions with an SER of between 0.9 and 1.1, one was classified as having a persistent curve.

MR Findings Compared with Nuclear Grades

MR morphology did not differ significantly among the low-, intermediate-, and high-nuclear-grade lesions ($P > .24$ for all comparisons, χ^2 test). Neither the initial uptake and delayed-phase classifications nor the kinetic parameters (E_1, E_{peak}, SER, T_{peak}) differed significantly across the nuclear grades of pure DCIS ($P > .06$ for all comparisons, χ^2 or independent samples t test).

MR Findings Compared with Mammographic Appearance

MR morphology did not differ significantly among the four mammographic classifications ($P > .14$ for all comparisons, χ^2 test). Lesions with amorphous or indistinct calcifications were smaller at MR imaging (average size, 23 mm) than were lesions with fine pleomorphic, fine linear, or fine linear-branching calcifications (average size, 33 mm; $P = .048$). The distribution of initial uptake was significantly similar among all mammographic appearance groups ($P > .42$ for all comparisons, χ^2 test). The χ^2 test revealed significant differences in the distribution of delayed-phase curve types: Nine (90%) of the 10 lesions with a mass appearance on mammograms—compared with 14 (45%) of the 31 lesions with fine pleomorphic, fine linear, or fine linear-branching calcifications ($P = .041$, χ^2 test) and four (22%) of the 18 lesions with amorphous or indistinct calcifications ($P = .002$, χ^2 test)—exhibited washout-type curves (Fig 5).

There were also significant differences in some quantitative parameters (Table 2). The mean SER for the pure DCIS lesions with amorphous or indistinct calcifications was 0.77, whereas the corresponding values for the lesions with fine pleomorphic, fine linear, or fine linear-branching calcifications and those with a masslike appearance at mammography were 0.95

and 1.34, respectively. Thus, on the basis of these SER values, the enhancement kinetic curves for the mass lesions strongly wash out relative to the first postcontrast point, while the curves for lesions with fine pleomorphic, fine linear, or fine linear-branching calcifications reach a plateau and the curves for lesions with amorphous or indistinct calcifications continue to increase ($P < .05$). The mean T_{peak} was 4.4 minutes for the amorphous or indistinct group; just under 3.5 minutes for the group with fine pleomorphic, fine linear, or fine linear-branching calcifications; and just under 2 minutes for the mass group ($P < .05$). The mean T_{peak} for the mammographically occult lesions was 2.5 minutes, significantly shorter than that for the lesions with an amorphous or indistinct appearance ($P = .025$). However, the enhancement kinetic characteristics of the mammographically occult lesions did not differ significantly from those of the other lesion groups ($P > .39$ for all comparisons), although these lesions demonstrated the smallest enhancement percentages. Four of the six occult lesions were of high grade.

Figure 5

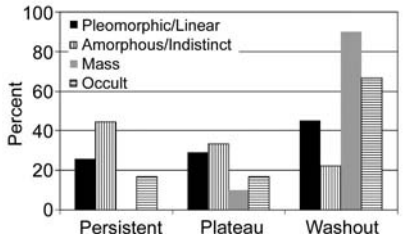

Figure 5: Graph illustrates distribution of qualitative BI-RADS–based enhancement characteristics of pure DCIS lesions assessed on the basis of mammographic appearance: amorphous or indistinct calcifications ($n = 18$); fine pleomorphic, fine linear, or fine linear-branching calcifications ($n = 31$); mass ($n = 10$); or occult lesion ($n = 6$).

Discussion

In our study, pure DCIS lesions typically appeared as nonmass-like, clumped or heterogeneous enhancement at MR imaging. In addition, the lesions did not always exhibit the typical malignant washout kinetic curves and could show persistent and plateau curve types. Our findings were concordant with those reported in the literature (13,16).

We also established several quantitative kinetic parameters of 79 pure DCIS lesions. In a previous study in which similar acquisition timing was used, the reported mean E_1 values for invasive and benign lesions were 273% and 163%, respectively (24). In our current study, the mean E_1 for pure DCIS lesions was 188%; this implies that these lesions enhance less than invasive cancers and more than benign lesions. The reported mean T_{peak} values for invasive and benign lesions were 173 and 430 seconds, respectively (24), whereas we calculated a mean T_{peak} of 212 seconds—again a value intermediate between the values for benign and malignant lesions. In the study of Esserman et al (25), the average SER for invasive lesions was 1.35, indicating a strong washout relative to the first postcontrast point. We calculated a lower mean SER of 0.93, which indicates that pure DCIS lesions plateau relative to the first postcontrast point.

The kinetic curve shape is related to the perfusion and diffusion of contrast media from the blood vessels to the extracellular space; it is the unique physiologic features and vasculature of invasive, benign, and pure DCIS lesions that ultimately explain the described differences in kinetic curves (26–28). It has been reported that perfusion rates increase as the lesion progresses from benign focus to DCIS to invasive cancer (22) and are associated with microvessel density in DCIS lesions (23). Guidi et al (29) observed an increase in vessel density around the ducts with DCIS, although with variable patterns. Heffelfinger et al (30,31) found that the expression of angiogenic growth factors, such as vascular endothelial growth factor, increases with the progression of the lesion from hyperplasia to DCIS.

We observed no significant difference in enhancement kinetic characteristics among the different nuclear grades of pure DCIS. This supports the previous findings of Viehweg et al (15). On the other hand, a few groups have observed a difference between low-grade pure DCIS and intermediate- and high-grade pure DCIS lesions. In one study (13), the difference may have existed because five of the 12 low-grade lesions studied did not enhance at all; in our study, we only considered DCIS lesions that enhanced at MR imaging. In other studies (22,23), the numbers of lesions consid-

Table 2

Kinetic Parameters of Pure DCIS Lesions Stratified according to Mammographic Appearance

Parameter	Mammographic Appearance*				*P* Value†		
	Fine Pleomorphic, Fine Linear, Fine Linear-branching Calcifications ($n = 31$)	Amorphous or Indistinct Calcifications ($n = 18$)	Occult ($n = 6$)	Mass ($n = 10$)	Amorphous vs Fine	Amorphous vs Mass	Fine vs Mass
E_1 (%)	204 ± 28	170 ± 30	152 ± 40	215 ± 34	. . .	. . .	. . .
E_{peak} (%)	251 ± 29	242 ± 32	182 ± 36	247 ± 39	. . .	. . .	. . .
SER	0.95 ± 0.06	0.77 ± 0.07	0.89 ± 0.14	1.34 ± 0.19	.05	.002	.01
T_{peak} (sec)	200 ± 20	265 ± 25	148 ± 39	109 ± 30	.05	<.001	.03

* Mean values ± standard errors of the mean.

† Fine refers to fine pleomorphic, fine linear, or fine linear-branching calcifications category. Amorphous refers to amorphous or indistinct calcifications category.

ered were perhaps too small (only three or four intermediate- and high-grade lesions) to yield significance.

To our knowledge, our study is the first investigation in which the conventional mammographic appearance of DCIS lesions was compared with the contrast medium uptake and washout in these lesions. There has been interest in the possibility that the conventional mammographic appearance of breast lesions may be a prognostic indicator (32–36). Tabar et al (34) reported that the survivals of women with masses or linear or linear-branching calcifications (ie, casting calcifications) are considerably worse than the survivals of women with other types of lesions, suggesting that the calcifications represent a duct-forming invasive cancer. In our study, lesions with fine pleomorphic, fine linear, or fine linear-branching calcifications—especially those that appeared as masses on conventional mammograms—were, according to conventional kinetic standards, more suspicious at MR imaging compared with lesions with amorphous or indistinct calcifications. In particular, DCIS lesions that appeared as masses at mammography exhibited, on average, typical malignant kinetic characteristics, with a short T_{peak} and strong washout (ie, SER).

Esserman et al (25) studied the relationships between the SERs of invasive tumors and both tumor vascularity and histologic grade. They found that higher SER was associated with higher vascularity and higher Scarff-Bloom-Richardson grade. In our study, the SERs of pure DCIS lesions of various grades were statistically equivalent. On the other hand, SERs did vary according to mammographic appearance. This suggests that the conventional mammographic appearance of pure DCIS might be related to the underlying physiologic and biologic characteristics of the lesion in a way that nuclear grade is not.

There are several limitations to the dynamic MR imaging examinations described herein, including the placement and size of the region of interest and performing the quantitative analysis by using signal intensity rather than contrast medium concentration, which can lead to errors due to variability in the native T1 of the tissue. In addition, various institutions use different imaging protocols and pulse sequences, making comparisons of quantitative parameters across institutions problematic. Even at our institution, we used two protocols, and this may have compromised the reliability of the kinetic parameters used. We attempted to minimize this effect by considering parameters based on signal intensities measured at the initial and last postcontrast time points (which were at similar times in the two protocols).

There were further limitations of our study: The MR and mammographic analyses were performed by one experienced radiologist, and the images were reviewed retrospectively. Although the MR analysis was performed without knowledge of nuclear grade or mammographic classification, there was still the question of reproducibility. Although the radiologist who performed these evaluations had 14 years of breast MR experience, a larger number of readers and a fully controlled blinded study would have been desirable. In addition, we did not perform a detailed analysis of the relationship between the histologic and imaging findings—for example, to compare the lesion extent at histologic analysis with that at MR imaging, as has been done elsewhere (20,37,38). With some preliminary conclusions in hand, we may now be in a better position to pursue a more detailed study involving more lesions, more radiologists, and improved histologic analysis.

The distinctive morphology and variable kinetic pattern of DCIS may prompt some to suggest that MR image acquisitions that emphasize spatial rather than temporal resolution are more sensitive to DCIS. Although spatial resolution is important (39), sufficient temporal resolution is also needed to distinguish the more slowly and moderately enhancing nonmass-like morphology of pure DCIS from enhancing parenchyma. Although the diagnostic utility of kinetic descriptors may be compromised by the variable kinetic pattern of DCIS, understanding the kinetic features is important for improving the detection of these lesions. For example, the longer T_{peak} and lower initial enhancement of pure DCIS lesions should be considered in some computer-aided detection schemes, in which the thresholds may be set too high and too early and thus run the risk of yielding a false-negative diagnosis. Conversely, setting thresholds too low may lead to more false-positive diagnoses and unnecessary biopsies; our results of enhancement kinetics quantification may help to balance these trade-offs.

In summary, we found that the variable enhancement kinetic characteristics of pure DCIS lesions were not associated with nuclear grade. Rather, lesions with a mammographic appearance of a soft-tissue mass or pleomorphic, linear, or linear-branching calcifications, as well as mammographically occult (ie, depicted at MR only) lesions, were more likely to exhibit plateau or washout enhancement characteristics than were lesions with amorphous or indistinct calcifications and might represent more aggressive disease. Recognition and understanding of the unique morphology and kinetic characteristics of pure DCIS at MR imaging might improve the detection of early-stage breast cancer.

References

1. Recht A, Rutgers EJ, Fentiman IS, Kurtz JM, Mansel RE, Sloane JP. The fourth EORTC DCIS consensus meeting (Heemskerk, the Netherlands, 23–24 January 1998): conference report. Eur J Cancer 1998;34:1664–1669.

2. DiPiro PJ, Meyer JE, Denison CM, Frenna TH, Harvey SC, Smith DN. Image-guided core breast biopsy of ductal carcinoma in situ presenting as a non-calcified abnormality. Eur J Radiol 1999;30:231–236.

3. Dershaw DD, Abramson A, Kinne DW. Ductal carcinoma in situ: mammographic findings and clinical implications. Radiology 1989;170:411–415.

4. Ikeda DM, Andersson I. Ductal carcinoma in situ: atypical mammographic appearances. Radiology 1989;172:661–666.

5. Stomper PC, Connolly JL, Meyer JE, Harris JR. Clinically occult ductal carcinoma in situ detected with mammography: analysis of 100 cases with radiologic-pathologic correlation. Radiology 1989;172:235–241.

6. Boetes C, Mus RD, Holland R, et al. Breast tumors: comparative accuracy of MR imaging relative to mammography and US for demonstrating extent. Radiology 1995;197:743–747.
7. Abraham DC, Jones RC, Jones SE, et al. Evaluation of neoadjuvant chemotherapeutic response of locally advanced breast cancer by magnetic resonance imaging. Cancer 1996;78:91–100.
8. Bone B, Aspelin P, Bronge L, Isberg B, Perbeck L, Veress B. Sensitivity and specificity of MR mammography with histopathological correlation in 250 breasts. Acta Radiol 1996;37:208–213.
9. Stomper PC, Herman S, Klippenstein DL, et al. Suspect breast lesions: findings at dynamic gadolinium-enhanced MR imaging correlated with mammographic and pathologic features. Radiology 1995;197:387–395.
10. Kuhl CK, Schild HH. Dynamic image interpretation of MRI of the breast. J Magn Reson Imaging 2000;12:965–974.
11. Kuhl CK, Mielcareck P, Klaschik S, et al. Dynamic breast MR imaging: are signal intensity time course data useful for differential diagnosis of enhancing lesions? Radiology 1999;211:101–110.
12. Menell JH, Morris EA, Dershaw DD, Abramson AF, Brogi E, Liberman L. Determination of the presence and extent of pure ductal carcinoma in situ by mammography and magnetic resonance imaging. Breast J 2005;11:382–390.
13. Neubauer H, Li M, Kuehne-Heid R, Schneider A, Kaiser WA. High grade and non-high grade ductal carcinoma in situ on dynamic MR mammography: characteristic findings for signal increase and morphological pattern of enhancement. Br J Radiol 2003;76:3–12.
14. Fischer U, Westerhof JP, Brinck U, Korabiowska M, Schauer A, Grabbe E. Ductal carcinoma in situ in dynamic MR-mammography at 1.5 T [in German]. Rofo 1996;164:290–294.
15. Viehweg P, Lampe D, Buchmann J, Heywang-Kobrunner SH. In situ and minimally invasive breast cancer: morphologic and kinetic features on contrast-enhanced MR imaging. MAGMA 2000;11:129–137.
16. Van Goethem M, Schelfout K, Kersschot E, et al. Comparison of MRI features of different grades of DCIS and invasive carcinoma of the breast. JBR-BTR 2005;88:225–232.
17. Orel SG, Mendonca MH, Reynolds C, Schnall MD, Solin LJ, Sullivan DC. MR imaging of ductal carcinoma in situ. Radiology 1997;202:413–420.
18. Gilles R, Zafrani B, Guinebretiere JM, et al. Ductal carcinoma in situ: MR imaging–histopathologic correlation. Radiology 1995;196:415–419.
19. Shiraishi A, Kurosaki Y, Maehara T, Suzuki M, Kurosumi M. Extension of ductal carcinoma in situ: histopathological association with MR imaging and mammography. Magn Reson Med Sci 2003;2:159–163.
20. Schouten van der Velden AP, Boetes C, Bult P, Wobbes T. The value of magnetic resonance imaging in diagnosis and size assessment of in situ and small invasive breast carcinoma. Am J Surg 2006;192:172–178.
21. Groves AM, Warren RM, Godward S, Rajan PS. Characterization of pure high-grade DCIS on magnetic resonance imaging using the evolving breast MR lexicon terminology: can it be differentiated from pure invasive disease? Magn Reson Imaging 2005;23:733–738.
22. Furman-Haran E, Schechtman E, Kelcz F, Kirshenbaum K, Degani H. Magnetic resonance imaging reveals functional diversity of the vasculature in benign and malignant breast lesions. Cancer 2005;104:708–718.
23. Oshida K, Nagashima T, Ueda T, et al. Pharmacokinetic analysis of ductal carcinoma in situ of the breast using dynamic MR mammography. Eur Radiol 2005;15:1353–1360.
24. Szabo BK, Aspelin P, Wiberg MK, Bone B. Dynamic MR imaging of the breast: analysis of kinetic and morphologic diagnostic criteria. Acta Radiol 2003;44:379–386.
25. Esserman L, Hylton N, George T, Weidner N. Contrast-enhanced magnetic resonance imaging to assess tumor histopathology and angiogenesis in breast carcinoma. Breast J 1999;5:13–21.
26. Su MY, Cheung YC, Fruehauf JP, et al. Correlation of dynamic contrast enhancement MRI parameters with microvessel density and VEGF for assessment of angiogenesis in breast cancer. J Magn Reson Imaging 2003;18:467–477.
27. Tuncbilek N, Unlu E, Karakas HM, Cakir B, Ozyilmaz F. Evaluation of tumor angiogenesis with contrast-enhanced dynamic magnetic resonance mammography. Breast J 2003;9:403–408.
28. Buadu LD, Murakami J, Murayama S, et al. Breast lesions: correlation of contrast medium enhancement patterns on MR images with histopathologic findings and tumor angiogenesis. Radiology 1996;200:639–649.
29. Guidi AJ, Fischer L, Harris JR, Schnitt SJ. Microvessel density and distribution in ductal carcinoma in situ of the breast. J Natl Cancer Inst 1994;86:614–619.
30. Heffelfinger SC, Miller MA, Yassin R, Gear R. Angiogenic growth factors in preinvasive breast disease. Clin Cancer Res 1999;5:2867–2876.
31. Heffelfinger SC, Yassin R, Miller MA, Lower E. Vascularity of proliferative breast disease and carcinoma in situ correlates with histological features. Clin Cancer Res 1996;2:1873–1878.
32. James JJ, Evans AJ, Pinder SE, Macmillan RD, Wilson AR, Ellis IO. Is the presence of mammographic comedo calcification really a prognostic factor for small screen-detected invasive breast cancers? Clin Radiol 2003;58:54–62.
33. Peacock C, Given-Wilson RM, Duffy SW. Mammographic casting-type calcification associated with small screen-detected invasive breast cancers: is this a reliable prognostic indicator? Clin Radiol 2004;59:165–170.
34. Tabar L, Tony Chen HH, Amy Yen MF, et al. Mammographic tumor features can predict long-term outcomes reliably in women with 1–14-mm invasive breast carcinoma. Cancer 2004;101:1745–1759.
35. Thurfjell E, Thurfjell MG, Lindgren A. Mammographic finding as predictor of survival in 1–9 mm invasive breast cancers: worse prognosis for cases presenting as calcifications alone. Breast Cancer Res Treat 2001;67:177–180.
36. Zunzunegui RG, Chung MA, Oruwari J, Golding D, Marchant DJ, Cady B. Casting-type calcifications with invasion and high-grade ductal carcinoma in situ: a more aggressive disease? Arch Surg 2003;138:537–540.
37. Esserman LJ, Kumar AS, Herrera AF, et al. Magnetic resonance imaging captures the biology of ductal carcinoma in situ. J Clin Oncol 2006;24:4603–4610.
38. Kumar AS, Chen DF, Au A, et al. Biologic significance of false-positive magnetic resonance imaging enhancement in the setting of ductal carcinoma in situ. Am J Surg 2006;192:520–524.
39. Harms SE. The use of breast magnetic resonance imaging in ductal carcinoma in situ. Breast J 2005;11:379–381.

Differentiation between benign and malignant breast lesions detected by bilateral dynamic contrast enhanced MRI: A sensitivity and specificity study

Sanaz A. Jansen, Xiaobing Fan, Gregory S. Karczmar, Hiroyuki Abe, Robert A. Schmidt, and Gillian M. Newstead*

Department of Radiology, University of Chicago, Chicago, IL 60637

Submitted as a full paper to Magnetic Resonance in Medicine
Word count: 3736
Short running head: Differentiation Benign Malignant Breast Lesions DCEMRI

*Corresponding Author:

Gillian Newstead, M.D.
Professor
Department of Radiology
University of Chicago
5841 S. Maryland Ave, MC 2026
Chicago, IL 60637

Phone: (773) 702-2781
Fax: (773) 834-9047
Email: gnewstead@radiology.bsd.uchicago.edu

ABSTRACT

The purpose of this study was to apply an empirical mathematical model (EMM) to kinetic data acquired under a clinical protocol to determine if the sensitivity and specificity can be improved compared with qualitative BI-RADS® descriptors of kinetics. 3D DCEMRI data from 100 patients with 34 benign and 79 malignant lesions were selected for review under an IRB approved protocol. The sensitivity and specificity of the delayed phase classification was 91% and 18%, respectively. The EMM was able to accurately fit these curves. There was a statistically significant difference between benign and malignant lesions for several model parameters: the uptake rate, initial slope, signal enhancement ratio, and curvature at the peak enhancement (at most $p = 0.04$). These results demonstrated that EMM analysis provided at least the diagnostic accuracy of the kinetic classifiers described in the BI-RADS® lexicon, and offered a few key advantages. It can be used to standardize data from institutions with different dynamic protocols, and can provide a more objective classification with continuous variables so that thresholds can be set to achieve desired sensitivity and specificity. This suggests that the EMM may be useful for analysis of routine clinical data.

Key words: Malignant, Breast, DCEMRI, Sensitivity.

INTRODUCTION

Improvements in breast cancer detection are largely responsible for increasing survival among breast cancer patients (1). Dynamic contrast enhanced magnetic resonance imaging (DCEMRI) is being used in breast imaging for several purposes, including determining extent of malignant disease and post treatment evaluation (2,3). DCEMRI has a high sensitivity to breast cancer, with a lower specificity (4-6). When analyzing DCEMRI, the radiologist assesses both the lesion morphology and kinetics of contrast enhancement. Some studies have suggested that the morphologic information from DCEMRI is more diagnostically useful than the kinetic information (7,8), implying that there may be room for improvement in extracting more diagnostically relevant information from kinetic data.

Ideally, DCEMRI protocols would acquire data with high spatial and high temporal resolution, to fully exploit both the morphologic and kinetic information. Unfortunately, with currently available equipment and techniques, there is always trade off between spatial and temporal resolution in DCEMRI (7). As a result, the signal intensity vs. time—or kinetic—curves typically have only 3-7 data points (9-11) for 3D DCEMRI, which presents a challenge for differentiating benign from malignant lesions. To simplify analysis of the kinetic curves, radiologists qualitatively asses the initial rise and delayed phase according to the BI-RADS® lexicon. Several reports have demonstrated that DCEMRI data from malignant lesions tend to exhibit 'washout' curves, while benign lesions tend to show persistent signal increase with time after contrast injection (12,13). Some groups have performed semi-quantitative analysis of these curves—for example, calculating the time to peak enhancement—to better distinguish between the benign and malignant lesions (10). However, semi-quantitative parameters have limited use since they are susceptible to errors due to noise, and with varying timing of acquisitions across institutions, comparison of these parameters between institutions is problematic.

There have been several studies of pharmacokinetic compartment modeling on breast 3D DCEMRI data, to relate kinetic curves to the underlying physiology of the lesions (14-18). However, for low time resolution 3D DCEMRI data, the accuracy of physiological parameters

obtained from compartmental models is questionable. In addition these models require an arterial input function (AIF), which is difficult to estimate accurately. As an alternative to these approaches, mathematical equations can be used to fit the kinetic curves. For example, Heiberg et al. (19) used a fifth order polynomial to fit the kinetic curves (5-7 points), but the coefficients of the polynomial did not show a significant difference between benign and malignant breast lesions. Recently, a 5-parameter empirical mathematical model (EMM) was developed to describe contrast uptake and washout behavior (20), and this model successfully distinguishes between benign and malignant lesions. Unfortunately, the EMM was performed with special protocols that allow acquisition of data with high temporal resolution, but are not clinically feasible (15,20). The limited temporal resolution in conventional 3D bilateral DCEMRI implies that complicated mathematical models cannot be directly applied to kinetic curves to obtain a unique solution.

In this study, a modified EMM with only three parameters was used to analyze 3D bilateral DCEMRI breast data that was acquired according to clinical protocols, with sparse time resolution of 68 seconds. Primary model parameters were determined by fitting the curves to the modified EMM. Secondary diagnostic parameters, such as initial area under curve ('**AUC_{30}'**)(21,22), initial slope of enhancement ('**$Slope_{ini}$**')(10,21,23), the time to peak enhancement ('**T_{peak}**')(10), signal enhancement ratio ('**SER'**)(11), and enhancement curvature at peak ('**κ_{peak}**') (24) were derived mathematically from the primary parameters after fitting the kinetic curves. The sensitivity and specificity to malignant lesions using these parameters was also evaluated by using receiver operating characteristic (ROC) analysis, and was compared to the kinetic curve classification according to the BI-RADS® lexicon. In addition to comparing benign vs. malignant lesions, the kinetic characteristics of subtypes of benign and malignant lesions were also studied.

METHODS

Patients

Diagnostic MR imaging is performed at this institution routinely for several clinical purposes: diagnostic imaging, evaluating extent of known disease, post-treatment and surgical evaluation and as a screening tool in high risk women. Bilateral 3D DCEMRI data from 100 female patients was acquired consecutively between May 2002 and June 2003 and reviewed for study under an Institutional Review Board approved protocol, with informed consent waived and under full HIPAA compliance. The age range of the subjects was 24 to 81 years (mean age = 56.2 ± 13.3 years). Based on the consensus opinion of two experienced pathologists, there were 34 benign and 79 malignant lesions used in this study.

MR Imaging

MR imaging was performed on a 1.5T GE Signa scanner (GE Healthcare, Milwaukee, WI) using a dedicated 4 channel breast coil (Invivo, Orlando, FL) with the patient in the prone position. One pre and five post-contrast images were acquired in the coronal plane using a 3D T_1-weighted spoiled grass sequence (TR/TE = 7.7/4.2 msec, flip angle = 30˚, slice thickness = 3 mm, and in plane resolution = 1.4 mm), without fat saturation. The first post-contrast acquisition was started 20 seconds after contrast injection and the remaining images were acquired every 68 seconds. Gadodiamide (Omniscan; Nycomed-Amersham, Princeton, NJ) was injected intravenously at a dose of 0.1 mmol/kg followed by a 20 ml saline flush at the rate of 2.0 ml /sec.

All kinetic analysis was performed by experienced radiologists by using coronal and reconstructed axial and sagittal views to assess the lesion. To generate the kinetic curve, the radiologist traced a small region of interest (ROI) around what was perceived to be the most enhancing part of the lesion on the first post-contrast image. The average ROI size was 7.1 pixels; thus the selected ROIs were small, and contained the most enhancing contiguous pixels in the lesion, as perceived by the radiologist. The plot of signal intensity vs. time for this ROI was assessed by the radiologist according to the BI-RADS® lexicon, which describes the “initial

rise" and "delayed phase" of the kinetic curve. The "initial rise" is classified as rapid, medium or slow. The "delayed phase" refers to the portion of the kinetic curve after two minutes and is classified as persistent (the signal intensity continues rise), plateau (the signal intensity levels off) and washout (the signal intensity decreases).

Modified Empirical Mathematical Model

The kinetic curve obtained above was analyzed quantitatively using the modified empirical mathematical model (EMM)(24) First, the average DCEMRI signal intensity as a function of time ($S(t)$) in the selected ROI was calculated. Next, signal changes after contrast injection were calculated as: $\Delta S = (S_n - S_0)/S_0$, where S_0 is the average signal intensity within the ROI in the precontrast scan, and S_n is the signal intensity within the ROI at the n^{th} post contrast time point. The following modified EMM was used to describe the lesion contrast uptake and washout and to fit the data:

$$\Delta S(t) = A \cdot \left(1 - e^{-\alpha t}\right) \cdot e^{-\beta t}, \qquad [1]$$

where A is the upper limit of the signal intensity, α (min^{-1}) is the rate of signal increase, β (min^{-1}) is the rate of the signal decrease during washout. The goodness of fit parameter R^2 was calculated for each lesion. The signal intensity modeled here is dependent on the noncontrast T_1 of the lesions. This is consistent with routine clinical practice, since Radiologists typically evaluate changes in signal intensity following contrast injection. Variations in the native tissue T_1 values will affect the measured signal intensity, however since T_1 values of benign and malignant lesions show considerable overlap (25-28), the results here may not be strongly affected.

Derived Diagnostic Parameters

Semi-quantitative diagnostic parameters used commonly in the literature were easily derived from the modified EMM parameters. After some simple mathematical manipulations, we obtained the following derivations for diagnostic parameters:

(a) **Initial area under curve ('AUC_τ'):** The 'AUC_τ' can be calculated by integration of the kinetic curve, i.e.:

$$\mathrm{AUC}_\tau = A \cdot \left[\left(1 - e^{-\beta\tau}\right) \Big/ \beta + \left(e^{-(\alpha+\beta)\tau} - 1\right) \Big/ (\alpha+\beta) \right], \qquad [2]$$

where τ is the time over which signal intensity was integrated. In this study we used τ = 30 seconds.

(b) **Initial slope of enhancement ('$Slope_{ini}$'):** The initial slope of the kinetic curve can be calculated by taking the derivative of Eq. [1] at an initial time $t << 1$:

$$Slope_{\mathrm{ini}} \approx A\alpha . \qquad [3]$$

Thus the initial slope is the product of the uptake rate α and the amplitude of enhancement A.

(c) **Time to peak of enhancement ('T_{peak}'):** The time at which the kinetic curve reached peak can be solved by setting the derivative of Eq. [1] equal to zero:

$$T_{\mathrm{peak}} = \frac{1}{\alpha} \log\left(1 + \frac{\alpha}{\beta}\right). \qquad [4]$$

Please notice that when $\beta \leq 0$, the curves did not reach the peak within the duration of the experiment. In these cases, we used the last point as the peak intensity.

(d) **Signal enhancement ratio ('SER')**: The signal intensity change at the first time point (ΔS_1) relative to the last time point (ΔS_L) was used to calculate the '**SER'** using the following formula:

$$SER = \frac{\Delta S_1}{\Delta S_L} = \frac{1 - e^{-\alpha t_1}}{1 - e^{-\alpha t_L}} \cdot e^{(t_L - t_1)\beta}, \qquad [5]$$

where t_1 = 60 s and t_L = 300 s used in this study. A '**SER'** value greater than 1.1 indicates the signal intensity decreases with respect to its value at 60 seconds; '**SER**' less than 0.9 indicates that signal intensity continues to rise; and '**SER**' between 0.9 and 1.1 represents a plateau relative to intensity at 60 seconds.

(e) **Enhancement curvature at peak ('κ_{peak}'):** The curvature at the peak of enhancement was calculated from the definition of curvature formula at time of 'T_{peak}':

$$\kappa_{peak} \approx -A\alpha\beta \,. \qquad [6]$$

Data analysis and Statistical evaluation

For the qualitative evaluation according to the BI-RADS® lexicon, distributions of initial rise and delayed phase were determined for benign and malignant lesions. To compare these distributions the chi-squared (χ^2) test was used, with a p value < 0.05 indicating statistical significance.

The 3D bilateral DCEMRI data were processed using software written in IDL (Research Systems, Inc., Boulder, CO). The average values of the diagnostic parameters were calculated separately for benign and malignant lesions. In addition, the benign and malignant lesions were further divided into pathologic subtypes. For malignant lesions these subtypes were: invasive ductal carcinoma (IDC), ductal carcinoma in situ (DCIS), invasive lobular carcinoma (ILC) and other. For benign lesions these subtypes were: fibrocystic change (FCC), fibroadenoma, papilloma and other. Two-tailed unequal variance Student's t-tests were performed to evaluate which parameters showed significant differences between the benign and malignant breast lesions, with a p value < 0.05 indicating statistical significance.

In order to determine whether modified EMM parameters varied within pathologic subtypes of benign and malignant lesions (for example, if the parameter '**α**' varied significantly among DCIS, ILC and IDC lesions) ANOVA calculations were used, with a p value < 0.05 indicating statistical significance. The ANOVA analysis was performed on the three classified subtypes of malignant lesions (DCIS, ILC and IDC) and the three classified subtypes of benign lesions (fibroadenoma, papilloma and FCC). We also performed a multivariate analysis using a stepwise logistic regression algorithm in Matlab (The MathWorks, Inc., Natick, MA) in order to determine whether a combination of primary and derived EMM parameters could better separate benign from malignant lesions. We used backwise regression (that is, the initial model included all parameters) and the minimum p value for removal of 0.1. Receiver operating characteristic

(ROC) analysis was performed to compare the diagnostic capability of the parameters derived from the modified EMM with the diagnostic performance of the qualitative BI-RADS® categories of initial rise and delayed phase. ROCKIT software (ROCKIT 0.9B Beta Version, Charles E. Metz, University of Chicago(29)) was used to generate the ROC curves and perform statistical comparisons between them via the bivariate and area test.

RESULTS

BI-RADS® Classification

The distribution of initial uptake and delayed phase for all lesions as well as the breakdown of benign and malignant lesions into pathology subtypes is shown in Table 1. Malignant and benign lesions did not have statistically significantly different distributions of initial rise, but differed in delayed phase distribution with 65% and 38% showing 'washout' curves, respectively ($p = 0.03$). Similarly, DCIS and IDC lesions were significantly different in delayed phase, with 50% and 78% showing 'washout', respectively ($p = 0.04$). Considering 'washout' and 'plateau' to be indicative of malignancy (10,13) the sensitivity and specificity were 91% (95% confidence interval (CI) 83-96%) and 18% (95% CI 7-35%), respectively. For initial phase criteria, considering 'rapid' to be indicative of malignancy, the sensitivity and specificity were 89% (95% CI 79-95) and 26% (95% CI 13-44%), respectively. In most prior studies of the kinetics of benign and malignant lesions, only IDC lesions were considered (10,13). When considering only the IDC lesions, the sensitivity of 'washout' and 'plateau' as described in the BI-RADS® lexicon improved to 97% (95% CI 85-100%), and the sensitivity of 'rapid' improved to 92% (95% CI 78-98%).

Modified EMM parameters

The modified EMM was able to accurately fit the curves, with a goodness of fit parameter R^2 greater than 0.90 for all cases studied here. Some typical examples of the modified EMM fits are shown in Fig. 1 for various benign (top row – FCC, fibroadenoma, and papilloma) and malignant lesions (bottom row - DCIS, IDC, and ILC). The distribution of the primary

parameters for all the sub-categories of benign and malignant lesions is shown in Fig. 2. Upon visual inspection, substantial overlap between benign and malignant lesions was evident for the EMM parameters. After fitting all the kinetic curves, the five derived diagnostic parameters were calculated using the Eqs. [2-6].

The average values of all primary and derived parameters were calculated and are summarized in Table 2. From calculated averaged parameters, it can be seen that malignant lesions had significantly faster contrast uptake ('**α'**), steeper initial slope ('**Slope$_{ini}$'**), larger enhancement ratio (**'SER'**) and sharper curvature ('**κ_{peak}'**) than benign lesions. Two tailed unequal variance t-test showed that there was a statistically significant difference between benign and malignant lesions for the parameters of contrast uptake rate '**α'** ($p < 0.03$), initial slope '**Slope$_{ini}$'** ($p < 0.04$), signal enhancement ratio '**SER'** ($p < 0.0007$), and the curvature at the peak '**κ_{peak}**'($p < 0.02$). To evaluate diagnostic performance, ROC curves were generated for all parameters, with calculated 'A_z' values shown in Fig. 3. 'A_z' had the smallest area under ROC curve ('**A_z**'), while **'SER'** had the largest. The ROC curves for the two parameters (Fig. 4) with the largest **'A_z'** values, '**α'** (blue line with solid square) and '**SER',** (red line with solid circle) are statistically equivalent under the bivariate and area test. From these ROC curves we can see that at a sensitivity of ~90% the specificity was ~20-30%, which was within the CI of the specificity achieved with the BI-RADS delayed phase and initial rise descriptors.

It is interesting to study further the kinetic properties of the subtypes of benign and malignant lesions. The calculated average values showed that the primary as well as diagnostic parameters for FCC were very similar to DCIS, which contributed to the majority of the overlap between the benign and malignant lesions. Performing t-test comparisons between these groups (DCIS vs. FCC) yields statistical equivalence ($p > 0.063$ for all parameters). On the other hand, the contrast uptake and washout rates for IDC were much faster than benign lesions. As a result, IDC lesions had the largest '**AUC_{30}**', deepest '**Slope$_{ini}$'**, highest '**SER'** and sharpest '**κ_{peak}**'. In addition, for all primary and derived parameters there was a statistically significant difference (at least $p < 0.02$) between IDC and DCIS lesions. This suggests that the diagnostic accuracy of the modified EMM parameters may be improved if we consider only IDC lesions. To explore this,

Fig. 4 also shows ROC curves (lines with open symbols) for '**α'** and '**SER'** when testing benign vs. IDC lesions only. As shown in the figure, these ROC curves demonstrate considerable improvement in the $\boldsymbol{'A'_z}$ values compared to their benign vs. all malignant lesions counterparts. At a sensitivity of ~95% the specificity was ~10-30%, which was within the CI achieved with the BI-RADS® classifications.

To test whether a combination of parameters could improve the sensitivity and specificity, multivariate analysis was performed. However, the recommended model selected by backward stepwise regression included only the parameter **SER**. Based on these results, it would seem that combinations of the EMM primary and derived parameters will not improve sensitivity and specificity.

Finally, ANOVA analysis was used to study the variation of the primary and derived parameters within benign and malignant sub-categories. Three parameters ('**α', '$\mathbf{T_{peak}}$'**, **'SER'**) varied significantly by subtype for benign lesions ($p < 0.03$ for all), whereas all but one ('***A'*, 'α', '$\mathbf{T_{peak}}$', '$\mathbf{AUC_{30}}$', '$\mathbf{Slope_{ini}}$', '$\boldsymbol{\kappa_{peak}}$'**, '**SER'**) varied significantly for malignant subtypes ($p <$ 0.007 for all).

DISCUSSION

In this study we found that 68% of malignant curves exhibited 'washout', which is similar to prior reports, however 38% of benign curves also showed 'washout', which is higher than many reports (13). This may be because the benign lesions considered in this study were histologically proven benign — in other words, these lesions were suspicious enough to warrant biopsy. Since most obviously benign lesions have 'persistent' type curves and would not be sent to biopsy, this may skew the delayed phase distribution in this study away from the 'persistent' curve type. Szabo et al (10) considered only histologically proven benign lesions, and found that 24% of benign lesions showed 'washout' type curves, a value closer to the one presented here. Because of the large number of benign lesions with 'plateau' and 'washout' type curves in this study, using these descriptors from the BI-RADS® kinetic classification provided high sensitivity and low specificity in diagnosing malignant lesions.

The results demonstrated that the modified EMM fit the 3D DCEMRI data very well, for all cases. All the secondary diagnostic parameters could be easily calculated from the EMM parameters. Thus, we were able to calculate parameters, such as '$\mathbf{AUC_{30}}$' and 'κ_{peak}', which could not be calculated directly from kinetic data comprised of only 6 points. The sensitivity and specificity of the BI-RADS® delayed phase and initial rise classifications were 89-91% and 18-26%, respectively. Using the primary model parameter 'α' or the derived parameter '**SER**', at ~90 % sensitivity the specificity was ~20-30%, which was statistically equivalent to the corresponding BI-RADS results. However, unlike the BI-RADS® classification, the EMM can be used to achieve a continuous spectrum of sensitivity and specificity. For example, at a sensitivity of ~80% the specificity was ~40%.

The diagnostic accuracy of the model parameters may be compromised by the relatively large number of DCIS and ILC lesions in this study, which showed significant overlap with benign lesions. Indeed, most other studies usually focus only on IDC lesions (10). We found that when considering benign vs. IDC lesions only, the 'plateau' and 'washout' descriptors from the BI-RADS® lexicon had sensitivity and specificity of 97% and 18%, respectively. Similarly, the

'rapid' descriptor from the BI-RADS® lexicon had sensitivity and specificity of 92% and 26%, respectively. The corresponding values for '**α**' and '**SER**' were comparable to the BI-RADS® results. However, at a reasonable sensitivity of ~80%, the specificity of the model parameters improved greatly to ~60%. The multivariate analysis did not yield a combination of parameters that improved results compared with individual parameters. This may be due to several factors; we have considered a small number of lesions, and some parameters may depend on each other mathematically, which in turn may reflect a biological dependence. Further investigation of the relationship that EMM parameters have with each other, and with the underlying biology of breast lesions is needed.

We have studied several subtypes of benign and malignant lesions, each having unique underlying biology. Fibroadenomas involve a proliferation of both epithelial and mesenchymal cells, and often present as encapsulated, well circumscribed masses. Papillomas, on the other hand, grow confined in mammary milk ducts. FCC refers to a variety of benign mammary alterations, which are thought of as exaggerated physiological phenomena rather than diseases. These include proliferative lesions, such as intraductal hyperplasia, as well as fibrocystic disease. Moving to the malignant subtypes of cancer, ILCs involve cancer cells of lobular origin, which have invaded the surrounding stroma in a diffusely infiltrating fashion. IDCs, on the other hand, are cancer cells of ductal origin, which have well-defined but infiltrative margins. DCIS lesions are also cancer cells of ductal origin that are still confined to the mammary ducts.

The significant overlap of DCIS lesions with benign lesions may be related to similarities in the underlying biology and vasculature(30,31). Because DCIS is the earliest form of malignant breast disease, improving the detection of DCIS is important, and further investigation into the presentation of DCIS would be interesting(32). The ANOVA results in this study indicate that most of the modified EMM parameters varied significantly across the sub-types of DCIS, ILC and IDC. Uptake and the sharpness and magnitude of washout tended to increase from DCIS to ILC to IDC. DCIS and IDC lesions showed the most difference in all parameters, with DCIS lesions having on average a much longer time to peak enhancement (3.6 minutes)

compared with IDC lesions (2 minutes). On the other hand, only three parameters ('**SER'**, '$\mathbf{T_{peak}}$**', 'α'**) showed significant variations among benign lesions; fibroadenomas exhibited a smaller uptake rate and much longer time to peak enhancement than papillomas.

The modified EMM does not make assumptions about the underlying physiology of the lesion. Some assumptions required by two compartment or multi compartment models (15) can lead to fitting errors and subsequent diagnostic errors. On the other hand, this lack of direct correspondence to identifiable physiologic or anatomic features is also the main disadvantage of the modified EMM approach. This problem can be addressed by deriving equations that connect parameters of the modified EMM to physiologic and anatomic parameters associated with various models (i.e. two or more compartment models). The parameters '$\boldsymbol{A}$**'**, '**α'**, and '**β'** in the modified EMM can be directly compared with two compartment models described in Eqs. [13-16] of Armitage et al (33). For example to compare the EMM with the Tofts model described in Eq. [13] of Armitage et al, it can be seen that the $\boldsymbol{A} = Dv_eK^{trans}/V_p(K^{trans} - k_{out}v_e)$, $\beta = k_{out}$, and $\alpha + \beta = K^{trans}/v_e$, where D is the dose of administered contrast agent, v_e is the extravascular extracellular space volume fraction, K^{trans} is the transfer constant, V_p is the volume of the plasma, and k_{out} is rate constant for contrast media elimination. With such relationships, the empirical model can be related to a physiologically motivated model.

There are other limitations to this study:

- Sparse sampling may result in fitting errors. In particular, prior work has suggested that high temporal resolution was required to sample the kinetic curve uptake and transition part of uptake and washout accurately(24)

- Pre-clinical studies suggest that specificity is improved when the tail of the washout curve is sampled for at least 15 minutes; the curves studied here are truncated at about 6 minutes (20).

- Using signal intensity rather than contrast concentration may result in errors due to variability of the native T_1 of the tissue. However, in the present application of the EMM we used signal intensity rather than contrast concentration to follow conventional clinical practice, and to minimize noise amplification.

- The present model does not account for variations in the arterial input function (AIF) and this omission can introduce variability and systematic error. The EMM is designed to analyze and accurately fit the signal intensity curves or contrast concentration vs. time curves, and these are a function of the AIF and the tissue response to the AIF. The effect of AIF can be removed by deconvoluting it from the contrast concentration curves, so that an impulse response function can be obtained. Future work will focus on deriving deconvolution algorithms and developing mathematical models for the impulse response function.

- To characterize the kinetics of the lesion, only a small ROI was used which results in lower SNR. In addition, one small ROI may not be a reliable representation of the entire lesion, especially for heterogeneously enhancing lesions. Although the ROI was placed on the most rapidly enhancing area of the lesion, as is clinical practice, there is no guarantee this is the region of most diagnostic utility. Also, the ROI was chosen manually, resulting in variations in size and placement.

- Although the total number of lesions studied was relatively large, when considering subtypes of benign and malignant lesions (such as fibroadenoma, or ILC) only a few cases were found, raising the issue of statistical validity. In particular, the numbers of lesions may be too small to perform reliable comparisons of the subtypes of benign and malignant lesions presented here.

- Recent parallel imaging techniques render the data we have used here slightly outdated, and the EMM will need to be tested with these new methods. We expect that the EMM will succeed with newer data, since the temporal resolution is comparable to that used in the studies described here. However, with the improved spatial resolution of parallel imaging, the ROI selection could likely be refined.

Despite the shortcomings summarized above, these results show that in our patient group, analysis of conventional 3D DCEMRI data with the EMM provides at least the diagnostic accuracy of qualitative kinetic parameters described in the BI-RADS® lexicon, and offers a few key advantages. It can be used to standardize kinetic data between institutions—currently, when radiologists are presented with an outside MRI for evaluation, there is no way to relate the kinetic findings of the outside case to experience at the home institution. For example, if MR

images at the outside institution are acquired every 90 seconds, and at the home institution the dynamic protocol acquires images every 60 seconds, the EMM can be used to present the outside kinetic data with 60 second time resolution. The EMM can be automated and can provide a more objective classification. The EMM provides continuous variables so that thresholds can be set to achieve desired sensitivity and specificity. It also offers an opportunity to relate semi-quantitative parameters (such as '**SER'**) to more fundamental EMM parameters. More importantly, this model allows for more flexibility in improving sensitivity and specificity in the future by correcting for arterial input functions. This model may become valuable as new protocols are being implemented at higher field strength and become more available. With the development of parallel imaging techniques, it is now possible to acquire images with relatively high spatial resolution while still acquiring 6 or 7 kinetic data points. Thus, optimizing the diagnostic utility of kinetic data will be more and more important, and these preliminary results have demonstrated that the EMM may be useful for analysis of routine clinical data.

Acknowledgments

The authors wish to thank Dr. Yulei Jiang and Marieke Heisen for assistance with statistical analysis. We would like to thank the Segal Foundation, the Biological Sciences Division at the University of Chicago, DOD grant W81XWH-06-1-0329 and NIH grants R21 CA104774-01A2 and 2 R01 CA078803-05A2 for financial support.

Table 1. Distributions of BI-RADS® categories for the qualitative assessment of the initial rise and delayed phased of kinetic curves for benign and malignant lesions, as well as the subtypes of benign and malignant lesions considered here. Numbers in parentheses are percentages.

		Initial			***Delayed***		
Type of lesions	**No. cases**	***Rapid***	***Medium***	***Slow***	***Washout***	***Plateau***	***Persistent***
All Benign	**34**	**25 (74%)**	**8 (24%)**	**1 (3%)**	**13 (38%)**	**15 (44%)**	**6 (18%)**
FCC	16	11	4	1	3	11	2
Fibroadenoma	4	2	2	0	2	1	1
Papilloma	7	6	1	0	4	2	1
Others	7	6	1	0	4	1	2
All Malignant	**79**	**70 (87%)**	**7 (9%)**	**2 (3%)**	**51 (65%)**	**21 (27%)**	**7 (9%)**
DCIS	30	26	3	1	15	10	5
IDC	36	33	3	0	28	7	1
ILC	7	6	0	1	4	2	1
Others	6	5	1	0	4	2	0

Table 2. The primary and secondary diagnostic parameters derived from the EMM in malignant and benign lesions. Reported values are mean ± standard deviation for all cases. Numbers in bold indicate that there was a statistic significantly difference between benign and malignant lesions.

Type of lesions	**No. cases**	A	α (min^{-1})	β (min^{-1})	AUC_{30}	$Slope_{ini}$ (min^{-1})	$*T_{peak}$ (min)	κ_{peak}	**SER**
All Benign	**34**	4.2±2.2	**1.6±1.1**	0.045±0.047	0.55±0.35	**6.1±4.6**	3.4±1.8	**-0.30±0.49**	**0.88±0.30**
FCC	16	3.9±1.8	1.3±1.0	0.039±0.046	0.48±0.39	5.3±5.5	4.0±1.6	-0.23±0.56	0.78±0.28
Fibroadenoma	4	6.5±2.6	0.69±0.22	0.050±0.066	0.48±0.25	4.4±2.4	4.2±1.4	-0.22±0.25	0.65±0.19
Papilloma	7	3.6±1.9	2.5±1.1	0.050±0.022	0.62±0.28	7.5±3.6	2.0±1.2	-0.33±0.14	1.08±0.7
Others	7	4.3±2.8	2.0±1.1	0.050±0.063	0.66±0.36	7.4±4.4	3.2±2.0	-0.45±0.64	1.04±0.30
All Malignant	**79**	4.0±2.2	**2.1±1.1**	0.058±0.061	0.71±0.54	**8.7±8.3**	2.8±1.9	**-0.67±1.18**	**1.14±0.48**
DCIS	30	2.8±1.9	1.8±0.9	0.037±0.058	0.40±0.23	4.3±2.6	3.6±2.0	-0.18±0.31	0.96±0.35
IDC	36	4.9±2.0	2.6±1.3	0.072±0.062	1.01±0.62	13.1±10.2	2.0±1.5	-1.12±1.57	1.31±0.55
ILC	7	3.1±2.1	1.5±0.4	0.054±0.062	0.44±0.26	4.6±2.7	3.2±2.0	-0.35±0.40	1.04±0.30
Others	6	5.6±1.4	1.6±0.9	0.087±0.046	0.78±0.38	8.5±4.7	2.3±1.0	-0.82±0.89	1.14±0.57

* For those curves which did not reach a peak within the duration of the experiment, we assumed a time to peak of 5 min.

Figure's Captions:

Figure 1. Examples of MRI signal enhancement vs. time curves (open circles) are shown for a variety of lesions types and fitted with the modified EMM (solid lines). The top row consists of benign lesions, from left to right: fibrocystic change (FCC), fibroadenoma and papilloma. The bottom row consists of malignant lesions, from left to right: ductal carcinoma *in situ* (DCIS), invasive ductal carcinoma (IDC) and invasive lobular carcinoma (ILC).

Figure 2. The distributions of the primary EMM parameters are shown according to lesion type. From top to bottom the primary EMM parameters are the amplitude A, the uptake rate α, and the washout rate β. The open circles display the values of the primary EMM parameter for every case in that subtype of benign lesion, and × marks the average value: fibrocystic change (FCC, n=16), fibroadenoma (n=4), papilloma (n=7), and other benign (n=7). Similarly, the open triangles represent the values of each primary EMM parameter for every case in that subtype of malignant lesion, and × marks the average value: ductal carcinoma *in situ* (DCIS, n=30), invasive ductal carcinoma (IDC, n=36), invasive lobular carcinoma (ILC, n=7), and other malignant (n=6).

Figure 3. The bar graph of the area under the ROC curve (Az) is shown for each EMM primary and derived parameter. The area under an ROC curve (Az) gives a measure of how well the diagnostic parameter performs; the larger the area under the curve, the better the performance. The Az values (and corresponding standard error) were determined from the fitted binormal ROC curves generated by the ROCKIT software. The standard errors are almost the same for all the cases.

Figure 4. Fitted binormal ROC curves generated by the ROCKIT software are shown for selected parameter α (blue line with solid squares) and **SER** (red line with solid circles). The $\mathbf{A_z}$ values were improved by comparing benign lesions with IDC lesions only, as shown by the ROC curves for α (blue line with open squares) and **SER** (red line with open circles).

Figure 1.

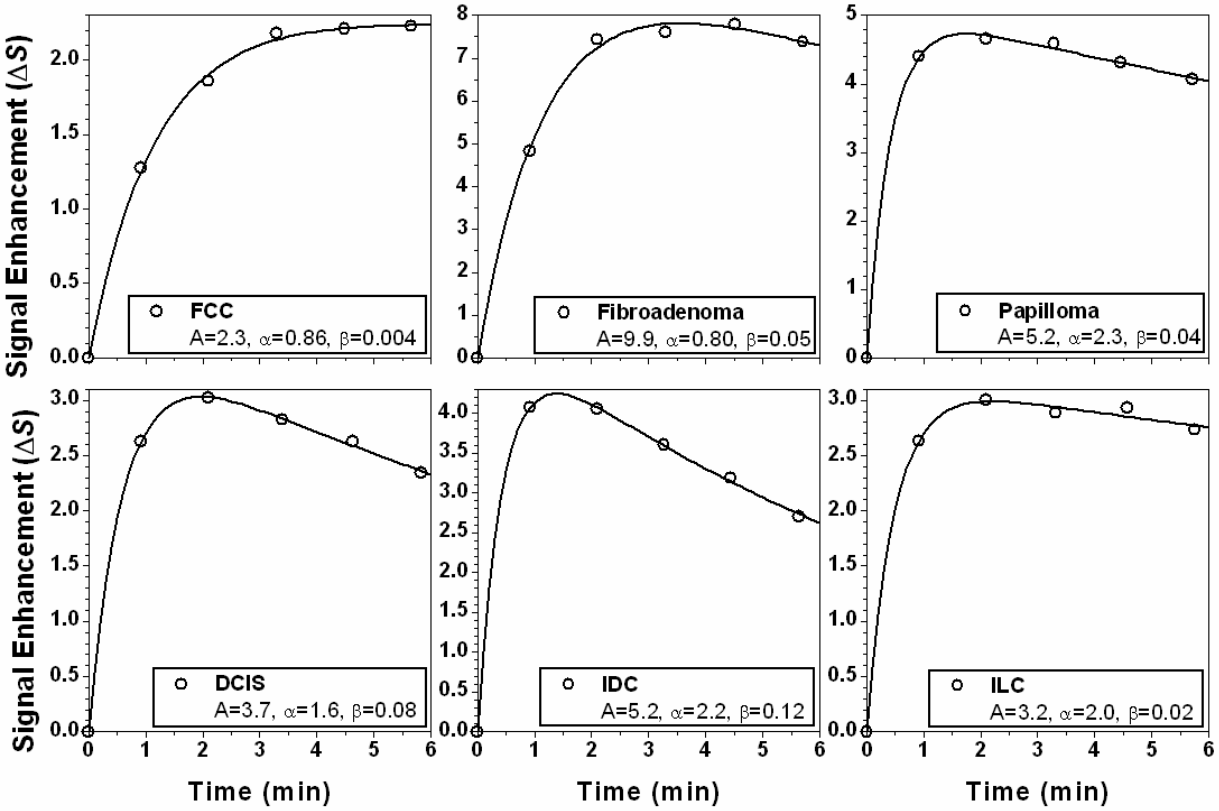
Signal Enhancement (ΔS)
FCC
A=2.3, α=0.86, β=0.004
Fibroadenoma
A=9.9, α=0.80, β=0.05
Papilloma
A=5.2, α=2.3, β=0.04
DCIS
A=3.7, α=1.6, β=0.08
IDC
A=5.2, α=2.2, β=0.12
ILC
A=3.2, α=2.0, β=0.02
Time (min)

Figure 2.

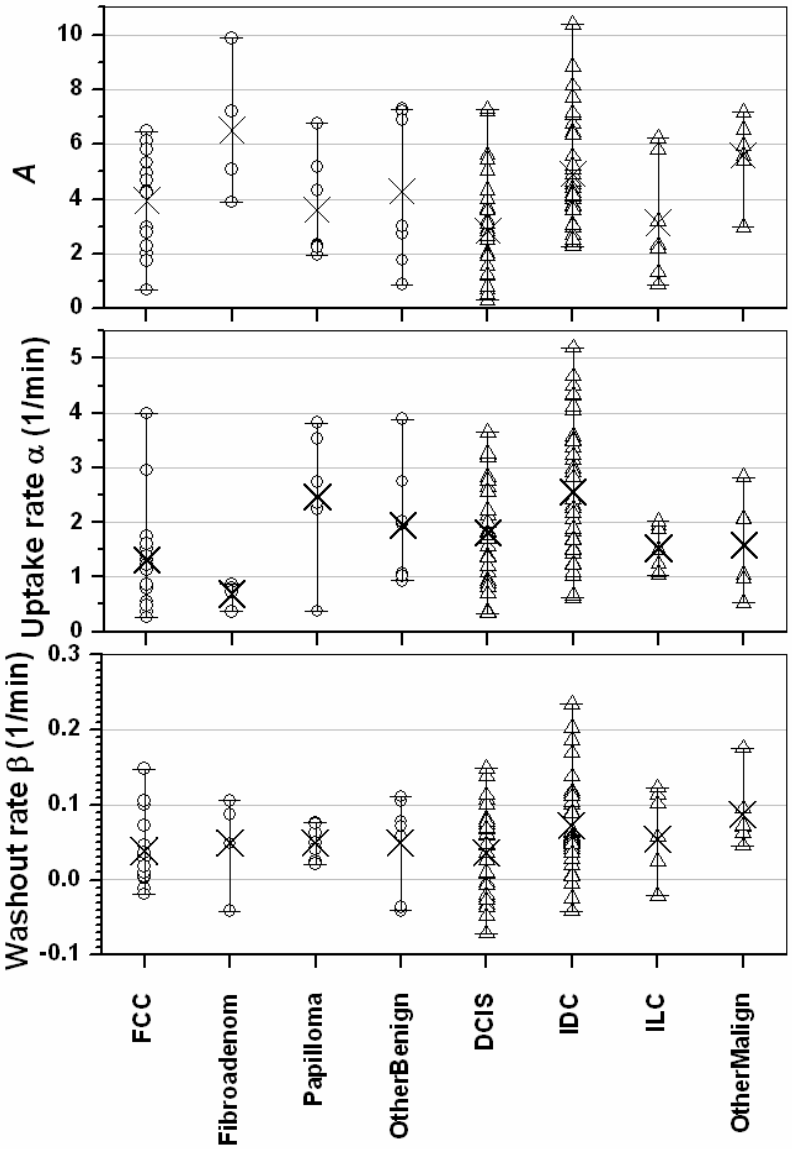
A
Uptake rate α (1/min)
Washout rate β (1/min)
FCC
Fibroadenom
Papilloma
OtherBenign
DCIS
IDC
ILC
OtherMalign

Figure 3.

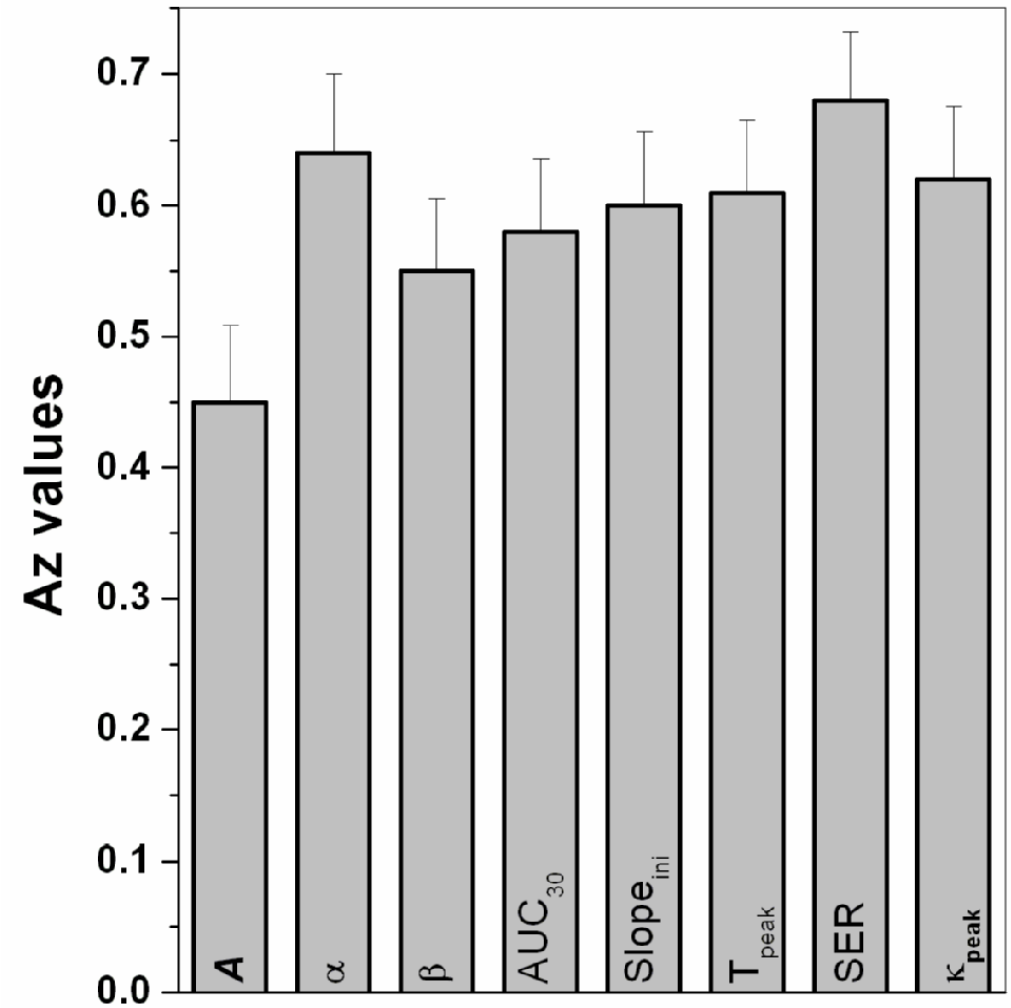
Az values
0.0
0.1
0.2
0.3
0.4
0.5
0.6
0.7
A
α
β
AUC30
Slopeini
Tpeak
SER
κpeak

Figure 4.

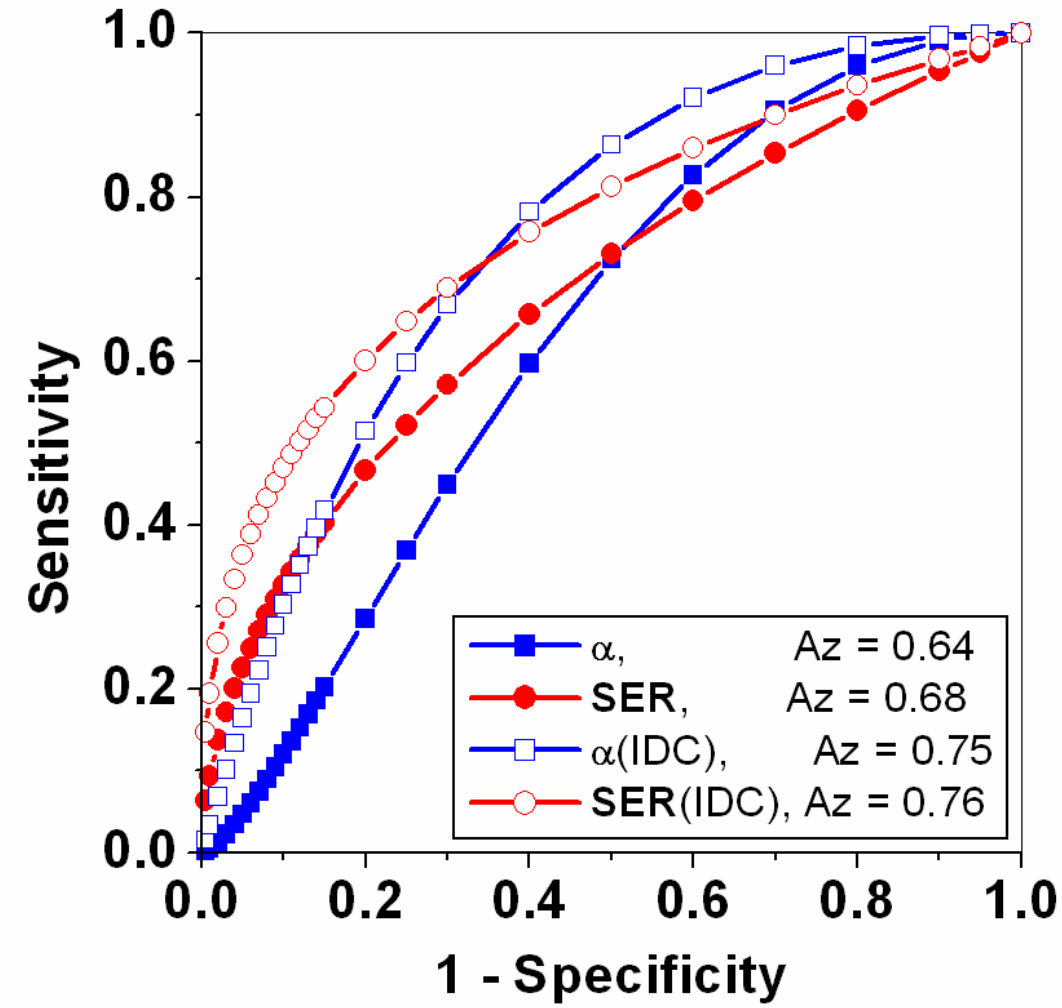
1.0
0.8
0.6
0.4
0.2
0.0
Sensitivity
0.0
0.2
0.4
0.6
0.8
1.0
1 - Specificity
α, Az = 0.64
SER, Az = 0.68
α(IDC), Az = 0.75
SER(IDC), Az = 0.76

References

1. Tabar L, Dean PB. Mammography and breast cancer: the new era. Int J Gynaecol Obstet 2003;82(3):319-326.
2. Abraham DC, Jones RC, Jones SE, Cheek JH, Peters GN, Knox SM, Grant MD, Hampe DW, Savino DA, Harms SE. Evaluation of neoadjuvant chemotherapeutic response of locally advanced breast cancer by magnetic resonance imaging. Cancer 1996;78(1):91-100.
3. Boetes C, Mus RD, Holland R, Barentsz JO, Strijk SP, Wobbes T, Hendriks JH, Ruys SH. Breast tumors: comparative accuracy of MR imaging relative to mammography and US for demonstrating extent. Radiology 1995;197(3):743-747.
4. Warren RM, Pointon L, Thompson D, Hoff R, Gilbert FJ, Padhani A, Easton D, Lakhani SR, Leach MO. Reading protocol for dynamic contrast-enhanced MR images of the breast: sensitivity and specificity analysis. Radiology 2005;236(3):779-788.
5. Heywang-Kobrunner SH, Bick U, Bradley WG, Jr., Bone B, Casselman J, Coulthard A, Fischer U, Muller-Schimpfle M, Oellinger H, Patt R, Teubner J, Friedrich M, Newstead G, Holland R, Schauer A, Sickles EA, Tabar L, Waisman J, Wernecke KD. International investigation of breast MRI: results of a multicentre study (11 sites) concerning diagnostic parameters for contrast-enhanced MRI based on 519 histopathologically correlated lesions. Eur Radiol 2001;11(4):531-546.
6. Orel SG. MR imaging of the breast. Radiol Clin North Am 2000;38(4):899-913.
7. Kuhl CK, Schild HH, Morakkabati N. Dynamic bilateral contrast-enhanced MR imaging of the breast: trade-off between spatial and temporal resolution. Radiology 2005;236(3):789-800.
8. Goto M, Ito H, Akazawa K, Kubota T, Kizu O, Yamada K, Nishimura T. Diagnosis of breast tumors by contrast-enhanced MR imaging: comparison between the diagnostic performance of dynamic enhancement patterns and morphologic features. J Magn Reson Imaging 2007;25(1):104-112.
9. Bazzocchi M, Zuiani C, Panizza P, Del Frate C, Soldano F, Isola M, Sardanelli F, Giuseppetti GM, Simonetti G, Lattanzio V, Del Maschio A. Contrast-enhanced breast MRI in patients with suspicious microcalcifications on mammography: results of a multicenter trial. AJR Am J Roentgenol 2006;186(6):1723-1732.
10. Szabo BK, Aspelin P, Wiberg MK, Bone B. Dynamic MR imaging of the breast. Analysis of kinetic and morphologic diagnostic criteria. Acta Radiol 2003;44(4):379-386.
11. Esserman L, Hylton N, George T, Weidner N. Contrast-Enhanced Magnetic Resonance Imaging to Assess Tumor Histopathology and Angiogenesis in Breast Carcinoma. Breast J 1999;5(1):13-21.
12. Kuhl CK, Schild HH. Dynamic image interpretation of MRI of the breast. J Magn Reson Imaging 2000;12(6):965-974.
13. Kuhl CK, Mielcareck P, Klaschik S, Leutner C, Wardelmann E, Gieseke J, Schild HH. Dynamic breast MR imaging: are signal intensity time course data useful for differential diagnosis of enhancing lesions? Radiology 1999;211(1):101-110.
14. Cron GO, Kelcz F, Santyr GE. Improvement in breast lesion characterization with dynamic contrast-enhanced MRI using pharmacokinetic modeling and bookend T(1) measurements. Magn Reson Med 2004;51(5):1066-1070.

15. Armitage P, Behrenbruch C, Brady M, Moore N. Extracting and visualizing physiological parameters using dynamic contrast-enhanced magnetic resonance imaging of the breast. Med Image Anal 2005;9(4):315-329.
16. Furman-Haran E, Degani H. Parametric analysis of breast MRI. J Comput Assist Tomogr 2002;26(3):376-386.
17. Furman-Haran E, Schechtman E, Kelcz F, Kirshenbaum K, Degani H. Magnetic resonance imaging reveals functional diversity of the vasculature in benign and malignant breast lesions. Cancer 2005;104(4):708-718.
18. Tofts PS, Berkowitz B, Schnall MD. Quantitative analysis of dynamic Gd-DTPA enhancement in breast tumors using a permeability model. Magn Reson Med 1995;33(4):564-568.
19. Heiberg EV, Perman WH, Herrmann VM, Janney CG. Dynamic sequential 3D gadolinium-enhanced MRI of the whole breast. Magn Reson Imaging 1996;14(4):337-348.
20. Fan X, Medved M, River JN, Zamora M, Corot C, Robert P, Bourrinet P, Lipton M, Culp RM, Karczmar GS. New model for analysis of dynamic contrast-enhanced MRI data distinguishes metastatic from nonmetastatic transplanted rodent prostate tumors. Magn Reson Med 2004;51(3):487-494.
21. Moate PJ, Dougherty L, Schnall MD, Landis RJ, Boston RC. A modified logistic model to describe gadolinium kinetics in breast tumors. Magn Reson Imaging 2004;22(4):467-473.
22. Evelhoch JL. Key factors in the acquisition of contrast kinetic data for oncology. J Magn Reson Imaging 1999;10(3):254-259.
23. Buadu LD, Murakami J, Murayama S, Hashiguchi N, Sakai S, Masuda K, Toyoshima S, Kuroki S, Ohno S. Breast lesions: correlation of contrast medium enhancement patterns on MR images with histopathologic findings and tumor angiogenesis. Radiology 1996;200(3):639-649.
24. Fan X MM, Karczmar GS, Yang C, Foxley S, Arkani S, Recant W, Zamora MA, Abe H, Newstead GM. Diagnosis of suspicious breast lesions using an empirical mathematical model for dynamic contrast-enhanced MRI. Magnetic Resonance Imaging 2007 (In press).
25. Kelcz F, Santyr GE, Cron GO, Mongin SJ. Application of a quantitative model to differentiate benign from malignant breast lesions detected by dynamic, gadolinium-enhanced MRI. J Magn Reson Imaging 1996;6(5):743-752.
26. Callicott C, Thomas JM, Goode AW. The magnetization transfer characteristics of human breast tissues: an in vitro NMR study. Phys Med Biol 1999;44(5):1147-1154.
27. Hulka CA, Smith BL, Sgroi DC, Tan L, Edmister WB, Semple JP, Campbell T, Kopans DB, Brady TJ, Weisskoff RM. Benign and malignant breast lesions: differentiation with echo-planar MR imaging. Radiology 1995;197(1):33-38.
28. Jacobs MA, Barker PB, Bluemke DA, Maranto C, Arnold C, Herskovits EH, Bhujwalla Z. Benign and malignant breast lesions: diagnosis with multiparametric MR imaging. Radiology 2003;229(1):225-232.
29. Metz CE, Herman BA, Shen JH. Maximum likelihood estimation of receiver operating characteristic (ROC) curves from continuously-distributed data. Stat Med 1998;17(9):1033-1053.

30. Arpino G, Laucirica R, Elledge RM. Premalignant and in situ breast disease: biology and clinical implications. Ann Intern Med 2005;143(6):446-457.
31. Kumar AS, Chen DF, Au A, Chen YY, Leung J, Garwood ER, Gibbs J, Hylton N, Esserman LJ. Biologic significance of false-positive magnetic resonance imaging enhancement in the setting of ductal carcinoma in situ. Am J Surg 2006;192(4):520-524.
32. Jansen S, Newstead G, Abe H, Shimauchi A, Schmidt R, Karczmar GS. MR Imaging of Pure Ductal Carcinoma in situ: Kinetics, Morphology and Comparison with Mammographic Presentation and Nuclear Grade. Radiology (in press) 2007.
33. Armitage P, Behrenbruch C, Brady M, Moore N. Extracting and visualizing physiological parameters using dynamic contrast-enhanced magnetic resonance imaging of the breast. Med Image Anal 2005;9(4):315-329.

DCEMRI of Breast lesions: Is kinetic analysis equally effective for both mass and non-mass-like enhancement?

Sanaz A. Jansen, Xiaobing Fan, Gregory S. Karczmar, Hiroyuki Abe, Robert A. Schmidt, Maryellen Giger and Gillian M. Newstead*

Address for all authors:

Department of Radiology
The University of Chicago
5841 S. Maryland Ave MC2026
Chicago, IL 60637

Submitted as a research article to Medical Physics
Word count: 2789
Running title: DCEMRI of Mass and Non-mass Breast Lesions

*Corresponding Author:

Gillian Newstead, M.D.
Professor
Department of Radiology
University of Chicago
5841 S. Maryland Ave, MC 2026
Chicago, IL 60637

Phone: (773) 702-2781
Fax: (773) 834-9047
Email: gnewstead@radiology.bsd.uchicago.edu

ABSTRACT

Purpose: To investigate whether the sensitivity and specificity of kinetic parameters can be improved by considering mass and non-mass breast lesions separately. The contrast media uptake and washout kinetics in benign and malignant breast lesions were analyzed using an empirical mathematical model (EMM), and model parameters were compared in lesions with mass-like and non-mass-like enhancement characteristics.

Materials and Methods: 34 benign and 78 malignant breast lesions were selected for review. Dynamic MR protocol: 1 pre and 5 post-contrast images acquired in the coronal plane using a 3D T1-weighted SPGR with 68 second timing resolution. An experienced radiologist classified the type of enhancement as mass, non-mass or focus, according to the BI-RADS® lexicon. The kinetic curve was analyzed quantitatively using a three parameter EMM. Several kinetic parameters were then derived from the EMM parameters: the initial slope (**'$\mathbf{Slope_{ini}}$'**)**,** curvature at the peak (**'$\boldsymbol{\kappa_{peak}}$'**), time to peak (**'$\mathbf{T_{peak}}$'**), area under the curve at 30 seconds ('**$\mathbf{AUC_{30}}$**') and the signal enhancement ratio ('**SER'**).

Results: The classification of type of enhancement yielded: 70 mass lesions, 38 non-mass, 4 focus. For mass lesions, the contrast uptake rate ('**α**'), contrast washout rate ('**β**')**, '$\mathbf{AUC_{30}}$'**, '**SER**', '**$\mathbf{Slope_{ini}}$**', '**$\mathbf{T_{peak}}$**' and '**$\boldsymbol{\kappa_{peak}}$**' differed significantly between benign and malignant lesions (p<0.03). For non-mass lesions, there were no statistically significant differences in any of the parameters for benign vs. malignant lesions (p>0.5).

Conclusions: Kinetic parameters could distinguish benign and malignant mass lesions effectively, but were not quite as useful in discriminating benign from malignant non-mass lesions. This suggests that to maximize diagnostic utility, it is better to classify lesion morphology as mass or non-mass-like enhancement prior to kinetic analysis.

Keywords: Non-mass lesions, malignant, DCE-MRI, sensitivity, specificity

INTRODUCTION

Dynamic contrast enhanced magnetic resonance imaging (DCEMRI) is being used in breast imaging for several purposes, including determining extent of malignant disease and post treatment evaluation (1,2). When analyzing lesion presentation on breast DCEMRI, the radiologist**s** assesses the morphology as well as the contrast media uptake and washout—or kinetics—of the lesion following the Breast Imaging Reporting and Data System (BI-RADS®) lexicon. According to the BI-RADS® lexicon, the first step in assessing lesion morphology is to classify the type of enhancement as mass, non-mass, focus (Figure 1). Then, subsequent descriptors of other lesion features (such as shape, distribution, margins, enhancement pattern) are selected, which differ depending on the type of enhancement. The BI-RADS® lexicon also classifies the initial rise of the kinetic curve, and the delayed phase as persistent, plateau or washout.

The level of suspicion for malignancy is determined by assessing both the morphologic as well as the kinetic characteristics of the lesion. Invasive cancers often present as heterogeneously enhancing masses with irregular or spiculated margins, and kinetic curves that typically rise rapidly and subsequently washout over time. Benign lesions, on the other hand, often present as homogeneously enhancing masses with smooth margins and tend to enhance more slowly and persistently take up contrast over time (3,4). To move beyond the qualitative BI-RADS® description of kinetics, many prior studies have applied mathematical models to DCEMRI kinetic data, such as the two-compartment model, to extract diagnostically useful parameters (5-11). However, for low time resolution 3D DCEMRI data, the accuracy of physiological parameters obtained from compartmental models is questionable. In addition these models require an arterial input function (AIF), which is difficult to estimate accurately. As an alternative to these approaches, mathematical equations can be used to fit the kinetic curves (11,12).

The majority of pre-invasive ductal carcinoma *in situ* (DCIS) lesions and some invasive cancers present as non-mass-like enhancement in a segmental or clumped distribution

(13-17). Benign lesions, such as atypical ductal hyperplasia, can also present with non-mass-like enhancement, as can normal parenchyma. DCIS is considered to be a non-obligate precursor of invasive cancer, and if treated has dramatically higher survival than invasive cancers (18,19). Yet the sensitivity and specificity of DCEMRI for detection of DCIS needs improvement (15,16,20-27), particularly given recent American Cancer Society guidelines recommending breast MRI in the screening of women at high risk of developing breast cancer(28). It is likely that mass-like and non-mass-like enhancement patterns reflect differences in the underlying physiology and vasculature of these lesions, which may in turn affect the kinetic characteristics. The kinetic parameters that can distinguish benign and malignant mass lesions may not work well on non-mass lesions, and vice versa. However, while there have been several studies on non-mass lesions such as DCIS, the efficacy of kinetic analysis in mass-like vs. non-mass-like enhancement has not been well characterized (29-33).

We are interested in whether kinetic analysis is more diagnostically useful in mass lesions compared with non-mass lesions. In addition to using conventional BI-RADS® descriptors of kinetics, we have also applied a mathematical model to the kinetic data. The limited temporal resolution in conventional 3D bilateral DCEMRI implies that complex mathematical models cannot be directly applied to kinetic curves to obtain a unique solution. In this study, a three parameter empirical mathematical model (EMM) was used to analyze 3D bilateral DCEMRI breast data. Thus, using both qualitative and quantitative means, we evaluated kinetic patterns of enhancement separately in (i) benign vs. malignant mass lesions, and (ii) benign vs. malignant non-mass lesions.

METHODS

Patients

At our institution, it is a routine protocol to obtain breast MR imaging, for evaluation of extent of malignant disease, for post-treatment evaluation of the cancer patient and for high-risk screening. The institutional review board approved our HIPAA compliant retrospective study with waiver of informed consent. Bilateral 3D DCEMRI data from 100 female patients acquired between May 2002 and June 2003 was reviewed for study. The age range of the subjects was 24 to 81 years (mean age = 56.2 ± 13.3 years). Based on the consensus opinion of two experienced pathologists, there were a total of 112 lesions of which 35 were benign and 77 malignant.

MRI Analysis

MR imaging was performed on a 1.5T GE Signa scanner (GE Healthcare, Milwaukee, WI) using a dedicated 4 channel breast coil (Invivo, Orlando, FL) with the patient in the prone position. One pre and five post-contrast images were acquired in the coronal plane using a 3D T_1-weighted spoiled grass sequence (TR/TE = 7.7/4.2 msec, flip angle = 30˚, slice thickness = 3 mm, and in plane resolution = 1.4 mm), without fat suppression. The first post-contrast acquisition was started 20 seconds after contrast injection and the remaining images were acquired every 68 seconds. 20cc of 0.5M Gadodiamide (Omniscan; Nycomed-Amersham, Princeton, NJ) was injected intravenously followed by a 20 ml saline flush at the rate of 2.0 ml /sec.

One experienced radiologist retrospectively reviewed the images and classified lesion morphology and kinetics. The type of enhancement was assessed according to the BI-RADS® lexicon as mass, non-mass or focus. To generate the kinetic curve, the radiologist traced a small region of interest (ROI) around what was perceived to be the most enhancing part of the lesion on the first post-contrast image. The plot of signal intensity vs. time for this ROI was assessed by the radiologist according to the BI-

RADS® lexicon, which describes the "initial rise" (rapid, medium, slow) and "delayed phase" (persistent, plateau, washout) of the kinetic curve.

Simplified Empirical Mathematical Model

The kinetic curve obtained above was analyzed quantitatively using a simplified empirical mathematical model (EMM). To implement the model, the average signal intensity as a function of time ($S(t)$) was first calculated in the selected ROI. Next, the relative signal changes after contrast injection were calculated: $\Delta S = (S_n - S_0)/S_0$, where S_0 is the average signal intensity in the pre-contrast scan, and S_n is the signal intensity at the nth post contrast time point. Then $\Delta S(t)$ was fit to:

$$\Delta S(t) = A \cdot \left(1 - e^{-\alpha t}\right) \cdot e^{-\beta t} \qquad [1]$$

where **'A'** is the upper limit of the signal intensity, 'α' (min^{-1}) is the rate of signal increase, and 'β' (min^{-1}) is the rate of the signal decrease during washout. This is a modified version of a more complicated five-parameter empirical mathematical model that has proven to be diagnostically useful (12).

From the primary EMM parameters '**A**', 'α' and 'β' we derived kinetic parameters that are commonly used in the literature: '**AUC_{30}**', '**$Slope_{ini}$**', '**T_{peak}**', '**SER**', '**κ_{peak}**' (10,34-38) which are described in Table 1.

Data analysis and Statistical evaluation

We compared the kinetic characteristics of benign and malignant lesions as evaluated by the BI-RADS® lexicon as well as the EMM. The kinetic characteristics of benign and malignant lesions within mass and non-mass lesions were compared: (i) benign vs. malignant mass lesions, and (ii) benign vs. malignant non-mass lesions. In addition, we also compared the kinetic characteristics of malignant mass vs. malignant non-mass lesions.

To compare the proportion of washout vs. plateau and persistent (or rapid vs. medium and slow) curves between benign and malignant lesions overall, as well as stratified by type of enhancement, we used the Pearson's χ^2 – test for significance, with a p value of < 0.05 indicating statistical significance.

The 3D bilateral DCEMRI data were processed using software written in IDL (Research Systems, Inc., Boulder, CO). After fitting the kinetic curve to the EMM. the goodness of fit parameter R^2 was calculated for each lesion. Two-tailed unequal variance Student's t-tests were performed to evaluate which modified EMM parameters showed significant differences between the benign and malignant breast lesions overall, as well as the subpopulations of mass and non-mass lesions, with a p value < 0.05 indicating statistical significance.

Receiver operating characteristic (ROC) analysis was performed to compare the diagnostic performance of the EMM parameters on mass lesions vs. non-mass lesions. ROCKIT software (ROCKIT 0.9B Beta Version, Charles E. Metz, University of Chicago) was used to generate the ROC curves.

RESULTS

Qualitative (BI-RADS) Kinetic Findings

Of the 112 lesions, 70 were classified as mass lesions, 44 of which were malignant and 26 benign. 38 were classified as non-mass lesions, with 31 malignant and 7 benign. Of the remaining 4 focus lesions, 2 were benign and 2 malignant. The distribution of the BI-RADS® assessments of initial uptake and delayed phase for all malignant and benign lesions is shown in Table 2. Overall, malignant lesions exhibited significantly higher proportion of curve showing 'rapid' initial rise, at 90% (69/77), compared with benign lesions, at 74% (26/35). Malignant and benign lesions also differed in delayed phase distribution with 65% (50/77) and 40% (14/35) classified as washout curves, respectively (p = 0.023).

The classification of initial rise and delayed phase for mass and non-mass lesions is also shown in Table 2. The kinetic curves of 77% (34/44) of mass-like malignant lesions were classified as 'washout', compared with 38% (10/26) of mass-like benign lesions (p=0.001). 73% (19/26) of benign mass lesions showed 'rapid' initial rise compared with 93% (41/44) of malignant mass lesions (p=0.049). However, there was no significant difference in the distribution of initial rise or delayed phase classification of non-mass malignant and non-mass benign lesions (p>0.65).

Quantitative (EMM) Kinetic Findings.

The EMM was able to accurately fit the curves, with a goodness of fit parameter R^2 greater than 0.90 for all lesions studied. Some examples of benign and malignant mass and non-mass lesions, along with the fitted kinetic curves, are shown in Figure 1. After fitting the kinetic curves, the five derived parameters were calculated using the equations in Table 1. The average values of all primary and derived parameters are displayed in Table 3. T-test comparisons demonstrated that malignant lesions had significantly faster

contrast uptake (**'α', p** = 0.047), steeper initial slope (**'$Slope_{ini}$', p =** 0.035), larger enhancement ratio ('**SER', p** = 0.001) and sharper curvature ('**κ_{peak}', p** = 0.018) than benign lesions.

All of the EMM parameters '**α', 'β', 'T_{peak}', 'AUC_{30}', 'SER', '$Slope_{ini}$**' and '**κ_{peak}**' except for '**A**' differed significantly between benign and malignant mass lesions (p < 0.035 for all, Figure 2). That is, kinetic curves of malignant mass lesions exhibited stronger contrast uptake ('**α**', '**AUC_{30}', '$Slope_{ini}$**'), earlier peak enhancement ('**T_{peak}**'), and sharper, stronger washout ('**SER'**, '**κ_{peak}**', '**β'**) compared with benign mass lesions. However, for non-mass lesions, there were no statistical differences in any of the primary or derived EMM parameters for benign vs. malignant lesions (p > 0.51 for all, Figure 2). Considering malignant lesions only, those with mass-like enhancement had significantly larger '**A' (**p=0.04**), 'β'** (p=0.04), '**AUC_{30}**' (**p**=0.03) and **'$Slope_{ini}$'** (p=0.04) compared with malignant non-mass lesions.

ROC analysis was used to evaluate the diagnostic accuracy of the primary and derived EMM parameters. ROC curves were generated for each parameter separately among mass and non-mass lesions. The A_z values in mass lesions ranged from 0.54 ('**A**') to 0.72 (**SER**), and in non-mass lesions from 0.52 ('**α**') to 0.60 ('**A**'). For all parameters except for '**A'**, the A_z values were higher in mass lesions, but this was not significant (p > 0.19), likely due to the small number of benign non-mass lesions considered. The ROC curves for these parameters are shown in Figure 3.

DISCUSSION

We have found that kinetic parameters could distinguish benign and malignant mass lesions more effectively, but were not useful in discriminating benign from malignant non-mass lesions. This was true both for the qualitative BI-RADS® and quantitative EMM measures of kinetics. Malignant mass lesions exhibited a higher proportion of washout type curves as well as a significantly higher initial uptake ('**α', 'AUC$_{30}$'**, '**Slope$_{ini}$**') and earlier, stronger washout ('**β', 'T$_{peak}$', 'SER', 'κ_{peak}**') compared with benign mass lesions. Conversely, the kinetic characteristics of malignant and benign non-mass lesions did not differ according to either the BI-RADS® lexicon or EMM. These results translated into diagnostic performance: the A_z values derived from ROC curves also demonstrated that the diagnostic performance of all primary and derived EMM parameters except one ('**A'**) was improved in mass lesions. Among malignant lesions, the parameters '**A'**, **'β', 'AUC$_{30}$'** and '**Slope$_{ini}$**' differed significantly between mass and non-mass lesions.

Kinetic curve shape is related to the perfusion, capillary permeability, and diffusion of contrast media from blood vessels to the extracellular space—these biological properties ultimately explain the differences between mass and non-mass lesions noted above. One important class of malignant lesions that most often displays non-mass-like enhancement is in situ lesions, in which neoplastic ductal epithelial cells remain confined to mammary ducts. The growth of vasculature associated with DCIS is not well understood. Guidi et al showed an increase in vessel density around ducts with DCIS, although with variable patterns (39). Heffelfinger found that the expression of angiogenic growth factors (such as VEGF) increases from hyperplasia to DCIS(40,41). The physiology of DCIS is distinct from invasive ductal carcinoma (IDC), in which cancer cells have invaded the surrounding stroma with well-defined but infiltrative margins. The vasculature associated with IDC lesions is dense and leaky (42,43). These physiological differences of DCIS and IDC lesions are likely related to the corresponding differences in MR presentation, in which IDC predominantly presents as a mass lesion on MRI (17).

Although most DCIS lesions display a distinctive non-mass-like enhancement at MR imaging, they do not exhibit a consistent kinetic pattern. Unlike invasive cancers, the kinetic curves of DCIS lesions can often exhibit persistent signal increase, or signal intensity that plateaus over time (13,14,16). Because of the variable kinetic pattern of DCIS lesions, some have suggested that kinetic information—specifically, the BI-RADS® qualitative assessment of delayed phase—is not useful in diagnosing DCIS lesions and instead, morphologic analysis should be favored (44). Our results support this prior work, in that we have found large overlap in the kinetic characteristics of benign and malignant non-mass lesions. However, given that the physiological basis of enhancement is likely different in non-mass vs. mass lesions, it may be that new quantitative kinetic parameters need to be developed that are tailored for non-mass lesions. We found that malignant non-mass lesions exhibited significantly lower contrast uptake compared with malignant mass lesions; this underscores the importance of early imaging to distinguish non-mass lesions from enhancing normal parenchyma which has a similar non-mass morphology. Perhaps other imaging techniques may be important; recent work by Bartella et al suggested that using proton spectroscopy to measure choline peaks yielded high sensitivity and specificity to malignant non-mass lesions (29).

There are several limitations to this study.

- While the total number of lesions studied was relatively large, there were only 7 non-mass-like benign lesions, which may be too small to perform reliable comparisons of the subtypes of benign and malignant lesions presented here.
- 40% of benign lesion kinetic curves were classified as ‘washout’, which is higher than many reports. The benign lesions considered were suspicious enough to warrant biopsy. Since most obviously benign lesions exhibit persistent type kinetic curves and would not be sent to biopsy, this may skew the delayed phase distribution in this study away from the persistent curve type. In other studies where only histologically proven benign lesions were considered, comparable values were found (36).

- The placement and size of the ROI was determined manually, and only one small ROI was used to characterize the whole lesion. This single ROI may not capture the heterogeneity of kinetic enhancement patterns in the lesion. In addition, partial volume effects may compromise the accuracy of the kinetic curve, especially in lesions with non-mass-like enhancement. It is possible that partial volume effects produce the observed differences between mass and non-mass lesion.

- Although the EMM fit the curves very well, sparse sampling of the kinetic curve may result in more fitting errors in the uptake phase. In addition, pre-clinical studies suggest that specificity of the EMM is improved when the tail of the washout curve is sampled for at least 15 minutes; the curves studied here were truncated at about 6 minutes (10,12).

Despite these shortcomings, our results suggest that kinetic analysis is not effective in non-mass lesions, while it may be very effective in mass lesions, and that the enhancement kinetics of malignant non-mass and mass lesions exhibit significant differences. This may be useful in computer aided detection and diagnosis (CAD) algorithms. By training classifiers on mass and non-mass lesions separately, it may be that (i) detection of non-mass lesions could be improved by choosing accurate thresholds (ii) the probability of malignancy in mass lesions may be improved, and (iii) new kinetic parameters that are diagnostically effective in cases of non-mass-like enhancement may be discovered. Future work will focus on a larger group of lesions with detailed pathology analysis, to investigate new parameters targeted at non-mass lesions. In addition, pixel by pixel analysis, acquiring high spatial/temporal resolution of MR images, or following the later phase of the kinetic curves for a longer time, could be used to help improve the differentiation of non-mass malignant from non-mass benign lesions.

Acknowledgements

We would like to thank the Segal Foundation, the Biological Sciences Division at the University of Chicago, DOD grant W81XWH-06-1-0329 and NIH grants R21 CA104774-01A2 and 2 R01 CA078803-05A2 for financial support.

Table 1: A list and description of the EMM parameters derived from the primary parameters A. α and β.

	Description	Equation
AUC_{30}	Area under the kinetic curve at 30 seconds (34,35).	$\mathrm{AUC}_\tau = A\cdot\left[\left(1-e^{-\beta\tau}\right)\Big/\beta+\left(e^{-(\alpha+\beta)\tau}-1\right)\Big/(\alpha+\beta)\right]$ Here we used $\tau = 30$.
$Slope_{ini}$ (min^{-1})	Initial slope of the kinetic curve (34,36,37),	$Slope_{\mathrm{ini}} \approx A\alpha$
T_{peak} (min)	Time to peak enhancement (36).	$T_{\mathrm{peak}} = \frac{1}{\alpha}\log\left(1+\frac{\alpha}{\beta}\right)$ Note that when $\beta \le 0$, the curves did not reach the peak within the duration of the experiment. In these cases, we used the last time point **T_{peak}**.
κ_{peak}	Curvature at the peak of enhancement **T_{peak}** (36).	$\kappa_{peak} \approx -A\alpha\beta$
SER	Signal enhancement ratio (38).	$SER = \frac{\Delta S_1}{\Delta S_L} = \frac{1-e^{-\alpha t_1}}{1-e^{-\alpha t_L}}\cdot e^{(t_L-t_1)\beta}$ Here, t_1 = 60 s and t_L = 300 s used in this study. A '**SER'** value greater than 1.1 indicates the signal intensity decreases with respect to its value at 60 seconds; '**SER**' less than 0.9 indicates that signal intensity continues to rise; and '**SER**' between 0.9 and 1.1 represents a plateau relative to intensity at 60 seconds.

345

Table 2. Distributions of BI-RADS® categories for the qualitative assessment of the initial rise and delayed phased of kinetic curves for benign and malignant lesions, as well as the subtypes of benign and malignant lesions considered here. There were 2 benign and 2 malignant lesions classified as focus type enhancement, which do not appear in the table below.

			Benign			**Malignant**		
			All (n=35)	Mass (n=26)	Non-mass (n=7)	**All (n=77)**	Mass (n=44)	Non-mass (n=31)
BIRADS® Initial Rise		*Rapid*	**26**	19	5	**69**	41	27
		Medium	**8**	6	2	**6**	3	3
		Slow	**1**	1	0	**2**	0	1
BIRADS® Delayed		*Washout*	**14**	10	2	**50**	34	16
		Plateau	**15**	12	3	**19**	9	9
		Persistent	**6**	4	2	**8**	1	6

Table 3. The primary and derived diagnostic parameters derived from the EMM in malignant and benign lesions. Reported values are mean ± standard deviation for all cases. Numbers in bold indicate that there was a statistic significantly difference between benign and malignant lesions.

EMM parameter	**All Benign (n=35)**	**All Malignant (n=77)**	***p* values**
A	4.2±2.2	4.1±2.2	p=0.703
α (min^{-1})	**1.6±1.1**	**2.1±1.1**	***p*=0.047**
β (min^{-1})	0.045±0.047	0.059±0.061	p=0.24
AUC_{30}	0.55±0.34	0.71±0.54	p=0.07
$Slope_{ini}$ (min^{-1})	**6.1±4.6**	**8.8±8.4**	***p*=0.04**
***T_{peak}** (min)	3.4±1.8	2.7±1.8	p=0.12
κ_{peak}	**-0.30±0.48**	**-0.68±1.19**	***p*=0.02**
SER	**0.88±0.31**	**1.14±0.49**	***p*=0.001**

* For those curves which did not reach a peak within the duration of the experiment, we assumed a time to peak of 5 min.

FIGURE CAPTIONS

Figure 1: Examples of four breast lesions with measured and EMM fitted kinetic curves. For each kinetic curve, the measured signal intensity values are indicated with triangles, and the fitted EMM curve with solid lines. From the top to bottom: benign mass lesion, malignant mass lesion, benign non-mass lesion and malignant non-mass lesion. The lesions are indicated by a white arrow.

Figure 2: The average value ± standard deviation for each EMM parameter in benign (white bars) and malignant (grey bars) lesions, stratified by type of enhancement as mass or non-mass.

Figure 3: Fitted binormal ROC curves generated by the ROCKIT software are shown for the EMM parameters with the highest, and lowest, A_z values in mass and non-mass lesions. '**SER'** (filled squares) and '**A'** (filled circles) had the highest A_z values in mass and non-mass lesions, respectively. '**A'** (open squares) and '**α'** (open circles) had the lowest A_z values in mass and non-mass lesions, respectively.

REFERENCES

1. Abraham DC, Jones RC, Jones SE, Cheek JH, Peters GN, Knox SM, Grant MD, Hampe DW, Savino DA, Harms SE. Evaluation of neoadjuvant chemotherapeutic response of locally advanced breast cancer by magnetic resonance imaging. Cancer 1996;78(1):91-100.
2. Boetes C, Mus RD, Holland R, Barentsz JO, Strijk SP, Wobbes T, Hendriks JH, Ruys SH. Breast tumors: comparative accuracy of MR imaging relative to mammography and US for demonstrating extent. Radiology 1995;197(3):743-747.
3. Kuhl CK, Mielcareck P, Klaschik S, Leutner C, Wardelmann E, Gieseke J, Schild HH. Dynamic breast MR imaging: are signal intensity time course data useful for differential diagnosis of enhancing lesions? Radiology 1999;211(1):101-110.
4. Kuhl CK, Schild HH. Dynamic image interpretation of MRI of the breast. J Magn Reson Imaging 2000;12(6):965-974.
5. Cron GO, Kelcz F, Santyr GE. Improvement in breast lesion characterization with dynamic contrast-enhanced MRI using pharmacokinetic modeling and bookend T(1) measurements. Magn Reson Med 2004;51(5):1066-1070.
6. Armitage P, Behrenbruch C, Brady M, Moore N. Extracting and visualizing physiological parameters using dynamic contrast-enhanced magnetic resonance imaging of the breast. Med Image Anal 2005;9(4):315-329.
7. Furman-Haran E, Degani H. Parametric analysis of breast MRI. J Comput Assist Tomogr 2002;26(3):376-386.
8. Furman-Haran E, Schechtman E, Kelcz F, Kirshenbaum K, Degani H. Magnetic resonance imaging reveals functional diversity of the vasculature in benign and malignant breast lesions. Cancer 2005;104(4):708-718.
9. Tofts PS, Berkowitz B, Schnall MD. Quantitative analysis of dynamic Gd-DTPA enhancement in breast tumors using a permeability model. Magn Reson Med 1995;33(4):564-568.
10. Fan X, Medved M, Karczmar GS, Yang C, Foxley S, Arkani S, Recant W, Zamora MA, Abe H, Newstead GM. Diagnosis of suspicious breast lesions using an empirical mathematical model for dynamic contrast-enhanced MRI. Magn Reson Imaging 2007;25(5):593-603.
11. Heiberg EV, Perman WH, Herrmann VM, Janney CG. Dynamic sequential 3D gadolinium-enhanced MRI of the whole breast. Magn Reson Imaging 1996;14(4):337-348.
12. Fan X, Medved M, River JN, Zamora M, Corot C, Robert P, Bourrinet P, Lipton M, Culp RM, Karczmar GS. New model for analysis of dynamic contrast-enhanced MRI data distinguishes metastatic from nonmetastatic transplanted rodent prostate tumors. Magn Reson Med 2004;51(3):487-494.
13. Jansen S, Newstead G, Abe H, Shimauchi A, Schmidt R, Karczmar GS. MR Imaging of Pure Ductal Carcinoma in situ: Kinetics, Morphology and Comparison with Mammographic Presentation and Nuclear Grade. Radiology (in press) 2007.
14. Neubauer H, Li M, Kuehne-Heid R, Schneider A, Kaiser WA. High grade and non-high grade ductal carcinoma in situ on dynamic MR mammography:

characteristic findings for signal increase and morphological pattern of enhancement. Br J Radiol 2003;76(901):3-12.
15. Menell JH, Morris EA, Dershaw DD, Abramson AF, Brogi E, Liberman L. Determination of the presence and extent of pure ductal carcinoma in situ by mammography and magnetic resonance imaging. Breast J 2005;11(6):382-390.
16. Van Goethem M, Schelfout K, Kersschot E, Colpaert C, Weyler J, Verslegers I, Biltjes I, De Schepper A, Parizel PM. Comparison of MRI features of different grades of DCIS and invasive carcinoma of the breast. Jbr-Btr 2005;88(5):225-232.
17. Kuhl C. The current status of breast MR imaging. Part I. Choice of technique, image interpretation, diagnostic accuracy, and transfer to clinical practice. Radiology 2007;244(2):356-378.
18. Recht A, Rutgers EJ, Fentiman IS, Kurtz JM, Mansel RE, Sloane JP. The fourth EORTC DCIS Consensus meeting (Chateau Marquette, Heemskerk, The Netherlands, 23-24 January 1998)--conference report. Eur J Cancer 1998;34(11):1664-1669.
19. Suzuki T, Toi M, Saji S, Horiguchi K, Aruga T, Suzuki E, Horiguchi S, Funata N, Karasawa K, Kamata N. Early breast cancer. Int J Clin Oncol 2006;11(2):108-119.
20. Kuhl CK, Schrading S, Bieling HB, Wardelmann E, Leutner CC, Koenig R, Kuhn W, Schild HH. MRI for diagnosis of pure ductal carcinoma in situ: a prospective observational study. Lancet 2007;370(9586):485-492.
21. Viehweg P, Lampe D, Buchmann J, Heywang-Kobrunner SH. In situ and minimally invasive breast cancer: morphologic and kinetic features on contrast-enhanced MR imaging. Magma 2000;11(3):129-137.
22. Gilles R, Zafrani B, Guinebretiere JM, Meunier M, Lucidarme O, Tardivon AA, Rochard F, Vanel D, Neuenschwander S, Arriagada R. Ductal carcinoma in situ: MR imaging-histopathologic correlation. Radiology 1995;196(2):415-419.
23. Shiraishi A, Kurosaki Y, Maehara T, Suzuki M, Kurosumi M. Extension of ductal carcinoma in situ: histopathological association with MR imaging and mammography. Magn Reson Med Sci 2003;2(4):159-163.
24. Schouten van der Velden AP, Boetes C, Bult P, Wobbes T. The value of magnetic resonance imaging in diagnosis and size assessment of in situ and small invasive breast carcinoma. Am J Surg 2006;192(2):172-178.
25. Orel SG. MR imaging of the breast. Radiol Clin North Am 2000;38(4):899-913.
26. Lee JM, Kaplan JB, Murray MP, Mazur-Grbec M, Tadic T, Stimac D, Liberman L. Underestimation of DCIS at MRI-guided vacuum-assisted breast biopsy. AJR Am J Roentgenol 2007;189(2):468-474.
27. Macura KJ, Ouwerkerk R, Jacobs MA, Bluemke DA. Patterns of enhancement on breast MR images: interpretation and imaging pitfalls. Radiographics 2006;26(6):1719-1734; quiz 1719.
28. Saslow D, Boetes C, Burke W, Harms S, Leach MO, Lehman CD, Morris E, Pisano E, Schnall M, Sener S, Smith RA, Warner E, Yaffe M, Andrews KS, Russell CA. American Cancer Society guidelines for breast screening with MRI as an adjunct to mammography. CA Cancer J Clin 2007;57(2):75-89.

29. Bartella L, Thakur SB, Morris EA, Dershaw DD, Huang W, Chough E, Cruz MC, Liberman L. Enhancing nonmass lesions in the breast: evaluation with proton (1H) MR spectroscopy. Radiology 2007;245(1):80-87.
30. Bartella L, Liberman L, Morris EA, Dershaw DD. Nonpalpable mammographically occult invasive breast cancers detected by MRI. AJR Am J Roentgenol 2006;186(3):865-870.
31. van den Bosch MA, Daniel BL, Mariano MN, Nowels KN, Birdwell RL, Fong KJ, Desmond PS, Plevritis S, Stables LA, Zakhour M, Herfkens RJ, Ikeda DM. Magnetic resonance imaging characteristics of fibrocystic change of the breast. Invest Radiol 2005;40(7):436-441.
32. Liberman L, Morris EA, Dershaw DD, Abramson AF, Tan LK. Ductal enhancement on MR imaging of the breast. AJR Am J Roentgenol 2003;181(2):519-525.
33. Liberman L, Morris EA, Lee MJ, Kaplan JB, LaTrenta LR, Menell JH, Abramson AF, Dashnaw SM, Ballon DJ, Dershaw DD. Breast lesions detected on MR imaging: features and positive predictive value. AJR Am J Roentgenol 2002;179(1):171-178.
34. Moate PJ, Dougherty L, Schnall MD, Landis RJ, Boston RC. A modified logistic model to describe gadolinium kinetics in breast tumors. Magn Reson Imaging 2004;22(4):467-473.
35. Evelhoch JL. Key factors in the acquisition of contrast kinetic data for oncology. J Magn Reson Imaging 1999;10(3):254-259.
36. Szabo BK, Aspelin P, Wiberg MK, Bone B. Dynamic MR imaging of the breast. Analysis of kinetic and morphologic diagnostic criteria. Acta Radiol 2003;44(4):379-386.
37. Buadu LD, Murakami J, Murayama S, Hashiguchi N, Sakai S, Masuda K, Toyoshima S, Kuroki S, Ohno S. Breast lesions: correlation of contrast medium enhancement patterns on MR images with histopathologic findings and tumor angiogenesis. Radiology 1996;200(3):639-649.
38. Esserman L, Hylton N, George T, Weidner N. Contrast-Enhanced Magnetic Resonance Imaging to Assess Tumor Histopathology and Angiogenesis in Breast Carcinoma. Breast J 1999;5(1):13-21.
39. Guidi AJ, Fischer L, Harris JR, Schnitt SJ. Microvessel density and distribution in ductal carcinoma in situ of the breast. J Natl Cancer Inst 1994;86(8):614-619.
40. Heffelfinger SC, Miller MA, Yassin R, Gear R. Angiogenic growth factors in preinvasive breast disease. Clin Cancer Res 1999;5(10):2867-2876.
41. Heffelfinger SC, Yassin R, Miller MA, Lower E. Vascularity of proliferative breast disease and carcinoma in situ correlates with histological features. Clin Cancer Res 1996;2(11):1873-1878.
42. Rice A, Quinn CM. Angiogenesis, thrombospondin, and ductal carcinoma in situ of the breast. J Clin Pathol 2002;55(8):569-574.
43. Furman-Haran E, Kelcz F, Degani H. Magnetic resonance imaging of breast cancer angiogenesis: a review. J Exp Clin Cancer Res 2002;21(3 Suppl):47-54.
44. Harms SE. The use of breast magnetic resonance imaging in ductal carcinoma in situ. Breast J 2005;11(6):379-381.

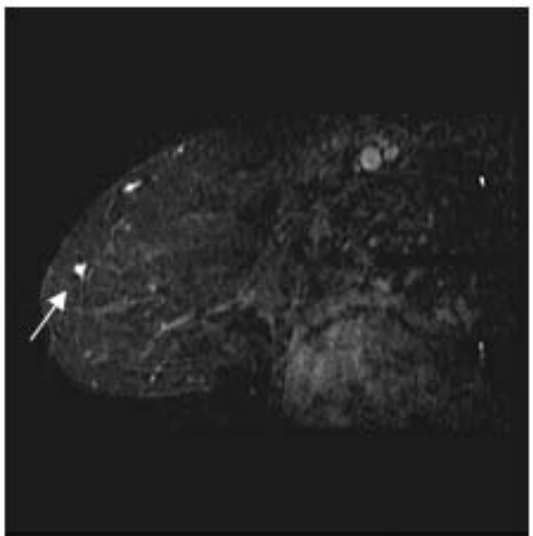

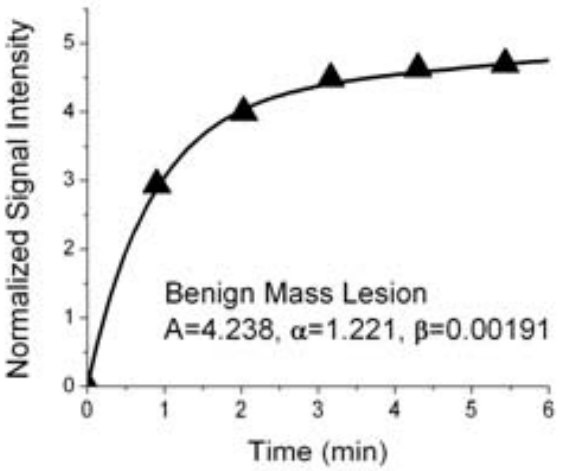
Normalized Signal Intensity
Time (min)
Benign Mass Lesion
A=4.238, α=1.221, β=0.00191

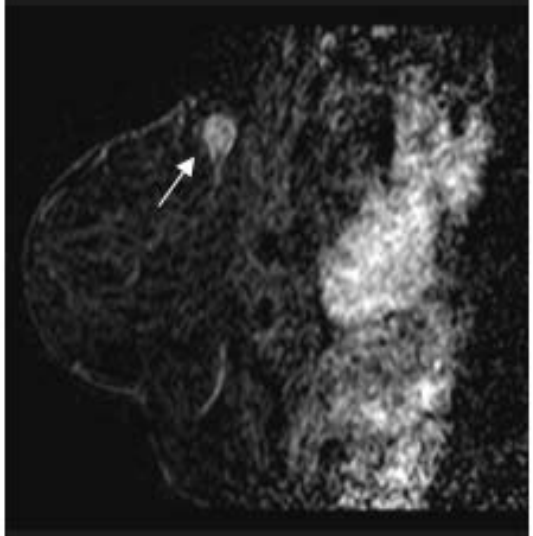

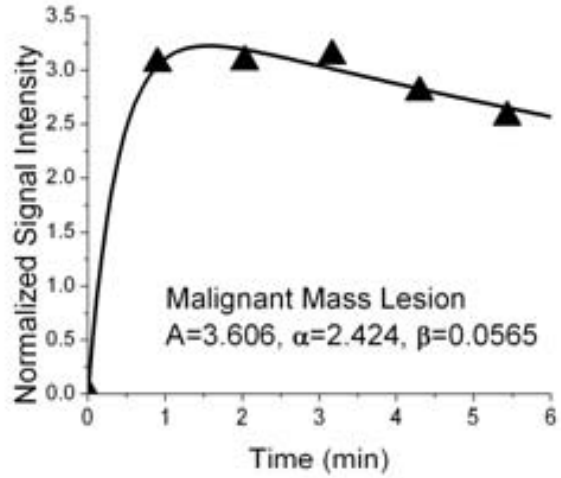
Normalized Signal Intensity
Time (min)
Malignant Mass Lesion
A=3.606, α=2.424, β=0.0565

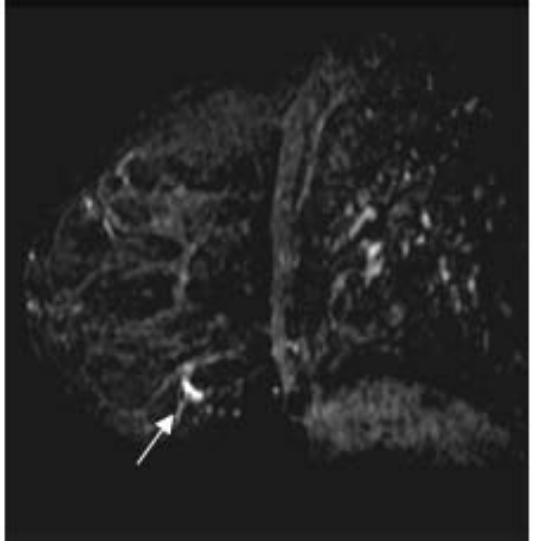

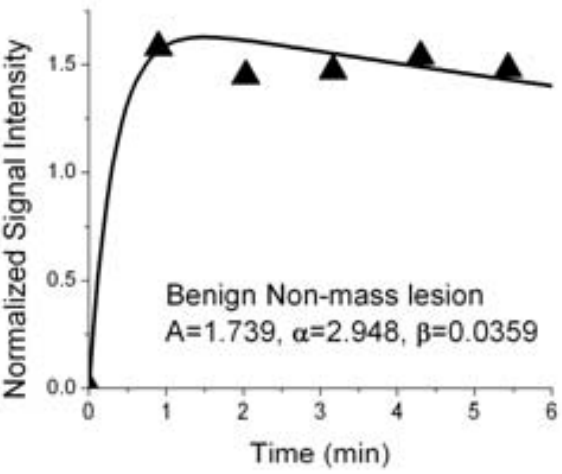
Normalized Signal Intensity
Time (min)
Benign Non-mass lesion
A=1.739, α=2.948, β=0.0359

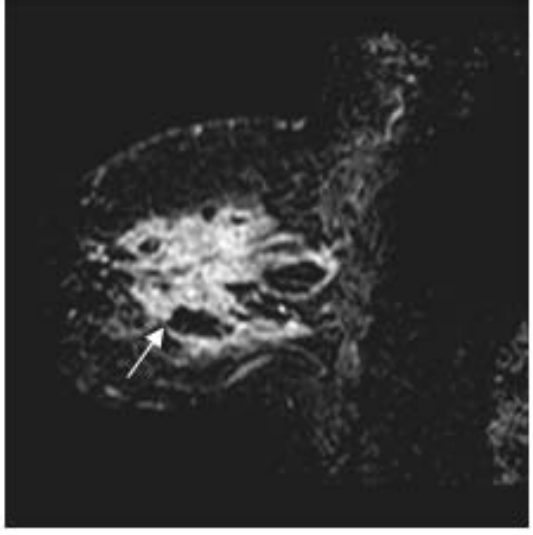

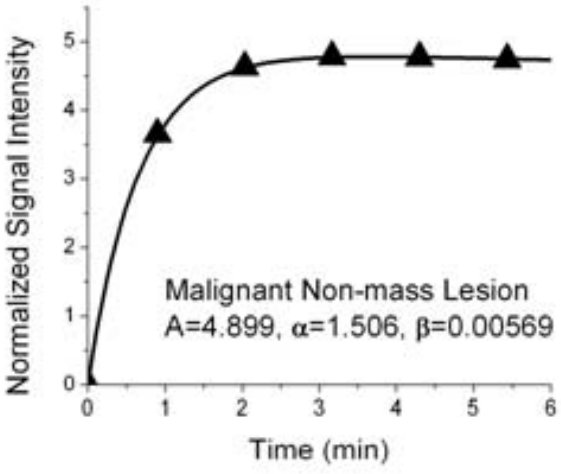
Normalized Signal Intensity
Time (min)
Malignant Non-mass Lesion
A=4.899, α=1.506, β=0.00569

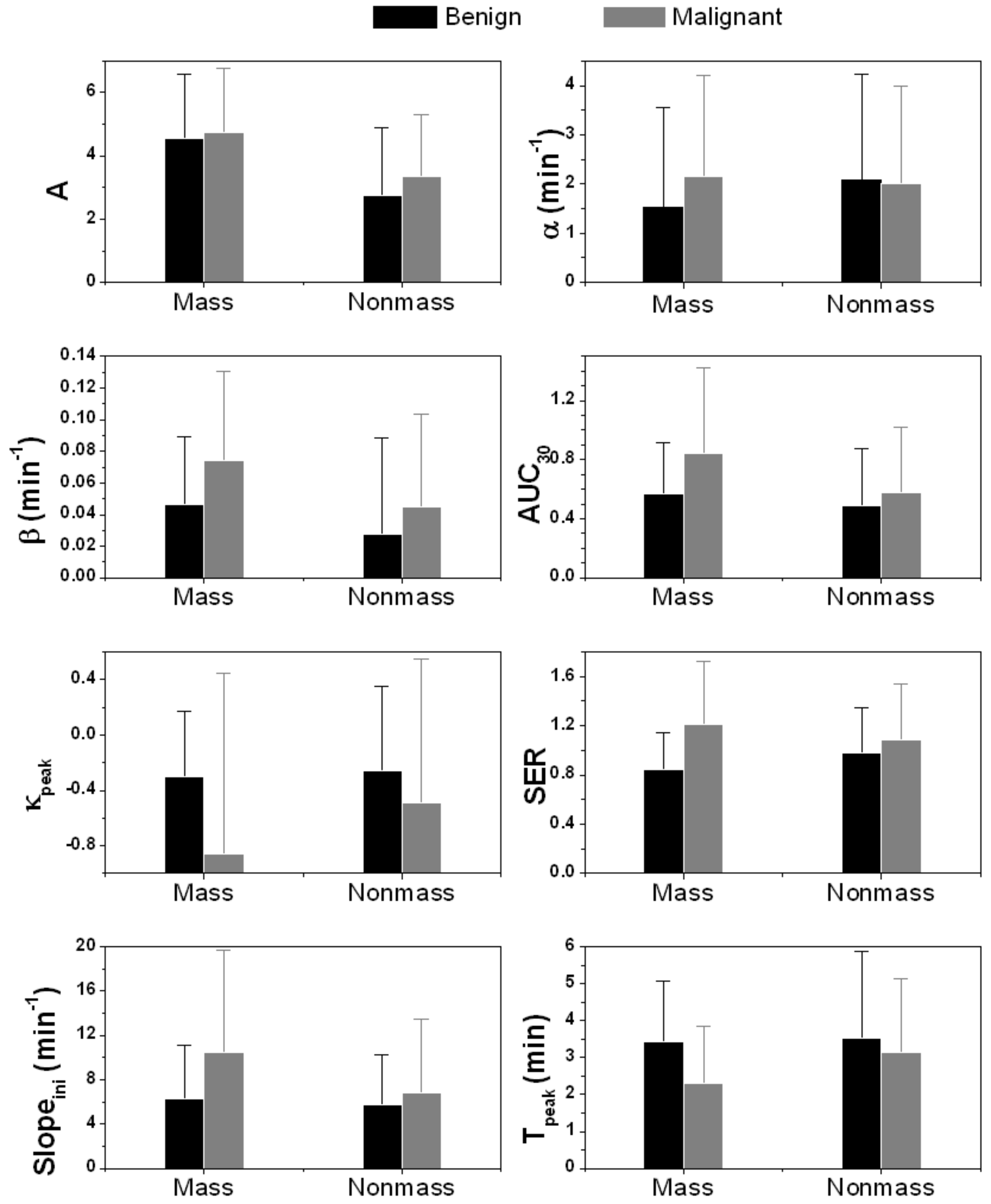
Benign
Malignant
A
α (min-1)
β (min-1)
AUC30
Kpeak
SER
Slopeini (min-1)
Tpeak (min)
Mass
Nonmass

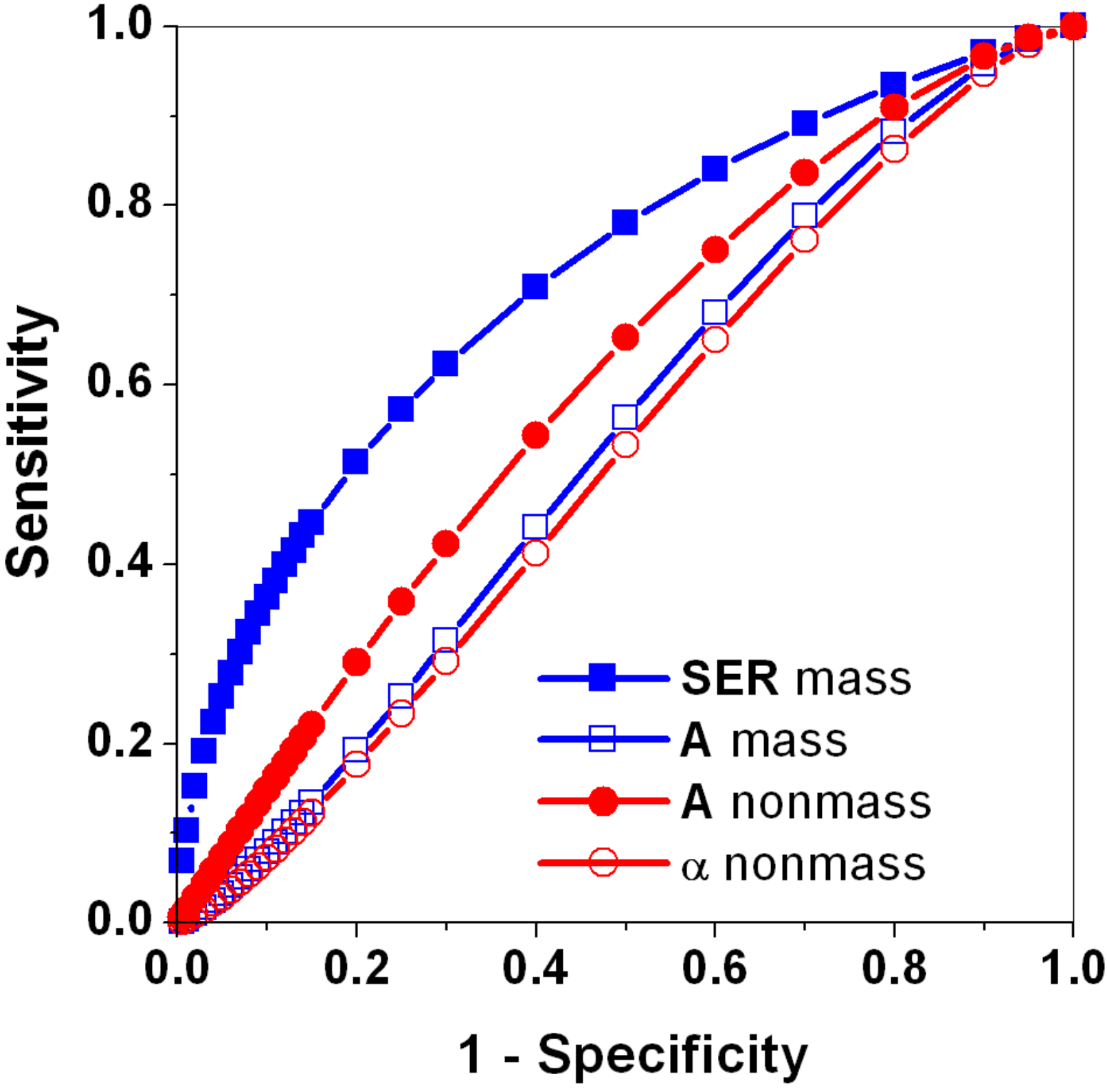
1.0
0.8
0.6
0.4
0.2
0.0
Sensitivity
0.0
0.2
0.4
0.6
0.8
1.0
1 - Specificity
SER mass
A mass
A nonmass
α nonmass

Detection of *in situ* mammary cancer in a transgenic mouse model: *in vitro* and *in vivo* MRI studies demonstrate histopathologic correlation

Short running head: Detection of *in situ* murine mammary cancer

S A Jansen[1], S D Conzen[2], X Fan[1], T Krausz[3], M Zamora[1], S Foxley[1], G M Newstead[1] and G S Karczmar[1*].

[1] University of Chicago, Department of Radiology 5841 S. Maryland Ave, MC 2026, Chicago, IL 60637

[2] University of Chicago, Department of Medicine & The Ben May Department for Cancer Research, 5841 S. Maryland Ave, MC 2115, Chicago, IL 60637

[3] University of Chicago, Department of Pathology 5841 S. Maryland Ave, MC 6101, Chicago, IL 60637

Submitted as a research paper to Physics in Medicine and Biology

*Corresponding Author:
Gregory Karczmar, Ph.D
Professor of Radiology and Medical Physics
University of Chicago
5841 S. Maryland Ave, MC 2026
Chicago, IL 60637
Phone: (773) 702-0214
Fax: (773) 834-9047
Email: gskarczm@uchicago.edu

ABSTRACT

Improving the prevention and detection of preinvasive ductal carcinoma *in situ* (DCIS) is expected to lower both morbidity and mortality from breast cancer. Transgenic mouse models can be used as a 'test bed' to develop new imaging methods and to evaluate the efficacy of candidate preventive therapies. We hypothesized that despite its microscopic size, early murine mammary cancer, including DCIS, might be accurately detected by MRI. C3(1) SV40 TAg female mice (n=23) between 10-18 weeks of age were selected for study. Eleven mice were subjected to *in vitro* imaging using a T_2-weighted spin echo (SE) sequence and 12 mice were selected for *in vivo* imaging using a T_1-weighted gradient echo (GE), a T_2-weighted spin echo (SE) and high spectral and spatial (HiSS) imaging sequences. The imaged glands were carefully dissected, formalin fixed, and paraffin embedded, and then H&E stained sections of all imaged glands were obtained, and the ratio of image-detected versus histologically-detected cancers was obtained. MR images were able to detect 12/12 intramammary lymph nodes, 1/1 relatively large (~5mm) tumor, 17/18 small (~1mm) tumors, and 13/16 ducts distended with DCIS greater than 300 microns. Significantly, there were no false positives—image detection always corresponded to a histologically detectable cancer in this model. These results indicate that MR imaging can reliably detect both preinvasive *in situ* and early invasive mammary cancers in mice with both high sensitivity and specificity. This technology is an important step towards the more effective use of non-invasive imaging in pre-clinical studies of breast cancer prevention, detection, and treatment.

Keywords: mouse, mammary, DCIS, MRI, cancer

INTRODUCTION

Women diagnosed with breast cancer today have significantly better survival outcomes compared with their counterparts of 30 years ago (Jemal *et al.*, 2004). This is attributed to improvements in treatment as well as improved detection of earlier stage cancer due to screening mammography (Berry *et al.*, 2005). Currently, 15-25% of newly diagnosed breast cancers are preinvasive ductal carcinoma *in situ* (DCIS) (Tsikitis and Chung, 2006), and with improvements in imaging these percentages are likely to increase. Women diagnosed with DCIS have the best prognosis with long-term survival rates of 97-99% (Morrow *et al.*, 2002). Half of all newly diagnosed invasive carcinomas are stage I, which is the earliest form of invasive breast cancer and does not involve metastatic spread to the lymph nodes (Li *et al.*, 2003). Some have suggested that improving the detection of early cancers is essential for further decreases in mortality rates (Duffy *et al.*, 2003). Thus, to help increase survival rates it is clearly essential to improve detection and effective treatment of early breast cancer.

Dynamic contrast enhanced MR imaging (DCEMRI) of the breast has been shown to improve the detection of early stage invasive cancers, and has recently been recommended by the American Cancer Society for the screening of women at high risk for developing breast cancer (Saslow *et al.*, 2007). However, initial reports studying the presentation of DCIS on DCEMRI found poorer sensitivity and specificity compared with x-ray mammography (Menell *et al.*, 2005; Orel *et al.*, 1997; Gilles *et al.*, 1995; Schouten van der Velden *et al.*, 2006). Although recent work has demonstrated that the sensitivity of DCEMRI for DCIS is increasing (Kuhl *et al.*, 2007), there is clearly room for improvement in diagnostic accuracy. It is anticipated that studies of the physiological and biological characteristics of early breast cancers will help improve imaging methods and analysis, because these insights will help to guide imaging approaches to find physiologically abnormal tissues seen in cancer.

Due to the urgency of surgery in early human breast cancer, studies of the natural history of such cancers in patients cannot be performed. Therefore, transgenic and xenografted mouse models of breast cancer are widely used to investigate the biological basis of human breast cancer, to evaluate new therapies, and to develop improved imaging methods. The usefulness of these mouse models depends on how closely they resemble human breast cancer. This is one reason why transgenic mouse models are appealing and have lead to improvements in detection and treatment of cancers: the tumors arise without additional carcinogens and the early tumors progress through the stages of disease, from *in situ* to invasive, closely mimicking their human counterpart. If mice are to be used as successful models of human cancer biology, then imaging methods that detect *in situ* tumors are required to accurately assess preventive, diagnostic, and therapeutic interventions. To date, however, there have been no reports of *in vivo* imaging of *in situ* or even non palpable invasive mammary gland cancers in mice (Seemann *et al.*, 2006; Jenkins *et al.*, 2005; Hsueh *et al.*, 2006; Tian *et al.*, 2003; Abbey *et al.*, 2004; Rodrigues *et al.*, 2004; Bremer *et al.*, 2005; Galie *et al.*, 2004; Artemov *et al.*, 2003; Rodriguez *et al.*, 2006; Robinson *et al.*, 2003; Geninatti Crich *et al.*, 2006). In fact, most imaging studies of mouse mammary cancer have focused on large tumors that are extremely advanced. Relative to DCIS and early invasive cancers, these more advanced cancers are not realistic models of the majority of newly diagnosed breast cancers in women.

In this project, our goal was to determine whether sensitive and specific MR imaging of early murine mammary cancer, including *in situ* carcinoma, is feasible. We studied the SV40Tag transgenic mouse model of breast cancer in which mammary cancer develops at about 16 weeks and progresses through similar stages as human breast cancer to invasive ductal carcinoma (IDC). We developed our imaging technique by first detecting microscopic cancers *ex vivo* in excised mammary glands. We then were able to advance to *in vivo* imaging of mammary glands with high sensitivity and specificity.

METHODS

Animals

Twenty three C3(1) SV40 large T antigen (Tag) transgenic mice were used for MR imaging (Maroulakou *et al.*, 1994). This mouse model targets expression of large Tag to the female mammary gland via the C3 promoter. Female mice develop mammary cancer that resembles human ductal breast carcinoma, including progression through atypical ductal hyperplasia (~8 weeks), DCIS (~12 weeks), and IDC (~16 weeks) (Green *et al.*, 2000). Eleven of the 23 mice were selected for *in vitro* imaging, and the remaining 12 for *in vivo* imaging. All procedures were carried out in accordance with our institution's Animal Care and Use Committee approval. Animals were anesthetized prior to imaging experiments, and anesthesia was maintained during imaging at 1.5% isoflorane. Body temperature was maintained with a warm air blower. The temperature, heart rate and respiration rate were monitored with data taken every minute and the signal from the respiration sensor was used to obtain gated images.

MRI Experiments

Imaging was performed with a Bruker 4.7 Tesla magnet equipped with a self-shielded gradient set that delivers maximum gradient strength of 20 gauss/cm.

In vitro: A homebuilt 6-leg low pass half-open birdcage coil (3 cm length × 2 cm width × 1 cm height) was built for mammary gland *in vitro* imaging using a multi-slice multiple spin echo sequence (rapid acquisition with refocused echoes (RARE) (Friedburg *et al.*, 1987), 4 RARE partitions, TR/TE: 4000/50 ms, field of view (FOV)=3.0× 1.5cm, number of excitations (NEX)=2, slice thickness=0.75 mm and inplane resolution= 117 microns). Twenty-two excised and fixed inguinal mammary gland specimens

were imaged from 11 mice between 8- 22 weeks of age. After imaging, hematoxylin and eosin (H&E) stained sections were obtained.

In vivo: Another homebuilt 8-leg low pass half-open birdcage coil (3 cm length × 3 cm width × 2 cm height) that produced high flux density in the mammary gland (Fan *et al.*, 2006b) was used for *in vivo* imaging. Several pulse sequences were evaluated. Initially, gradient echo (GE) images were obtained (fast low angle shot (FLASH) (Frahm *et al.*, 1986) TR/TE: 675/7 ms, FOV=3.0 × 3.0 cm, NEX=2, slice thickness=0.5mm, in-plane resolution=117 microns and flip angle=30°) across the entire sensitive volume of the coil to map out the whole gland. Based on this initial evaluation, slices that contained structures of interest (i.e., candidate cancers) were evaluated further: (i) FLASH GE with fat suppression, (ii) spin echo (SE) images (RARE, TR/TE: 3000/29 ms, RARE acceleration factor = 4, FOV=3.0 × 3.0 cm, NEX=2, slice thickness=0.5mm and in-plane resolution=117), (iii) SE with fat suppression, and (iv) high spectral and spatial (HiSS) resolution imaging (using echo-planar spectroscopic imaging (EPSI) (Mansfield, 1984) with a spectral resolution of ~ 6 Hz, FOV=3.0 × 3.0 cm, NEX=2, slice thickness=0.5mm and in-plane resolution=117 microns). The HiSS method has been detailed in prior work; briefly, HiSS acquisitions sample the entire free induction decay in each voxel, and after processing water peak-height images can be displayed – this provides complete fat suppression.

The inguinal mammary glands on the left side of twelve mice between the ages of 10-18 weeks were selected for imaging. The mice were sacrificed immediately after imaging, and the glands excised and submitted for sectioning and H&E staining. To facilitate spatial correlations between MR images and histology, a fine polyethylene mesh 3.0 cm × 2.0 cm in size with 3.0 mm spacing was embedded in partially deuterated agar and wrapped around each mouse. This agar grid produced a pattern on MRI that was used for registration of tissue sections and images. It also served to eliminate the air tissue interface near the mammary gland, which is expected to reduce susceptibility artifacts.

Image Analysis

Correlation of MRI with Histology: The H&E stained sections were evaluated by an experienced breast and mouse mammary gland pathologist (TK). Intramammary lymph nodes, invasive tumors and ducts distended with DCIS with diameters greater than 300 microns were identified. For the *in vitro* study, the H&E stained sections were acquired in the same orientation as the MR images and thus the two were easily compared. For the *in vivo* study, the agar grid allowed for comparisons between the H&E stained sections of the whole gland with the axial MR images, which represent cross sectional slices through the mammary gland. The sensitivity and specificity of MRI for lymph nodes, DCIS and invasive tumors was determined. The signal-to-noise ratio (SNR) of lymph nodes, DCIS and invasive tumors was calculated in the FLASH GE and RARE SE images. In addition, the contrast-to-noise ratio (CNR) of lymph nodes, DCIS and invasive tumors was calculated relative to muscle and normal mammary glandular tissue.

Lesion Morphology: The morphology of the lesions and lymph nodes detected by *in vivo* MRI were analyzed in the same standardized manner as lesions found in clinical breast MRI of women. For clinical examinations, the Breast Imaging- Reporting and Data System (BI-RADS) lexicon classifies the type, shape, margins and enhancement pattern of the lesion (ACR, 2003). In our study, the morphology of the lesions was classified based on a simplified version of the BI-RADS lexicon as follows: type (mass or non-mass), shape/distribution (for mass lesions: round, oval, lobular or irregular; for non-mass lesions: linear, ductal or segmental), margins (for mass lesions only: smooth or irregular) and pattern (for mass lesions: homogeneous or heterogeneous; for non-mass lesions: homogeneous, stippled or clumped).

RESULTS

In vitro MRI

H&E stained sections were obtained from six of the 22 excised mammary gland specimens. Analysis of the histologic slides confirmed that many stages of the development of mammary carcinoma were present in the specimens, including DCIS, small invasive tumors (<3mm) and large tumors (>3mm). Figure 1 shows four representative examples of the correlation between RARE SE MR images and histology. It can be seen that the MR images matched the H&E stained sections, demonstrating intramammary lymph nodes, DCIS, and both large and small invasive tumors. Review of the MR images of all 22 excised specimens demonstrated 6 large tumors (>3mm), 30 small tumors (< 3mm), 32 DCIS lesions and 22 lymph nodes.

In vivo MRI

Figure 2 demonstrates two representative examples illustrating the correlation between axial FLASH GE MR images and histology. The MR images correlated well with corresponding H&E stained sections of the mammary glands. H&E stained sections were obtained from the inguinal glands of all of the 12 mice selected for *in vivo* MR imaging. Based on histologic review, there were 12 lymph nodes, 1 large (~5mm) tumor, 18 small non-palpable tumors ~0.5-3 mm in size, and 16 ducts distended with DCIS greater than 300 microns in diameter. For lymph nodes, the sensitivity of FLASH GE imaging was 100% (12/12), for tumors larger than 5mm sensitivity was also 100% (1/1); for small tumors 0.5-3mm in size 94% (17/18) and for DCIS 81% (13/16). There were no false positives—an MR finding corresponded to cancer in all glands. Three more examples of early murine mammary cancer are shown in Figure 3.

In addition to GE images, other conventional gradient and spin echo images were also acquired of the mammary glands. The FLASH GE images with fat suppression provided the clearest images of early murine mammary cancer. In comparison, T_2 weighted RARE images with and without fat suppression did not depict the cancers or lymph nodes well, as shown for one case in Figure 4. This qualitative observation was validated by calculations of SNR and CNR, shown in Table 1. For FLASH GE images with fat suppression, the average SNR of lymph nodes, tumors and DCIS lesions were comparable to each other and to muscle, but were 3-4 times larger than normal mammary gland tissue. The average SNR of lymph nodes, tumors and DCIS lesions in RARE SE images with fat suppression were larger than muscle. However, unlike FLASH GE images, RARE SE images of early murine mammary cancers and lymph nodes had comparable SNR to the normal mammary gland tissue. Thus, because of the high background signal of the mammary gland tissue, early cancer was not well-visualized on RARE SE images. In contrast, HiSS water peak-height images provided excellent lesion visualization with complete fat suppression (Figure 4).

Lesion Morphology: The morphology of tumors, DCIS and lymph nodes was assessed on FLASH GE images with fat suppression. These images were acquired on a subset of slices and contained a total of 11 lymph nodes, 9 invasive tumors and 12 DCIS lesions. Nine of 9 invasive tumors were mass lesions, with a round (6/9) or irregular (3/9) shape, with smooth (6/9) or irregular (3/9) margins, and with a homogeneous (7/9) pattern. As with invasive tumors, 11/11 of lymph nodes were mass lesions, but the predominant shape was lobular (8/11) with smooth (10/11) margins, and a homogeneous (11/11) pattern. Eleven of 12 DCIS were non-mass lesions, with a linear (7/12) or ductal (4/12) shape, and a stippled (4/12), clumped (3/12) or homogeneous (5/12) pattern. Overall, the patterns show a similar distribution to human tumor morphologies.

DISCUSSION

In this study, we hypothesized that MR imaging techniques could be successfully applied to non-palpable, microscopic invasive and *in situ* murine mammary cancers. The importance of this accomplishment lies in the fact that (i) modeling early cancers in transgenic animals heretofore required sacrifice of the animals to assess the impact of potential therapies, and (ii) these early tumors are more realistic models of the most frequently detected human cancers, i.e. those tumors that are increasingly small. We found that MRI can reliably detect the microscopic stages of both *in situ* and invasive murine mammary cancers with both high sensitivity and specificity. To our knowledge, this is the first report of *in vivo* imaging of microscopic murine mammary cancer (Arkani *et al.*, May 2007). Abbey et al. used PET to image DCIS and early murine mammary cancer, however the correlation with histology was made *ex vivo* (Abbey *et al.*, 2004). In addition, MR imaging offers superior spatial resolution compared with PET for lesion localization and characterization. We next plan to combine the excellent anatomic detail of *in vivo* MRI with molecular imaging modalities such as PET and/or optical imaging.

We found that an open birdcage coil was better suited for this research than a volume coil because the mammary glands are attached to the skin of the mouse and are very thin (~ 1-5 mm) and therefore are close to the coil. We also found that gradient echo (GE) images with various modest T_1- weighting and fat suppression produced the clearest *in vivo* images of mammary glands and cancer compared with T_2-weighted spin echo (SE) images. This is primarily because the SNR of lymph nodes, tumors and DCIS was comparable to that of the surrounding normal mammary gland tissue. This may be due to incomplete fat suppression in the RARE SE. For the conventional SE and GE images, fat suppression was achieved via a spectrally selective saturation pulse. It could be that if the initial saturation pulse did not adequately suppress the fat signal, residual signal of the mammary fat pad remained and was further amplified by the four refocusing pulses in the RARE acquisition. To image murine mammary cancer, suppression of signal from the mammary fat pad is important. High spectral and spatial (HiSS) imaging techniques

allow calculation of water resonance peak height images and provide complete fat suppression. In addition, these images provide strong T_2* contrast without distortion (Fan *et al.*, 2006a). We found that HiSS imaging revealed distended ducts and irregularities in parenchymal texture, while providing excellent fat suppression (Figure 4).

Interestingly, we noted that the morphology of early murine mammary cancers on MRI is similar to the MR presentation of early human breast cancer: DCIS lesions were non-mass lesions and appeared in a ductal or linear shape (Jansen *et al.*, 2007; Esserman *et al.*, 2006), while small invasive cancers appeared as round masses with smooth margins. In clinical DCEMRI of the human breast, contrast is administered to visualize the lesion. However, in the present study we used non-contrast enhanced imaging techniques. This suggests that, in principle, contrast media may not be needed to visualize breast cancer lesions. Indeed, this is consistent with early work of Harms et al. using rotating delivery of excitation offresonance (RODEO) fat suppression, while more recent work using HiSS imaging of the breast has demonstrated that both benign and malignant lesions can be appreciated without contrast injection (Du *et al.*, 2002). This is consistent with the results obtained here with both fat-suppressed GE and HiSS imaging. In fact, evaluation of lesion morphology in the absence of contrast agent may be desirable because contrast agents may cause blooming (Fischer *et al.*, 2004; Penn *et al.*, 2006) and other changes in morphology. We plan to acquire and analyze the DCEMRI kinetic parameters of early murine mammary cancer for comparison with non-contrast-enhanced images.

The results of the present study suggest that in the future MR imaging can be used to assess the effectiveness of therapies for cancers of all stages—*in situ*, early invasive and advanced. Using the MR imaging techniques we have shown here, new contrast agents and imaging techniques that target DCIS and early invasive cancers can be developed, optimized, and evaluated. DCIS is generally considered to be a precursor of invasive cancer (Recht *et al.*, 1998). However, because its progression cannot be observed directly in women, the natural history of DCIS is not well understood. Evidence from studies

where DCIS was initially misdiagnosed as benign disease suggest that 14-53% of DCIS may progress to become invasive cancer (Erbas *et al.*, 2006). Autopsy studies have shown that DCIS is found in 5-14% of women, implying that there is a large pool of undetected DCIS in the general population (Erbas *et al.*, 2006). Although it is a preinvasive disease, due to the uncertainty of the natural history of individual lesions, DCIS is currently managed with obligate surgical excision (Duffy *et al.*, 2005). The techniques we report here provide a first step towards the use of non-invasive imaging to investigate the progression of DCIS in an animal model, and may allow us to study the characteristics of those tumors that become invasive cancers compared to those that do not. This information can be used to improve clinical management of early breast cancers.

In summary, the present study was designed to develop MR approaches to detecting early murine mammary cancer *in vivo*. We selected a transgenic mouse model with nearly 100% penetrance of mammary cancer. A logical extension of the work discussed here will be to test our MRI detection methods of early cancers in other mouse strains that develop mammary cancer with a much lower percentage penetrance. It will also be important to image thoracic mammary glands in addition to the inguinal glands reported on here. However, these experiments provide proof of principle that microscopic mammary tumors can indeed be detected and followed in a mouse model of breast cancer. This is an important step towards the more effective use of non-invasive imaging in pre-clinical studies of early breast cancer.

Acknowledgements

We would like to thank the Segal Foundation, the Florsheim Foundation, the Biological Sciences Division at the University of Chicago, the University of Chicago Cancer Center, DOD Award W81XWH-06-1-0329 and NIH grants R21 CA104774-01A2 and 1 R01 EB003108-04 for financial support. We would also like to thank Erica Markiewicz, Diana Pang, Brad Williams and So-young Kim for help with acquiring and imaging the mice.

Table 1. (a) The average signal-to-noise ratio (SNR) of muscle, normal mammary gland tissue (MGT), lymph nodes, tumors and DCIS lesions for FLASH gradient echo (GE) images with fat suppression (FS) and RARE spin echo (SE) images with fat suppression. (b) The average contrast-to-noise ratio (CNR) of tumors, DCIS and lymph nodes relative to muscle and normal mammary glandular tissue. Numbers are mean ± standard deviation.

(a) Average SNR

Pulse sequence	***Muscle***	***MGT***	***Tumor***	***DCIS***	***Lymph Node***
FLASH GE with FS	33.9±6.0	10.3±4.2	34.3±12.2	30.0±8.7	40.3±7.4
RARE SE with FS	26.5±3.0	39.0±5.5	50.0±5.4	38.9±8.6	44.4±7.5

(b) Average CNR

Pulse sequence	***Tumor-Muscle***	***DCIS-Muscle***	***Lymph node-Muscle***	***Tumor-MGT***	***DCIS-MGT***	***Lymph node-MGT***
FLASH GE with FS	3.78±6.1	-3.6±8.9	6.8±5.6	21.3±8.3	20.6±7.6	29.9±6.2
RARE SE with FS	21.7±5.2	13.2±7.3	18.0±5.9	7.08±3.4	2.46±5.2	5.4±6.8

Figure Captions.

Figure 1. *In vitro* MR images (RARE SE) with corresponding H&E stained sections of the different stages of mammary cancer. For each MR image, the display FOV is 0.8 cm × 0.48 cm. White arrowheads point to lymph nodes, thin black arrows to DCIS, and thick black arrows to invasive tumors. The lymph nodes here are approximately 2-3 mm in size, while invasive tumors range from approximately 2-4 mm in size. The ducts distended with DCIS range from one to a few hundred microns in diameter. In (a) approximately 120 micron ducts with very early DCIS are detected. In (b) the ducts are now distended further with DCIS to a few hundred microns in diameter, and an area of microinvasion—that is, where the cancer cells have penetrated through the basement membrane—is evident (thin grey arrow). This marks the beginning of the transition from *in situ* to invasive carcinoma. In (c) two relatively large ~ 4mm invasive tumors are shown. In (d) smaller ~ 2 mm invasive tumors and DCIS are demonstrated.

Figure 2. *In vivo* axial MR images (FLASH GE with fat suppression) and corresponding H&E stained sections. The MR images and H&E stained sections represent different orientations. During imaging, the mammary glands are attached to the skin of the mouse, and are therefore wrapped around the body of the mouse. For excision, the glands are peeled back from the body of the mouse and laid flat, so that coronal H&E stained sections can be obtained. Each axial MR image represents one cross-sectional slice through the mammary gland. We used an agar grid (a polyethylene mesh embedded in partially deuterated agar) to register the axial MR images with the H&E stained sections. (a) Lymph node (arrowhead) and DCIS (thin arrow). (b) Lymph node (arrowhead) and small tumor (thick arrow). For each MR image, the display FOV is 3.0 × 2.0 cm.

Figure 3: Examples of FLASH GE images with fat suppression of: a) DCIS (thin arrow), b) DCIS (thin arrow) and c) small tumor (thick arrow). The display FOV is 3.0 × 2.0 cm. In b) and c) the agar grid is visible wrapped around the mouse.

Figure 4: Demonstration of the same axial slice of a) lymph node (arrowhead) and b) DCIS (thin arrow), for three different imaging acquisitions, from left to right: FLASH GE with fat suppression, RARE SE with fat suppression and high spectral and spatial imaging (HiSS), which yields water peak height images (shown). The display FOV is 3.0 × 2.0 cm. The FLASH GE with fat suppression produced clearer images of the cancer and lymph node compared with SE. The HiSS images show the lymph node and DCIS along with excellent fat suppression.

Figure 1. *In vitro* MR images (RARE SE) with corresponding H&E stained sections of the different stages of mammary cancer. For each MR image, the display FOV is 0.8 cm × 0.48 cm. White arrowheads point to lymph nodes, thin black arrows to DCIS, and thick black arrows to invasive tumors. The lymph nodes here are approximately 2-3 mm in size, while invasive tumors range from approximately 2-4 mm in size. The ducts distended with DCIS range from one to a few hundred microns in diameter. In (a) approximately 120 micron ducts with very early DCIS are detected. In (b) the ducts are now distended further with DCIS to a few hundred microns in diameter, and an area of microinvasion—that is, where the cancer cells have penetrated through the basement membrane—is evident (thin grey arrow). This marks the beginning of the transition from *in situ* to invasive carcinoma. In (c) two relatively large ~ 4mm invasive tumors are shown. In (d) smaller ~ 2 mm invasive tumors and DCIS are demonstrated.

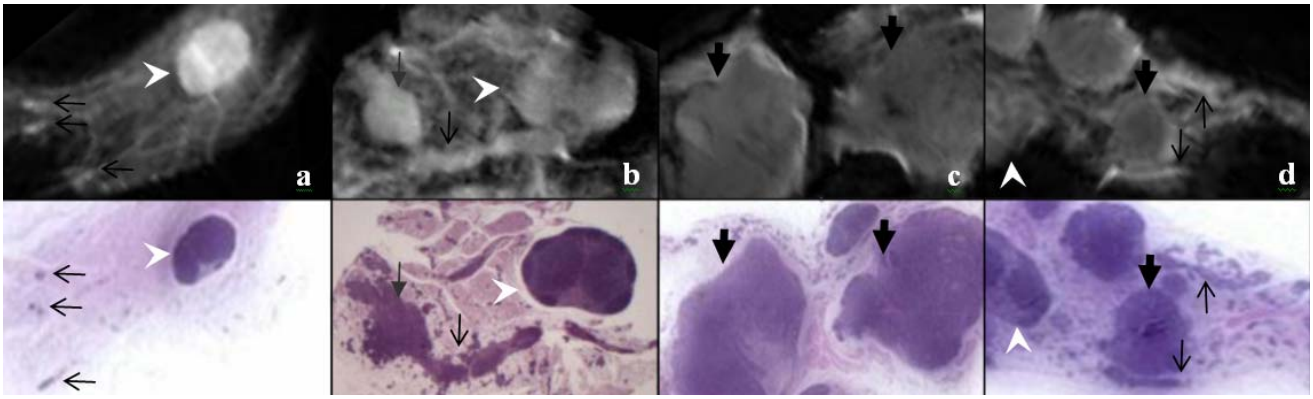

Figure 2. *In vivo* axial MR images (FLASH GE with fat suppression) and corresponding H&E stained sections. The MR images and H&E stained sections represent different orientations. During imaging, the mammary glands are attached to the skin of the mouse, and are therefore wrapped around the body of the mouse. For excision, the glands are peeled back from the body of the mouse and laid flat, so that coronal H&E stained sections can be obtained. Each axial MR image represents one cross-sectional slice through the mammary gland. We used an agar grid (a polyethylene mesh embedded in partially deuterated agar) to register the axial MR images with the H&E stained sections. (a) Lymph node (arrowhead) and DCIS (thin arrow). (b) Lymph node (arrowhead) and small tumor (thick arrow). For each MR image, the display FOV is 3.0 × 2.0 cm.

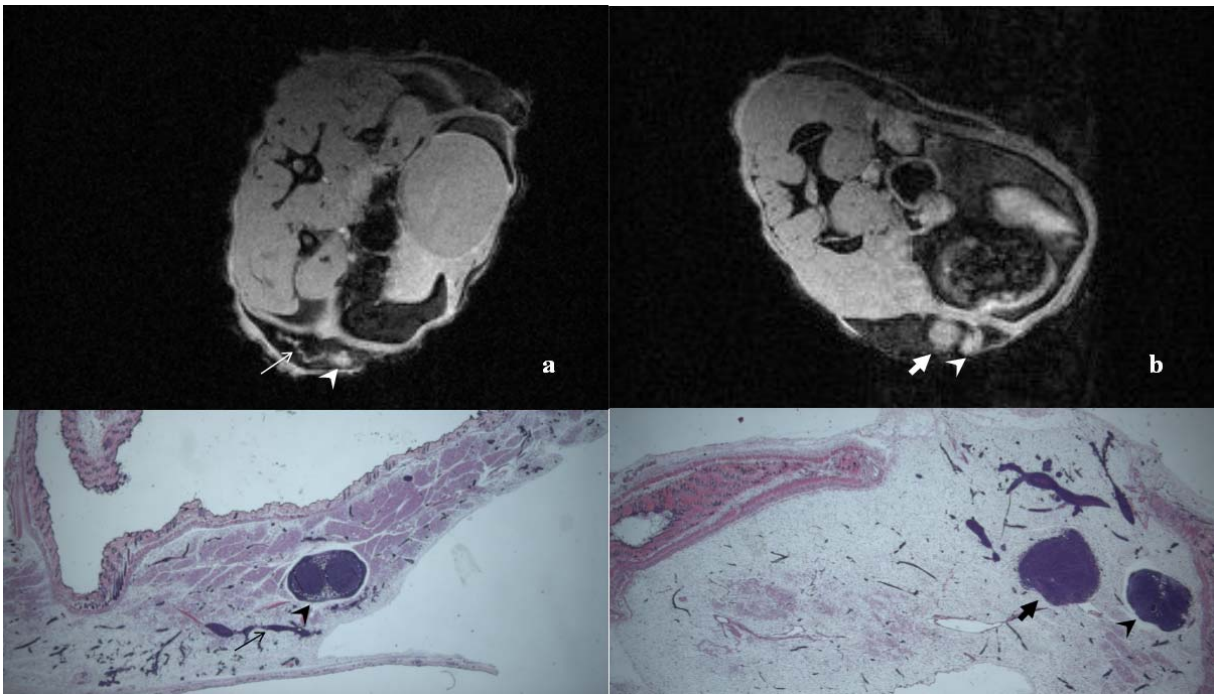

Figure 3: Examples of FLASH GE images with fat suppression of: a) DCIS (thin arrow), b) DCIS (thin arrow) and c) small tumor (thick arrow). The display FOV is 3.0 × 2.0 cm. In b) and c) the agar grid is visible wrapped around the mouse.

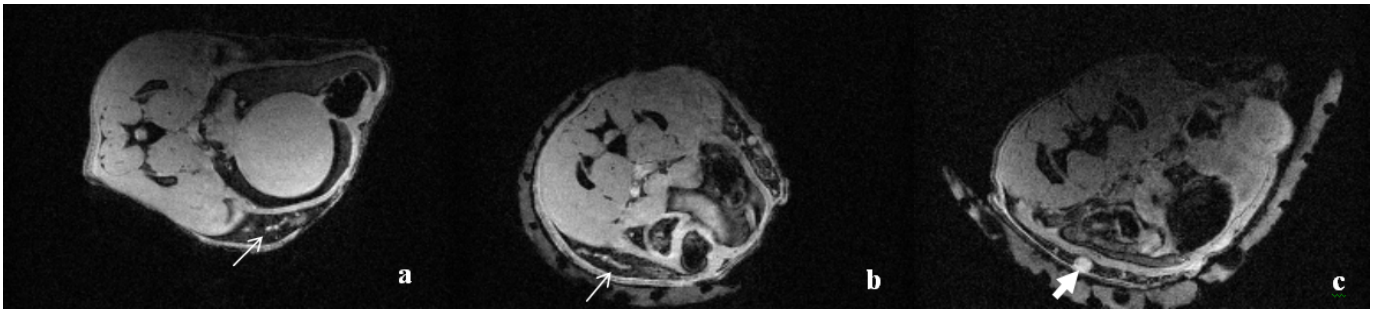

Figure 4: Demonstration of the same axial slice of a) lymph node (arrowhead) and b) DCIS (thin arrow), for three different imaging acquisitions, from left to right: FLASH GE with fat suppression, RARE SE with fat suppression and high spectral and spatial imaging (HiSS), which yields water peak height images (shown). The display FOV is 3.0 × 2.0 cm. The FLASH GE with fat suppression produced clearer images of the cancer and lymph node compared with SE. The HiSS images show the lymph node and DCIS along with excellent fat suppression.

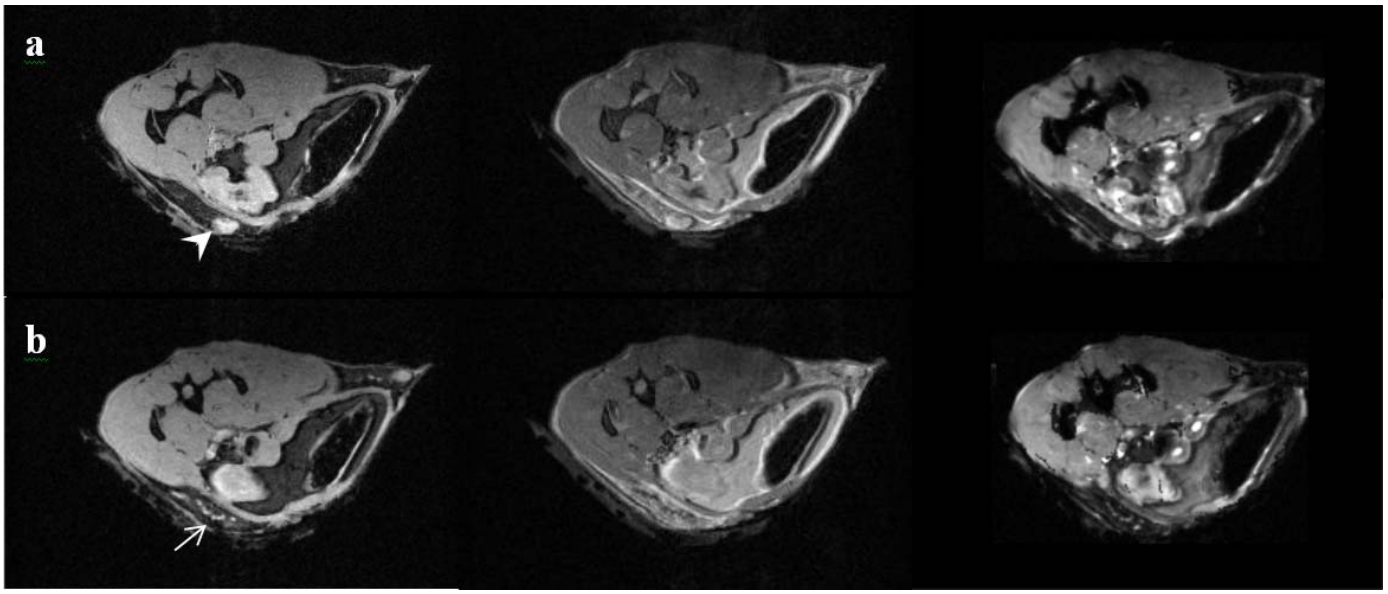

References:

American Cancer Society. Breast Cancer Facts & Figures 2005-2006 *Atlanta: American Cancer Society, Inc. http://www.cancer.org/downloads/STT/CAFF2005BrFacspdf2005.pdf. Accessed March 2007.*

Abbey C K, Borowsky A D, McGoldrick E T, Gregg J P, Maglione J E, Cardiff R D and Cherry S R 2004 In vivo positron-emission tomography imaging of progression and transformation in a mouse model of mammary neoplasia *Proc Natl Acad Sci U S A* **101** 11438-43

ACR 2003 *American College of Radiology (ACR) Breast Imaging Reporting and Data System Atlas (BI-RADS)* (Reston, VA.

Arkani S, Conzen S, Krausz T, Newstead G and Karczmar G S May 2007 MRI of Ductal Carcinoma in situ and Other Early Mammary Cancers in Transgenic Mice *Poster Presentation at International Society for Magnetic Resonane in Medicine.*

Artemov D, Mori N, Ravi R and Bhujwalla Z M 2003 Magnetic resonance molecular imaging of the HER-2/neu receptor *Cancer Res* **63** 2723-7

Berry D A, Cronin K A, Plevritis S K, Fryback D G, Clarke L, Zelen M, Mandelblatt J S, Yakovlev A Y, Habbema J D and Feuer E J 2005 Effect of screening and adjuvant therapy on mortality from breast cancer *N Engl J Med* **353** 1784-92

Bremer C, Ntziachristos V, Weitkamp B, Theilmeier G, Heindel W and Weissleder R 2005 Optical imaging of spontaneous breast tumors using protease sensing 'smart' optical probes *Invest Radiol* **40** 321-7

Du W, Du Y P, Bick U, Fan X, MacEneaney P M, Zamora M A, Medved M and Karczmar G S 2002 Breast MR imaging with high spectral and spatial resolutions: preliminary experience *Radiology* **224** 577-85

Duffy S W, Agbaje O, Tabar L, Vitak B, Bjurstam N, Bjorneld L, Myles J P and Warwick J 2005 Overdiagnosis and overtreatment of breast cancer: estimates of overdiagnosis from two trials of mammographic screening for breast cancer *Breast Cancer Res* **7** 258-65

Duffy S W, Tabar L, Vitak B, Day N E, Smith R A, Chen H H and Yen M F 2003 The relative contributions of screen-detected in situ and invasive breast carcinomas in reducing mortality from the disease *Eur J Cancer* **39** 1755-60

Erbas B, Provenzano E, Armes J and Gertig D 2006 The natural history of ductal carcinoma in situ of the breast: a review *Breast Cancer Res Treat* **97** 135-44

Esserman L J, Kumar A S, Herrera A F, Leung J, Au A, Chen Y Y, Moore D H, Chen D F, Hellawell J, Wolverton D, Hwang E S and Hylton N M 2006 Magnetic resonance imaging captures the biology of ductal carcinoma in situ *J Clin Oncol* **24** 4603-10

Fan X, Abe H, Medved M, Foxley S, Arkani S, Zamora M A, Olopade O I, Newstead G M and Karczmar G S 2006a Fat suppression with spectrally selective inversion vs. high spectral and spatial resolution MRI of breast lesions: qualitative and quantitative comparisons *J Magn Reson Imaging* **24** 1311-5

Fan X, Markiewicz E J, Zamora M, Karczmar G S and Roman B B 2006b Comparison and evaluation of mouse cardiac MRI acquired with open birdcage, single loop surface and volume birdcage coils *Phys Med Biol* **51** N451-9

Fischer D R, Baltzer P, Malich A, Wurdinger S, Freesmeyer M G, Marx C and Kaiser W A 2004 Is the "blooming sign" a promising additional tool to determine malignancy in MR mammography? *Eur Radiol* **14** 394-401

Frahm J, Haase A and Matthaei D 1986 Rapid three-dimensional MR imaging using the FLASH technique *J Comput Assist Tomogr* **10** 363-8

Friedburg H, Henning J and Schumacher M 1987 [RARE-MR myelography in routine clinical practice. Experience with 175 cases] *Rofo* **146** 584-90

Galie M, D'Onofrio M, Calderan L, Nicolato E, Amici A, Crescimanno C, Marzola P and Sbarbati A 2004 In vivo mapping of spontaneous mammary tumors in transgenic mice using MRI and ultrasonography *J Magn Reson Imaging* **19** 570-9

Geninatti Crich S, Cabella C, Barge A, Belfiore S, Ghirelli C, Lattuada L, Lanzardo S, Mortillaro A, Tei L, Visigalli M, Forni G and Aime S 2006 In vitro and in vivo magnetic resonance detection of tumor cells by targeting glutamine transporters with Gd-based probes *J Med Chem* **49** 4926-36

Gilles R, Zafrani B, Guinebretiere J M, Meunier M, Lucidarme O, Tardivon A A, Rochard F, Vanel D, Neuenschwander S and Arriagada R 1995 Ductal carcinoma in situ: MR imaging-histopathologic correlation *Radiology* **196** 415-9

Green J E, Shibata M A, Yoshidome K, Liu M L, Jorcyk C, Anver M R, Wigginton J, Wiltrout R, Shibata E, Kaczmarczyk S, Wang W, Liu Z Y, Calvo A and Couldrey C 2000 The C3(1)/SV40 T-antigen transgenic mouse model of mammary cancer: ductal epithelial cell targeting with multistage progression to carcinoma *Oncogene* **19** 1020-7

Hsueh W A, Kesner A L, Gangloff A, Pegram M D, Beryt M, Czernin J, Phelps M E and Silverman D H 2006 Predicting Chemotherapy Response to Paclitaxel with 18F-Fluoropaclitaxel and PET *J Nucl Med* **47** 1995-9

Jansen S, Newstead G, Abe H, Shimauchi A, Schmidt R and Karczmar G S 2007 MR Imaging of Pure Ductal Carcinoma in situ: Kinetics, Morphology and Comparison with Mammographic Presentation and Nuclear Grade *Radiology (in press).*

Jemal A, Clegg L X, Ward E, Ries L A, Wu X, Jamison P M, Wingo P A, Howe H L, Anderson R N and Edwards B K 2004 Annual report to the nation on the status of cancer, 1975-2001, with a special feature regarding survival *Cancer* **101** 3-27

Jenkins D E, Hornig Y S, Oei Y, Dusich J and Purchio T 2005 Bioluminescent human breast cancer cell lines that permit rapid and sensitive in vivo detection of mammary tumors and multiple metastases in immune deficient mice *Breast Cancer Res* **7** R444-54

Kuhl C K, Schrading S, Bieling H B, Wardelmann E, Leutner C C, Koenig R, Kuhn W and Schild H H 2007 MRI for diagnosis of pure ductal carcinoma in situ: a prospective observational study *Lancet* **370** 485-92

Li C I, Malone K E and Daling J R 2003 Differences in breast cancer stage, treatment, and survival by race and ethnicity *Arch Intern Med* **163** 49-56

Mansfield P 1984 Spatial mapping of the chemical shift in NMR *Magn Reson Med* **1** 370-86

Maroulakou I G, Anver M, Garrett L and Green J E 1994 Prostate and mammary adenocarcinoma in transgenic mice carrying a rat C3(1) simian virus 40 large tumor antigen fusion gene *Proc Natl Acad Sci U S A* **91** 11236-40

Menell J H, Morris E A, Dershaw D D, Abramson A F, Brogi E and Liberman L 2005 Determination of the presence and extent of pure ductal carcinoma in situ by mammography and magnetic resonance imaging *Breast J* **11** 382-90

Morrow M, Strom E A, Bassett L W, Dershaw D D, Fowble B, Harris J R, O'Malley F, Schnitt S J, Singletary S E and Winchester D P 2002 Standard for the management of ductal carcinoma in situ of the breast (DCIS) *CA Cancer J Clin* **52** 256-76

Orel S G, Mendonca M H, Reynolds C, Schnall M D, Solin L J and Sullivan D C 1997 MR imaging of ductal carcinoma in situ *Radiology* **202** 413-20

Penn A, Thompson S, Brem R, Lehman C, Weatherall P, Schnall M, Newstead G, Conant E, Ascher S, Morris E and Pisano E 2006 Morphologic blooming in breast MRI as a characterization of margin for discriminating benign from malignant lesions *Acad Radiol* **13** 1344-54

Recht A, Rutgers E J, Fentiman I S, Kurtz J M, Mansel R E and Sloane J P 1998 The fourth EORTC DCIS Consensus meeting (Chateau Marquette, Heemskerk, The Netherlands, 23-24 January 1998)--conference report *Eur J Cancer* **34** 1664-9

Robinson S P, Rijken P F, Howe F A, McSheehy P M, van der Sanden B P, Heerschap A, Stubbs M, van der Kogel A J and Griffiths J R 2003 Tumor vascular architecture and function evaluated by non-

invasive susceptibility MRI methods and immunohistochemistry *J Magn Reson Imaging* **17** 445-54

Rodrigues L M, Stubbs M, Robinson S P, Newell B, Mansi J and Griffiths J R 2004 The C-neu mammary carcinoma in Oncomice; characterization and monitoring response to treatment with herceptin by magnetic resonance methods *Magma* **17** 260-70

Rodriguez O, Fricke S, Chien C, Dettin L, VanMeter J, Shapiro E, Dai H N, Casimiro M, Ileva L, Dagata J, Johnson M D, Lisanti M P, Koretsky A and Albanese C 2006 Contrast-enhanced in vivo imaging of breast and prostate cancer cells by MRI *Cell Cycle* **5** 113-9

Saslow D, Boetes C, Burke W, Harms S, Leach M O, Lehman C D, Morris E, Pisano E, Schnall M, Sener S, Smith R A, Warner E, Yaffe M, Andrews K S and Russell C A 2007 American Cancer Society guidelines for breast screening with MRI as an adjunct to mammography *CA Cancer J Clin* **57** 75-89

Schouten van der Velden A P, Boetes C, Bult P and Wobbes T 2006 The value of magnetic resonance imaging in diagnosis and size assessment of in situ and small invasive breast carcinoma *Am J Surg* **192** 172-8

Seemann M D, Beck R and Ziegler S 2006 In vivo tumor imaging in mice using a state-of-the-art clinical PET/CT in comparison with a small animal PET and a small animal CT *Technol Cancer Res Treat* **5** 537-42

Tian X, Aruva M R, Rao P S, Qin W, Read P, Sauter E R, Thakur M L and Wickstrom E 2003 Imaging oncogene expression *Ann N Y Acad Sci* **1002** 165-88

Tsikitis V L and Chung M A 2006 Biology of ductal carcinoma in situ classification based on biologic potential *Am J Clin Oncol* **29** 305-10

Why do Ductal Carcinoma in situ Lesions Enhance on Dynamic Contrast Enhanced MRI of the Breast? Using X-Ray Fluorescence and MRI to Track the Spatial Distribution of Gd-DTPA in Murine DCIS.

S. A. Jansen[1], T. Paunesku[2], G. Woloschak[2], S. Vogt[3], S. Conzen[4], G. M. Newstead[4], and G. Karczmar[4]
[1]University of Chicago, Chicago, IL, United States, [2]Northwestern University, [3]Argonne National Laboratory, [4]University of Chicago

Introduction: The early detection of breast cancer is a major prognostic factor in the management of the disease. In particular, detecting breast cancer in its pre-invasive form as ductal carcinoma *in situ* (DCIS) improves prognosis greatly compared with invasive tumors. Although dynamic contrast enhanced MR imaging (DCEMRI) of the breast has demonstrated high sensitivity to invasive breast cancer, the diagnostic accuracy of DCEMRI to DCIS needs improvement. Furthermore, the mechanism for contrast enhancement of DCIS lesions—which represent neoplastic cells that are still confined within the mammary ducts—on DCEMRI is not clear. The purpose of this study was to use transgenic mouse models of breast cancer to study DCEMRI of DCIS by (i) obtaining *in vivo* DCEMRI of murine DCIS lesions, (ii) use x-ray fluorescence (XRF) microscopy to identify the spatial distribution of Gd-DTPA following IV injection in mouse mammary glands, and (iii) determine if Gd-DTPA enters ducts distended with DCIS.

Methods: Fourteen C3(1) Sv40 TAg female transgenic mice were selected for DCEMRI following approval by the Animal Care and Use Committee. In this mouse model, mice develop mammary cancer similar to breast ductal carcinoma, including progression through DCIS and invasive cancer. On all fourteen mice, DCEMRI of the inguinal mouse mammary glands were obtained on a 4.7 T magnet, in conjunction with T_1 weighted gradient echo images for DCIS lesion localization. To prepare samples for XRF microscopy, mice were injected with 0.1 mM/kg Gd-DTPA, sacrificed after 2 minutes, and portions of the inguinal mammary glands were excised and frozen. Frozen sections were mounted on ~3x3mm silicon nitride "windows" for XRF; these sections contained portions of portions of lymph nodes, ducts distended with DCIS, and nearby blood vessels. Using the 2-ID XOR CAT at the Advanced Photon Source at Argonne National Laboratory, we performed XRF microscopy on the frozen section. Elemental concentrations of Gd, phosphorus (P) and iron (Fe) were determined in regions of interest in the ducts, lymph nodes and blood vessels. The DCEMRI were also compared with the XRF microscopy.

Results: DCEMRI demonstrated that ducts distended with DCIS exhibited contrast uptake along the length of the lesion (Figure 1). XRF microscopy verified that Gd-DTPA was present in lymph nodes, blood vessels as well as in portions of mammary ducts distended with DCIS (Figures 2, 3). As expected, Fe was also present in blood vessels, but not in the duct with DCIS.

Discussion: We have used transgenic mice to investigate contrast enhancement in DCEMRI. Our preliminary results indicate that: (i) murine DCIS lesions exhibit contrast uptake, which has not been observed before, and (ii) Gd-DTPA can leave blood vessels to enter ducts distended with DCIS. These ducts may have leaky basement membranes allowing gadolinium to diffuse inside. This is an important, new insight into the mechanism for contrast enhancement of DCIS lesions in DCEMRI. This observation may indicate that two compartment pharmacokinetic models may be invalid for DCIS lesions, as they ignore exchange of contrast with the mammary duct distended with DCIS (representing a 3rd compartment). These preliminary results point to future validation in more samples. Understanding the uptake of Gd in mammary ducts may lead to improvements in imaging methods, mathematical modeling of kinetic data and interpretation of DCEMRI.

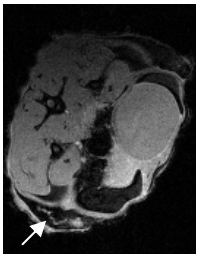

Figure 1: Axial MRI of mouse with duct distended with DCIS (arrow).

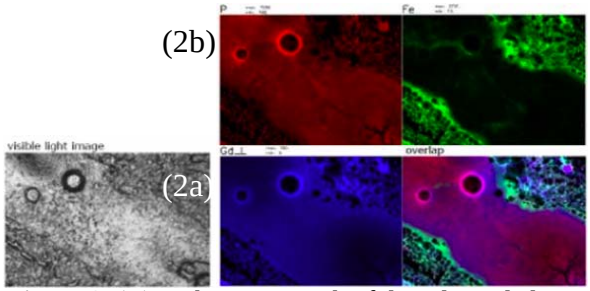

Figure 2. (a) Light micrograph of duct distended with DCIS. (b) Elemental concentration maps of P (red), Fe (green), Gd (blue) and the overlap demonstrating Gd (but not Fe) penetrated the mammary duct distended with DCIS.

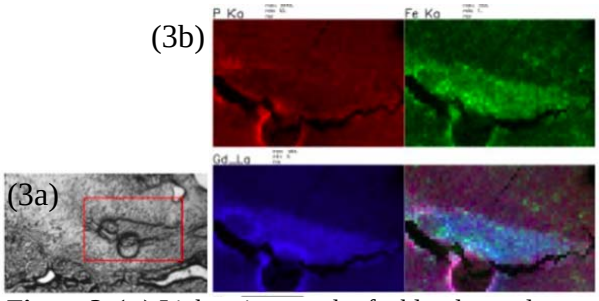

Figure 3. (a) Light micrograph of a blood vessel. (b) Elemental concentration maps of P (red), Fe (green), Gd (blue) and the overlap, demonstrating that Fe and Gd was present in the blood vessel.

Acknowledgments: We would like to thank the Segal Foundation, DOD grant W81XWH-06-1-0329 and NIH grants R21 CA104774-01A2 and 2 R01 CA078803-05A2 for financial support.

Do all *in situ* cancers progress to invasive disease? A first look at progression of mammary cancer from *in situ* to invasive carcinoma *in vivo*.

S. A. Jansen[1], G. Newstead[2], S. Conzen[2], M. Zamora[2], T. Krausz[2], and G. Karczmar[2]
[1]University of Chicago, Chicago, IL, United States, [2]University of Chicago

Introduction: The early detection of breast cancer is a major prognostic factor in the management of the disease. In particular, detecting breast cancer in its pre-invasive form as ductal carcinoma *in situ* (DCIS) improves prognosis greatly compared with invasive tumors. However, a clinical concern is whether DCIS is being overdiagnosed and overtreated, as there is evidence to suggest that not all DCIS lesions will progress into invasive cancers. The purpose of this study was to investigate the progression of DCIS into invasive cancer using a transgenic mouse model. In order to accomplish this, DCIS and early invasive cancers would need to be reliably detected in mouse mammary glands, however there have been no prior published reports demonstrating this. Therefore, the first part of this study involved demonstrating that although *in situ* and early invasive cancers are difficult and small (< 1mm) targets, they can be reliably detected by MR imaging. Then, the progression of *in situ* to invasive disease was studied using *in vivo* MRI.
Methods: The Animal Care and Use Committee approved our study of 20 C3(1) SV40 TAg mice between 10-20 weeks of age. In 12 mice, a sensitivity/specificity study was performed to determine whether conventional MR imaging techniques could be used to reliably detect early mammary cancer and DCIS *in vivo*. For this, a pair of inguinal mammary glands in each mouse was imaged using a T_1-weighted gradient echo (GE) sequence, with fat suppression. H&E sections of the glands were obtained. We used a polyethylene grid embedded in partially deuterated agar to register tissue sections and MR images. On one representative H&E section, the tumors and ducts distended with DCIS were identified by an experienced pathologist. The MR images were examined to see if correlative structures were discernable. The remaining 8 mice were selected for serial imaging every two weeks from 10-20 weeks of age. For each, the onset of DCIS, the onset of invasive tumors and the size of the lesion over time was measured.
Results: GE images were able to detect 1/1 large (~5mm) tumor, 17/18 small (~1mm) tumors, and 13/16 ducts distended with DCIS greater than 300 microns. There were no false positives—a clear MR finding corresponded to cancer in all glands. Having reliably detected DCIS with GE, we then moved to studying the progression of disease. DCIS lesions developed at an average age of 14.5 weeks of age, and small tumors developed at an average age of 17.3 weeks. 4 of 8 mice not progress from DCIS to invasive cancer within the study period (Figure 1).
Discussion: The results presented here demonstrate for the first time that i) MRI can reliably detect *in situ* cancer (300 microns) and small, non-palpable tumors (< 1 mm), ii) MRI may be used to track the progression of breast cancer through the full range of development, from *in situ* to invasive carcinoma, and iii) some DCIS lesions did not progress significantly during the study window, illustrating that this model offers the opportunity to influence factors that predict and influence DCIS progression. One significant application of this work is in pre-clinical imaging of drug evaluation. MR imaging has long been used to assess the effects of novel therapies on mammary cancers—however, the tumors imaged in these studies have been large and palpable, representing a better model for advanced rather than early human disease. With the results presented here, MR imaging could be used to assess efficacy of therapies on cancers of all stages of disease (*in situ*, early and advanced). These preliminary results point to future work performing serial imaging in larger numbers of mice, and further investigating MR markers that can predict invasion.

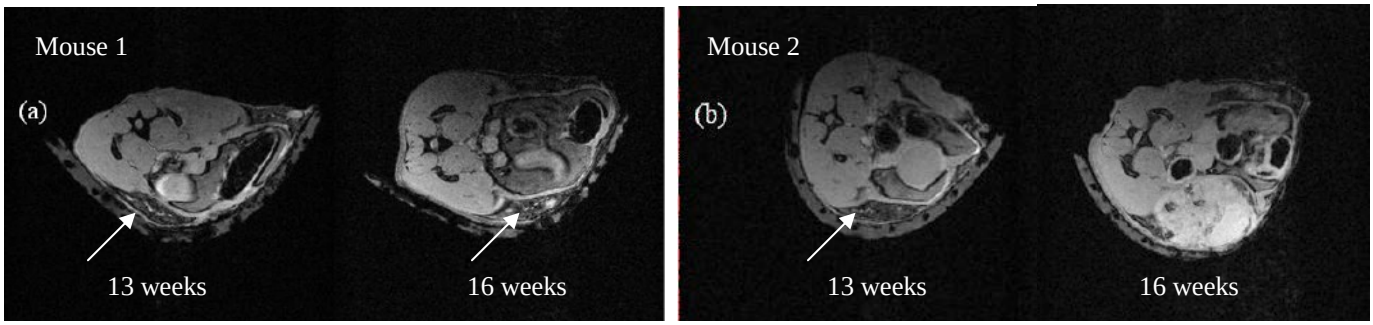

Figure 1: Axial MRI from two mice, at ages 13 and 16 weeks (a) Mouse 1: DCIS (white arrow) is present at 13 weeks and has not progressed significantly at age 16 weeks. (b) Mouse 2: DCIS is again present at 13 weeks, and at 16 weeks has progressed to a large palpable tumor.

Acknowledgments: We would like to thank the Segal Foundation, DOD grant W81XWH-06-1-0329 and NIH grants R21 CA104774-01A2 and 2 R01 CA078803-05A2 for financial support.

Are Kinetic Parameters Diagnostically Useful for Breast Lesions Exhibiting Nonmass-like Enhancement?

S. A. Jansen[1], X. Fan[2], G. Karczmar[2], M. Giger[2], H. Abe[2], and G. Newstead[2]
[1]University of Chicago, Chicago, IL, United States, [2]University of Chicago

Introduction: When analyzing lesion presentation on breast DCEMRI, the radiologist assesses both the morphology as well as the contrast media uptake and washout—or kinetics—of the lesion. The first step in assessing lesion morphology is to classify the type of enhancement as mass, nonmass or focus (Figure 1); subsequent descriptors (such as shape or enhancement pattern) are selected, which differ depending on the type of enhancement. The purpose of this study was to investigate whether the sensitivity and specificity of kinetic parameters can be improved by considering mass and nonmass breast lesions separately. The contrast media uptake and washout kinetics in benign and malignant breast lesions were analyzed using an empirical mathematical model (EMM), and model parameters were compared in lesions with mass-like and nonmass-like enhancement characteristics.

Methods: 34 benign and 78 malignant lesions were selected for review. One pre and five post-contrast images were acquired in the coronal plane using 3D T_1-weighted SPGR (TR/TE = 7.7/4.2 msec, flip angle = 30˚, slice thickness = 3 mm, and in plane resolution = 1.4 mm, 68 sec acquisition). An experienced radiologist classified the type of enhancement as mass, nonmass or focus, according to the BI-RADS lexicon. The radiologist then traced a small region of interest (ROI) around what was perceived to be the most enhancing part of the lesion on the first post-contrast image. The kinetic curve represents the signal intensity in the ROI vs. time. The kinetic curve was analyzed quantitatively using a three parameter EMM[1]: $\Delta S(t) = A \cdot \left(1 - e^{-\alpha t}\right) \cdot e^{-\beta t}$ where **A** is the upper limit of signal intensity, **α** is the rate of signal increase, **β** is the rate of signal decrease during washout. Several kinetic parameters were then derived from the EMM parameters: the initial slope (**$Slope_{ini}$**), curvature at the peak (**κ_{peak}**), time to peak (**T_{peak}**), area under the curve at 30 seconds (**AUC_{30}**) and the signal enhancement ratio (**SER**). The kinetic characteristics of benign and malignant lesions within mass and nonmass lesions were compared: (i) benign vs. malignant mass lesions, and (ii) benign vs. malignant nonmass lesions. Receiver operating characteristic (ROC) analysis was performed to compare the diagnostic performance of the EMM parameters on mass lesions vs. nonmass lesions.

Results: The type of enhancement found was: 70 mass lesions, 38 nonmass, 4 focus. For mass lesions, the EMM parameters **α**, **β**, **AUC_{30}**, **SER**, **$Slope_{ini}$**, **T_{peak}** and **κ_{peak}** differed significantly between benign and malignant lesions (p<0.03). For nonmass lesions, there were no statistically significant differences in any of the parameters for benign vs. malignant lesions (p>0.5). ROC curves were generated for each parameter; for all except **A** the A_z values were higher in mass lesions. The ROC curves for the primary and derived parameter with the highest A_z value for mass lesions (**SER**, **β**) are shown in Figure 2a, and for nonmass lesions (**A**, **$Slope_{ini}$**) in Figure 2b.

Discussion: Kinetic parameters could distinguish benign and malignant mass lesions, but were not useful in discriminating nonmass-like benign from malignant lesions. This suggests that the diagnostic utility of kinetic analysis of breast lesions, e.g., in computer aided diagnosis schemes, is likely improved if performed after identifying the lesion as mass or nonmass enhancement. Given that the physiological basis of enhancement is likely different in nonmass vs. mass lesions, it may be that new quantitative kinetic parameters need to be developed that are tailored for nonmass lesions. This task is of particular importance given that the majority of preinvasive ductal carcinoma *in situ* lesions present as nonmass-like enhancement. Future work will focus on a larger group of lesions with detailed pathology analysis, to investigate new parameters targeted at nonmass lesions. In addition, pixel by pixel analysis, acquiring high spatial/temporal resolution of MR images, or following the later phase of the kinetic curves for a longer time, could be used to help improve the differentiation of nonmass malignant from nonmass benign lesions.

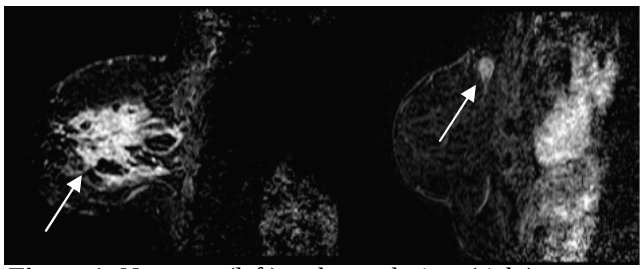

Figure 1: Nonmass (left) and mass lesion (right).

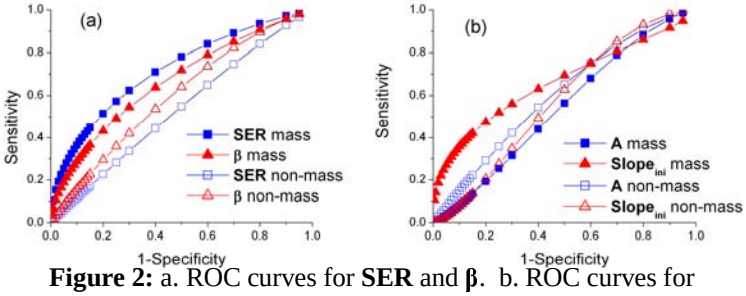

Figure 2: a. ROC curves for **SER** and **β**. b. ROC curves for **A** and **$Slope_{ini}$**

References: 1. Fan et al, JMRI, 2007 Jun;25(5):593-603.

Are Kinetic Parameters related to Prognostic Indicators in < 2.0 cm Invasive Ductal Carcinomas?

S. A. Jansen[1], G. Karczmar[2], A. Shimauchi[2], H. Abe[2], and G. Newstead[2]
[1]University of Chicago, Chicago, IL, United States, [2]University of Chicago

Introduction: Tumor size is strongly correlated with prognosis in breast cancer—the larger and more advanced a tumor, the worse the prognosis. In addition, there are other factors that contribute to prognosis, for example lesions that are estrogen receptor (ER) negative, poorly differentiated (nuclear grade III) or have positive lymph nodes tend to have poorer outcome. These other prognostic indicators are in turn correlated with tumor size: advanced tumors frequently exhibit positive nodes, ER negativity and poorer differentiation. Since kinetics of contrast media uptake and washout measured by MRI are related to the underlying physiology and biology of lesions, it is possible that kinetic parameters could be used as surrogates for prognostic indicators. Prior studies have found that lesions with poorer prognosis have more suspicious enhancement kinetics[1], but these studies have included large tumors; it could be that the kinetic patterns they have found are simply a reflection of the tumor size, rather than being correlated to specific markers. The purpose of this study was to separate the effect of lesion size from the assessment of the relationship between MR parameters and certain prognostic indicators. We evaluated the morphologic and kinetic characteristics of 71 small T1 (< 2.0 cm) invasive ductal carcinoma (IDC) lesions, and classified these findings by ER status, nuclear grade and node invasion.
Methods: 71 patients with 71 histologically proven T1 IDC lesions were selected for IRB approved review. Grade classification: 15 grade I, 32 grade II and 21 grade III, with 3 unclassified. 19 were ER negative and 47 ER positive lesions with 5 unclassified. 18 were node positive and 47 node negative, with 6 unknown. Dynamic MR protocol: 1 pre and 5 post-contrast images using a T1-weighted SPGR with 68 second timing resolution. Analysis of kinetic curve shape and morphology was made by an experienced radiologist according to the BI-RADS lexicon. In addition, several quantitative parameters were derived from the kinetic curves:

$$E_1 = 100 \times \frac{S_1 - S_0}{S_0},\ E_{peak} = 100 \times \frac{S_{peak} - S_0}{S_0}, SER = \frac{S_1 - S_0}{S_{last} - S_0},$$

where $\mathbf{E_1}$ and $\mathbf{E_{peak}}$ are the initial and peak enhancement percentages, respectively, **SER** is the signal enhancement ratio (a measure of washout), and $\mathbf{T_{peak}}$ is the time to peak enhancement.
Results: The predominant MR morphology was homogeneous(44%) mass-like enhancement(87%), with a round shape(51%), irregular margins(51%), and average size=1.6 cm. 93% of kinetic curves exhibited 'rapid' initial uptake and 69% a delayed phase 'washout'. Mean kinetic parameters: $\mathbf{E_1}$=304%, $\mathbf{E_{peak}}$=346%, **SER**=1.12, $\mathbf{T_{peak}}$=147sec. Node negative lesions were significantly smaller on MRI than node positive lesions (p=0.001), but did not exhibit statistically significantly different enhancement kinetics. Grade III lesions exhibited stronger washout (**SER**=1.34) compared with grade I and II lesions (**SER**=0.98, p=0.03). ER negative lesions showed a stronger washout (**SER**=1.40) compared with ER positive (**SER**=0.97, p=0.01) lesions.
Discussion: We have found that enhancement kinetics in < 2.0cm cancers were associated with ER status and grade, but did not depend on whether the cancer had spread to lymph nodes. Compared with ER positive and grade I and II lesions, ER negative and poorly differentiated tumors showed stronger washout. Previous reports have demonstrated that higher **SER** values correlated with higher vascularity[2]; our results suggest increased vasculature in small aggressive tumors compared to small less aggressive tumors. By considering only small cancers, our results suggest that kinetic parameters are related to certain prognostic indicators irrespective of lesion size. An improved understanding of kinetic and morphologic presentation of small IDC lesions, and the characteristics of poorly differentiated and ER negative lesions, may improve interpretation of DCEMRI exams. If these preliminary results can be validated in a larger trial with more detailed kinetic analysis, they would suggest that reliable surrogates for these molecular markers can be measured non-invasively, in real-time and with high spatial resolution by MRI. Although preliminary, this study may point to a role for DCEMRI in guiding biopsies, selecting hormone based therapy and assessing lesion differentiation.

References:
1. Szabo et al, Eur Radiol. 2003 Nov; 13(11): 2425-35.
2. Esserman et al, Breast J 1999 Jan; 5(1): 13-21.

Non-mass vs. mass-like enhancement: Which kinetic parameters distinguish benign and malignant breast lesions?

Purpose: To analyze contrast media uptake and washout kinetics in benign and malignant breast lesions using semi-quantitative kinetic parameters and to compare results obtained for lesions with mass-like and non-mass-like enhancement characteristics.

Materials and Methods: 129 benign and 327 malignant lesions were selected for review. Dynamic MR protocol: 1 pre and 3 or 5 post-contrast images acquired in the coronal plane using a T1-weighted SPGR with 68 second timing resolution. An experienced radiologist classified the type of enhancement according to the BI-RADS lexicon (mass, non-mass or focus) and generated a kinetic curve by tracing a region of interest around the most enhancing part of the lesion. The kinetic curve was analyzed using several quantitative parameters: the initial and peak enhancement percentage (E1 and Epeak), the time to peak enhancement (Tpeak) and the signal enhancement ratio (SER), which measures the amount of signal washout.

Results: The type of enhancement found was: 300 mass lesions (213 malignant and 87 benign), 130 non-mass (106 malignant and 24 benign) and 27 focus (6 malignant and 21 benign). For lesions with mass-like enhancement, the EMM parameters E1, SER and Tpeak differed significantly between benign (average E1=223%, SER=0.75, Tpeak=228 sec) and malignant lesions (average E1=305%, SER=1.13, Tpeak=140 sec, $p<0.00001$). For lesions with non-mass like enhancement, only the parameter SER differed significantly between benign (SER=0.76) and malignant lesions (SER=0.95, $p=0.01$). Restricting analysis to just malignant lesions, all parameters—E1, Epeak, Tpeak and SER—differed significantly when comparing mass vs. non-mass malignant lesions.

Significance of the Conclusions: Kinetic parameters capturing both the initial (E1) and washout phase of the curve (Tpeak, SER) could distinguish benign and malignant mass lesions, but only one parameter (SER) was useful in discriminating non-mass-like benign from malignant lesions. This suggests that to maximize diagnostic utility, the first step before kinetic analysis should be to classify lesion morphology as mass or non-mass-like enhancement. Furthermore, better understanding of the physiology of non-mass lesions may lead to new, diagnostically useful kinetic parameters.

The kinetic and morphologic characteristics of mammographically occult, MR visible breast cancers: How different are the "extra" cancers found at MR imaging?

Purpose: To evaluate the MR morphology and kinetics of lesions that are occult on conventional x-ray mammography, and to investigate if these characteristics differ compared to lesions that are visible on both mammography and DCEMRI.

Materials and Methods: 33 MR visible, mammographically occult lesions as well as 99 mammographically visible malignant lesions were selected for review. The lesions were classified as ductal carcinoma in situ (DCIS), invasive ductal carcinoma (IDC), invasive lobular carcinoma (ILC) and 'other'. Dynamic MR protocol: 1 pre and 3 or 5 post-contrast images with 68 sec timing. Analysis of kinetic curve shape and morphology was made by an experienced radiologist according to the BI-RADS lexicon. Several quantitative kinetic parameters were derived: the initial and peak enhancement percentage (E1 and Epeak), the time to peak enhancement (Tpeak) and the signal enhancement ratio (SER, a measure of washout).

Results: Among the mammographically occult lesions, there were 15 IDC, 9 DCIS, 6 ILC and 3 'other' malignant lesions. The predominant morphology was homogeneous (39%) or heterogeneous(33%) mass-like (67%) enhancement, with irregular(39%) or smooth(18%) margins, and mean lesion size=2.03cm. 76% of lesion curves exhibited 'rapid' initial rise and 70% a delayed phase 'washout'. The average kinetic parameters were: E1=225%, Epeak=266%, SER=1.03 and Tpeak=160 seconds. Among the mammographically visible lesions, there were 68 IDC, 19 DCIS, 7 ILC and 5 'other' malignant lesions. There was no significant difference in the kinetic parameters of mammographically occult IDC lesions, or DCIS lesions, compared with their mammographically visible counterparts.

Significance of the conclusions: Kinetic parameters from DCEMRI data have been related to several biological factors, such as vascularity and hormone receptor status, some of which are a measure of the aggressiveness of disease. Some have suggested that the benefit of DCEMRI of the breast is not clear; perhaps MR only lesions may not develop into life-threatening cancers. In our study, we found that among similar subtypes of cancer (i.e., IDC and DCIS lesions), the kinetic characteristics of occult cancers were similar to that of mammographically visible cancers. If these results could be verified in a larger study, it would suggest that the 'extra' cancers detect by DCEMRI and incorporated into patient management may yield future survival benefits.

A new approach to studying the progression of breast cancer in mice: High resolution MRI of early cancer and DCIS

SA Jansen MSc, S Conzen MD, M Zamora BS, X Fan PhD, T Krausz MD, GM Newstead MD and GS Karczmar PhD.
University of Chicago, Departments of Radiology, Oncology and Pathology

Abstract

To follow the progression of breast cancer, non-invasive imaging methods are needed, since small developing cancers are not visible to the eye. The purpose of this study was to investigate whether *in vivo* MR imaging could be used to detect early mammary cancer in mice. We found that MRI could detect invasive tumors < 1mm in size, and ducts distended with DCIS 300 microns in size.

Background

• Better understanding of the progression of breast cancer is needed to develop improved therapies. Mouse models are often used as pre-clinical models of breast cancer progression.

• Imaging is needed to study the full progression of breast cancer—from hyperplasia to ductal carcinoma in situ (DCIS) to invasive cancer—since early cancers are too small to be visible to the eye. However, there have been no prior reports of *in vivo* imaging of early breast cancer in mice.

• Thus, the purpose of this study was to determine whether MR imaging could detect early murine mammary cancer—including DCIS– with histopathologic correlation. If successful, MR imaging could be used to track the development and progression of mammary cancer *in vivo*.

Methods

Twelve C3(1) SV40 TAg transgenic mice between 10-18 weeks of age were used. A pair of inguinal mammary glands in each mouse was imaged using a T1-weighted gradient echo (GE) sequence with 117 micron in plane resolution. H&E sections of the glands were obtained. We used a polyethylene grid embedded in partially deuterated agar to register tissue sections and MR images. On one representative H&E section from each mouse, the tumors and ducts distended with DCIS were identified by an experienced pathologist. The MR images were examined to see if correlative structures were discernable. Two mice were selected for serial imaging at 13 weeks and 16 weeks of age.

Results

GE images were able to detect 1/1 large (5mm) tumor, 17/18 small (1mm) tumors, and 13/16 ducts distended with DCIS greater than 300 microns. There were no false positives—a clear MR finding corresponded to cancer in all glands. Both of the mice selected for serial imaging exhibited DCIS at 13 weeks: in one the DCIS did not progress significantly at 16 weeks, in the other the DCIS had progressed to a large invasive tumor.

Correlating MR images with histology

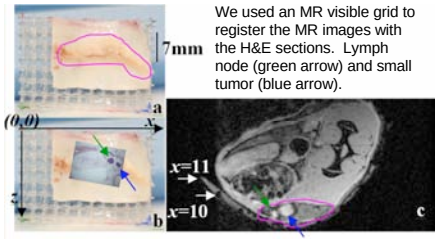

We used an MR visible grid to register the MR images with the H&E sections. Lymph node (green arrow) and small tumor (blue arrow).

Examples of murine DCIS and early invasive tumors (< 1mm)

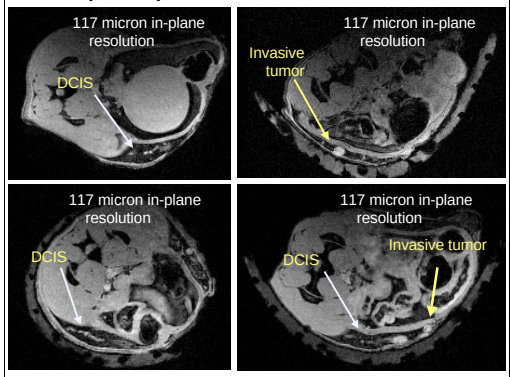

Prior MRI studies[1,2] of murine mammary cancer study tumors that are at least 5-10 times the size of the lesions we have detected.

Murine and Human DCIS

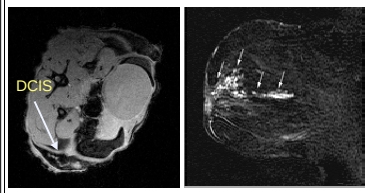

The morphology of murine DCIS (left) is similar to that found in women (right). In this example they both exhibit a ductal distribution.

A first look at progression of DCIS in Sv40 TAg model

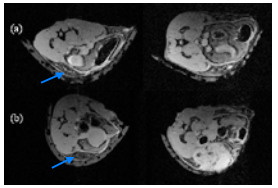

(a) Left. 13 week old mouse, with DCIS (blue arrow). *Right.* Same mouse at 16 weeks continuing to exhibit only DCIS.

(b) Left. 13 week old mouse, with DCIS (blue arrow). *Right.* Same mouse at 16 weeks, demonstrating large tumor.

Discussion

These results demonstrate for the first time that:

i. MRI can reliably detect *in situ* murine mammary cancer (300 microns) and small, non-palpable tumors (< 1 mm),

ii. MRI may be used to track the progression of mammary cancer through the full range of development, from *in situ* to invasive carcinoma,

With these techniques, MRI could be used to study the natural history of mammary cancer in mice, and evaluate effects of therapies on localized non-palpable and spontaneous tumors.

References

1. Rodrigues et al. *Magma, 2004.*
2. Artemov et al. *Cancer Res, 2003.*

How does ER/PR and Her2/Neu status affect the MR characteristics of invasive ductal carcinoma?

Sanaz Arkani Jansen MSc, Hiroyuki Abe MD, Akiko Shimauchi MD, Gregory S. Karczmar PhD and Gillian M. Newstead MD.

University of Chicago, Department of Radiology

Abstract

The purpose was to perform a systematic evaluation of the MR kinetic characteristics of 145 invasive ductal carcinoma (IDC) lesions classified by estrogen receptor (ER), progesterone receptor (PR) and Her2/Neu gene amplification status. The kinetic characteristics of ER and PR positive and negative lesions showed some statistically significant differences (p <0.03), with ER negative lesions showing the strongest initial enhancement, shortest time to peak enhancement and strongest washout.

Introduction

• Dynamic contrast enhanced breast MR imaging (DCEMRI) provides both morphologic and functional characterization of lesions via contrast media uptake and washout (or "kinetic") curves. Prior reports have shown that kinetic curves are related to the underlying lesion biology and physiology.

•Molecular markers such as estrogen receptor (ER), progesterone receptor (ER), and human epidermal growth factor receptor 2 (HER2/neu) are important for guiding treatment choices for breast cancer patients. Her2/neu positive and ER negative lesions tend to have poorer prognosis.

• Since kinetics of contrast media uptake and washout measured by MRI are related to the underlying physiology and biology of lesions it is possible that kinetic parameters could be used as surrogates for molecular markers[1]. This would have the advantage that receptor status could be evaluated non-invasively and with high spatial resolution.

•The purpose of this study was to perform a systematic evaluation of the kinetic characteristics of 145 invasive ductal carcinoma (IDC) lesions classified by ER, PR and Her2/Neu status.

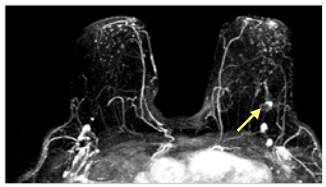

The kinetic curve represents how quickly contrast is taken up, and washed out, by the lesion

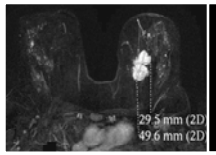

Triple negative (ER, PR, Her2/Neu) grade III IDC. Kinetic curve shows rapid initial rise and sharp washout. This pattern is typically associated with lesions with dense and leaky vasculature, and is the kinetic curve pattern most suspicious for malignancy.

Triple positive (ER, PR, Her2/Neu) grade II IDC. Kinetic curve shows rapid initial rise and persistent signal increase. This curve type is usually associated with benign lesions, and a small proportion of invasive cancers.

Methods

138 patients with 145 histologically proven IDC lesions with known ER, PR and Her2/Neu status were selected for IRB approved review. These lesions were classified as: ER positive (n=101), ER negative (n=44), PR positive (n=76), PR negative (n=69), Her2/Neu positive (n=25) and Her2/Neu negative (n=120). Dynamic MR protocol: 1 pre and 3-5 post-contrast T1-weighted SPGR sequence with 68 s timing. Several quantitative parameters were derived from the kinetic curves, as shown below. These parameters were compared in: (i) ER negative vs. positive, (ii) PR negative vs. positive and (iii) Her2/Neu negative vs. positive lesions.

$$E_1 = 100 \times \frac{S_1 - S_0}{S_0}$$

Initial enhancement percentage

$$E_{peak} = 100 \times \frac{S_{peak} - S_0}{S_0}$$

Peak enhancement percentage

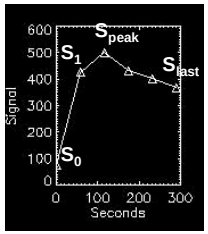

$$SER = \frac{S_1 - S_0}{S_{last} - S_0}$$

Signal enhancement ratio, measures washout rate

T_{peak}

Time to peak enhancement

Results

• Compared with ER positive cancers, ER negative lesions exhibited: stronger initial enhancement, stronger washout and a shorter time to peak enhancement ($p < 0.03$ for all).
• PR negative lesions exhibited a stronger washout compared with PR positive lesions ($p < 0.01$).
• Kinetic parameters did not differ for Her2/Neu negative and positive lesions.

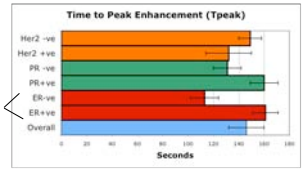

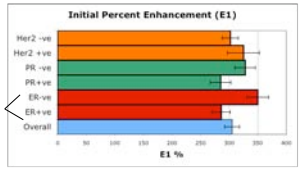

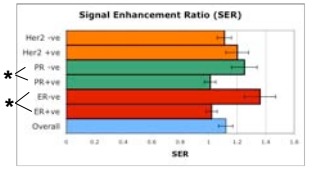

Figures: Average kinetic parameters values. Statistically significant differences are noted with an asterisk.

Conclusions

ER and PR negative lesions showed stronger washout (**SER**) compared with their positive counterparts. Previous reports have demonstrated that higher **SER** values correlated with higher vascularity[2]. These results imply:

- ER and PR negative lesions possess higher vascularity compared to their positive counterparts.
- PR and in particular ER status may be related to tumor angiogenesis in a way that Her2/Neu status is not.
- Parameters derived from DCEMRI measurements may be directly linked to some molecular markers. Thus, there may be a future role of DCEMRI in selection of effective neoadjuvant therapy.

References

1. Szabo et al. *Eur Radiol. 2003.*
2. Esserman et al. *Breast J. 1999.*

Are the MRI characteristics of malignant breast lesions different for African American women?

Sanaz Arkani Jansen MSc, Hiroyuki Abe MD, Akiko Shimauchi MD, Gregory S. Karczmar PhD, Olufunmilayo Olopade MD, and Gillian M. Newstead MD.
University of Chicago, Departments of Radiology and Oncology

Abstract

Recently, disparities in breast cancer mortality and stage at diagnosis in African American vs. Caucasian women have been investigated. The purpose of this study was to compare the MR morphologic and kinetic presentation of 122 malignant lesions in African American and Caucasian women. We found no significant differences in MR morphology, kinetics, lesion size or types of cancer found among African American vs. Caucasian women.

Introduction

- Disparities in breast cancer mortality and stage at diagnosis between African American and Caucasian women has been a topic of recent interest, with evidence to suggest earlier onset of more aggressive cancer in African American women. This disparity has been attributed to differences in quality of medical care and genetic background.
- Dynamic contrast enhanced MRI (DCEMRI) of breast cancers is being used increasingly due to its high sensitivity and accuracy in determining extent of disease. DCEMRI provides both morphologic and functional lesion characterization via contrast media uptake and washout (or 'kinetic') curves, which are related to tumor blood flow.
- The purpose of this study was to compare the MR presentation of malignant breast lesions in African American and Caucasian women.

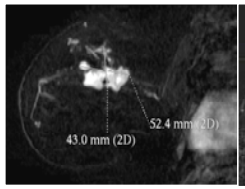

IDC in Caucasian woman.

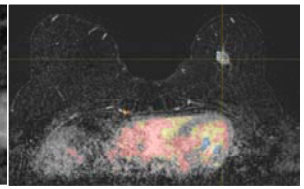

IDC in African American woman.

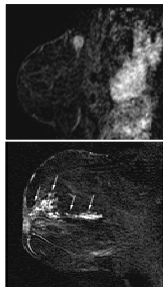

Grade II IDC in Caucasian woman. Kinetic curve shows rapid initial rise and sharp washout This pattern is typically associated with lesions with dense and leaky vasculature, and is the kinetic curve pattern most suspicious for malignancy.

Intermediate grade DCIS in African American woman. Kinetic curve shows rapid initial rise and plateau. This kinetic curve pattern is found in both benign and malignant lesions.

Methods

108 patients with 122 histologically proven malignant lesions were selected for review: 51 African American patients with 59 lesions (average age 58 yrs) and 57 Caucasian women with 63 lesions (average age 55 yrs). The malignant lesions were classified as ductal carcinoma in situ (DCIS), invasive ductal carcinoma (IDC), invasive lobular carcinoma (ILC) and 'other'. Dynamic MR protocol: 1 pre and 3 or 5 post contrast images, 68 second timing. The number of IDC lesions positive for Her2/Neu over-expression was determined. Analysis of kinetic curve shape and morphology was made by an experienced radiologist, and several quantitative parameters were derived from the kinetic curves, as shown below. The kinetic and morphology characteristics of malignant lesions were compared in African American vs. Caucasian women.

$$E_1 = 100 \times \frac{S_1 - S_0}{S_0}$$

Initial enhancement percentage

$$E_{peak} = 100 \times \frac{S_{peak} - S_0}{S_0}$$

Peak enhancement percentage

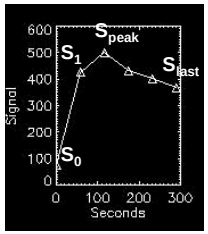

$$SER = \frac{S_1 - S_0}{S_{last} - S_0}$$

Signal enhancement ratio, measures washout rate

T_{peak}

Time to peak enhancement

Results

The mean lesion size was 2.1 cm. There was no difference in the MR morphology, size or kinetics of malignant lesions by race. When considering only IDC lesions, again no significant differences in morphology, size or kinetics by race were demonstrated. Her2/Neu was over-expressed in 19% (6/31) of IDC lesions in African American women, and 16% (5/31) of Caucasians.

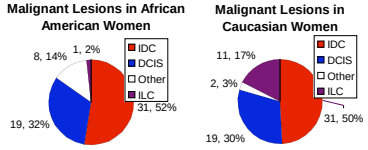

African American and Caucasian women exhibited a similar distribution of types of cancers.

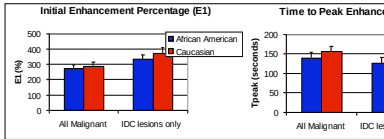

The average E_1 and T_{peak} was similar in African American and Caucasian women.

Conclusions

- Despite recent evidence of racial disparities in breast cancer stage at diagnosis, in our study, we found no difference in the lesion size, MR morphologic or kinetic presentation of malignant lesions between African American and Caucasian women.
- At our institution, comparable numbers of African American and Caucasian women present for diagnostic breast evaluation, implying a similar level of care upon which biological differences can be explored. Our results indicate that newly diagnosed breast cancers in African American and Caucasian women share many similarities. This points to future work on follow-up of the efficacy of treatment and survival in these patients.

DCEMRI of Breast lesions: Is kinetic analysis equally effective for both mass and non-mass-like enhancement?

Purpose: To analyze contrast media uptake and washout kinetics in benign and malignant breast lesions using an empirical mathematical model (EMM) and to compare results obtained for these lesions with mass-like and non-mass-like enhancement characteristics.

Materials and Methods: 34 benign and 78 malignant lesions were selected for a HIPAA compliant IRB approved review. Dynamic MR protocol: One pre and five post-contrast images acquired in the coronal plane using a T_1-weighted SPGR with 68 second timing resolution. An experienced radiologist classified the type of enhancement according to the BI-RADS lexicon (mass, non-mass or focus) and generated a kinetic curve by tracing a region of interest around the most enhancing part of the lesion. The kinetic curve was analyzed quantitatively using the EMM: $\Delta S(t) = A \cdot \left(1 - e^{-\alpha t}\right) \cdot e^{-\beta t}$, where A is the upper limit of signal intensity, α is the rate of signal increase (min^{-1}), β is the rate of signal decrease during washout (min^{-1}). Several secondary parameters were also derived from this equation including the initial slope (**$Slope_{ini}$**), curvature at the peak (**κ_{peak}**), area under the curve at 30 seconds (**AUC30**) and the signal enhancement ratio (**SER**).

Results: The type of enhancement found was: 70 mass, 38 non-mass, 4 focus. EMM parameters **α, SER, $Slope_{ini}$**, and **κ_{peak}** differed significantly between benign and malignant lesions ($p<0.048$). For lesions with mass-like enhancement, the EMM parameters **α, AUC30, SER, $Slope_{ini}$** and **κ_{peak}** ($p<0.03$) differed significantly between benign and malignant lesions. For lesions with non-mass like enhancement, there were no statistically significant differences in any of the parameters for benign v.s. malignant lesions ($p>0.5$).

Conclusions: Kinetic parameters could distinguish benign and malignant mass lesions, but were not useful in discriminating non-mass-like benign from malignant lesions. This suggests that to maximize diagnostic utility, the first step before kinetic analysis should be to classify lesion morphology as mass or non-mass-like enhancement. Since non-mass-like lesions are diffuse, kinetic analysis on a pixel-by-pixel basis may lead to more effective discrimination between malignant and benign lesions.

Clinical Relevance/Application: The diagnostic utility of kinetic analysis of breast lesions, for example in computer aided diagnosis schemes, is likely improved if performed after identifying the lesion as mass-like or non-mass-like enhancement.

DCEMRI of malignant breast lesions: Should a fixed volume of contrast be injected, or a fixed dose?

Purpose: At our institution a fixed volume of contrast is injected into each patient presenting for dynamic contrast enhanced MRI of the breast, regardless of weight. The purpose was to study the MR morphologic and kinetic presentation of malignant lesions in overweight and obese women compared with normal weight women.

Materials and Methods: 111 patients with 125 histologically proven malignant lesions were selected for an IRB approved review. The BMI of each patient was calculated yielding: 2 underweight (2 lesions), 27 normal weight (31 lesions), 49 overweight (54 lesions), and 33 obese (38 lesions). The lesions were classified as ductal carcinoma in situ (DCIS), invasive ductal carcinoma (IDC), invasive lobular carcinoma (ILC) and 'other'. Dynamic MR protocol: 1 pre and 5 post-contrast (20 cc of 0.5M gadodiamide) images, 68 sec timing resolution. Analysis of kinetic curve shape and morphology was made by an experienced radiologist according to the BI-RADS lexicon. Quantitative parameters were derived from the kinetic curves including initial and peak enhancement percentage (E1 and Epeak), and time to peak enhancement (Tpeak). The parameters were then normalized to more closely reflect their values if the contrast was administered at a fixed dose of 0.1mmol/kg.

Results: Overall, there were 63 IDC, 39 DCIS, 13 ILC and 10 'other' malignant lesions. 85% of lesion curves exhibited 'rapid' initial rise and 62% a delayed phase 'washout'. The average E1=284%, Epeak=334%, Tpeak=155sec. Malignant lesions in obese women had a lower E1 and Epeak compared with normal weight women ($p<0.04$). The morphology and size of lesions did not differ significantly between the BMI groups. When considering IDC lesions only, obese women again demonstrated significantly lower E1 and Epeak ($p<0.03$). After normalizing the dose to 0.1mmol/kg, the kinetic parameters of all BMI groups were statistically equivalent.

Conclusions: Malignant lesions in obese women exhibited lower E1 and Epeak but similar kinetic curve shape compared with normal weight women. Our findings suggest that (i)obesity may have an affect on tumor blood flow, (ii)contrast should be administered at a fixed dose (0.1 mmol/kg) rather than a fixed volume (20cc) to achieve similar enhancement levels in heavier women.

Clinical Relevance/Applications: Obese women exhibit lower contrast uptake than normal weight women when injected with a fixed volume of contrast, suggesting that contrast be administered at a fixed dose.

Sanaz (Sunny) Arkani Jansen

CONTACT INFORMATION

Department of Radiology
Committee on Medical Physics
5841 S. Maryland Ave MC 2026
University of Chicago
Chicago, IL 60637 USA

Voice: (773) 834-8008
E-mail: sarkani@uchicago.edu
Web: http://home.uchicago.edu/~sarkani

RESEARCH INTERESTS

Detection and evaluation of of early breast cancer, particularly ductal carcinoma *in situ*, in human breast cancer and mouse models of breast cancer.

EDUCATION

University of Chicago, Chicago, Illinois USA

Ph.D. Candidate, Medical Physics

- Advisors: Gregory Karczmar and Gillian Newstead

M.S., Physics, 2003

University of Toronto, Toronto, Ontario Canada

B.Sc., Mathematics and Physics, 2001

PROFESSIONAL & ACADEMIC EXPERIENCE

University of Chicago, Chicago, Illinois USA

Graduate Student and Research Assistant (Medical Physics) **September, 2004 - present**
Includes current Ph.D. research and graduate course work in medical physics. I also continue to maintain and expand a clinical breast MRI database that currently includes over 800 malignant lesions and 300 benign lesions.

Research Associate (Radiology) **January, 2004 -August, 2004**
Includes research under the supervision of Dr. Gillian Newstead and work on developing a clinical database of breast MRI examinations since 2002.

Graduate Student and Teaching Assistant (Physics) **September, 2001 - December, 2003**
Includes graduate course work and research in the department of Physics. Teaching assistant for five physics courses, duties included discussion section/lab leading, assignment preparation, grading, and tutoring.

University of Toronto, Toronto, Ontario Canada

Research Assistant **May, 1999 - August, 2001**
Summer research in the departments of mathematics and physics, using statistical methods to model mixing boundries of ozone in the stratosphere.

Teaching Course in Mammography Austin, TX USA
Finding Cancer in its Early Stages , Faculty: Laszlo Tabar, Ward Parsons, Ed Hendrick **October, 2007**

HONORS AND AWARDS

Trainee Research Prize:
Radiological Society of North America (RSNA) 2006 and 2007

Department of Defense Breast Cancer Predoctoral Award:
Detection and Evaluation of Early Breast Cancer via Magnetic Resonance Imaging: Studies of Mouse Models and Clinical Implementation 2005-2008

Student Travel Stipend:
International Society for Magnetic Resonance in Medicine 2005, 2007 and 2008

University of Chicago:
Deans Fellowship Biological Sciences Division 2004

Carl J. Vyborny Award 2007

National Sciences and Engineering Research Council (NSERC):
Postgraduate Scholarship 2001

Undergraduate Student Research Award 1999, 2000 and 2001

University of Toronto:
Prince of Wales Award

3T0 M&P Associates Scholarship 1998 and 1999

University of Toronto Scholar 1998

Trinity College Chancellor Scholarship 1998-2001

RESEARCH SKILLS

Computer Languages: C, IDL, Matlab
Computer Applications: MS Office, Filemaker Pro
Animal work: Physiological monitoring set up, tail veins, dissections
Pahthology techniques: Microscopy, cryosectioning

PUBLICATIONS

1. Sanaz A. Jansen, Hiroyuki Abe, Akiko Shimauchi, Gregory Karczmar, Robert Schmidt, Gillian Newsteadi. “Pure ductal carcinoma in situ: kinetic and morphologic MR characteristics compared with mammographic appearance and nuclear grade.” Radiology. 2007 Dec;245(3):684-91.
2. Sanaz A. Jansen, Xiaobing Fan, Gregory S. Karczmar, Hiroyuki Abe, Robert A. Schmidt, and Gillian M. Newstead. ”Differentiation between benign and malignant breast lesions detected by bilateral dynamic contrast enhanced MRI: A sensitivity and specificity study.” Magnetic Resonance in Medicine (in press).
3. Xiaobing Fan, Hiroyuki Abe, Milica Medved, Sean Foxley, Sanaz Arkani, Marta Zamora, Olopade OI, Gillian M Newstead, Gregory Karczmar. ”Fat suppression with spectrally selective inversion vs. high spectral and spatial resolution MRI of breast lesions: qualitative and quantitative comparisons.” J Magn Reson Imaging. 2006 Dec;24(6):1311-5.
4. Xiaobing Fan, Milica Medved, Gregory S. Karczmar, Cheng Yang, Sean Foxley, Sanaz Arkani, Wendy Recant, Marta A. Zamora, Hiroyuki Abe, Gillian M. Newstead. ”Diagnosis of suspicious breast lesions using an empirical mathematical model for dynamic contrast-enhanced MRI.” J Magn Reson Imaging. 2007 25:593-603.
5. Sean Foxley, Xiaobing Fan, Sanaz A. Jansen, Marta Zamora, Erica Markiewicz, Hikmat Al-Ahmadie and Gregory S. Karczmar. ”High spectral and spatial resolution MRI of age related changes in murine prostate.” Magnetic Resonance in Medicine (in press)
6. Sanaz A. Jansen, Xiaobing Fan, Gregory S. Karczmar, Hiroyuki Abe, Robert A. Schmidt, Maryellen Giger and Gillian M. Newstead.”DCEMRI of breast lesions: Is kinetic analysis equally effective for both mass and non-mass-like enhancement?” Medical Physics (provisionally accepted with revisions).
7. Sanaz A. Jansen, Suzanne Conzen, Thomas Krausz, Marta Zamora, Sean Foxley, Xiaobing Fan, Gillian Newstead and Gregory Karczmar. ”Detection of *in situ* mammary cancer in a transgenic mouse model:*in vitro* and *in vivo* MRI studies demonstrate histopathologic correlation.” Physics in Medicine and Biology (provisionally accepted with revisions).
8. Sanaz A. Jansen, Gregory Karczmar, Vicky Chen, Lindsay Zak, Maryellen Giger and Gillian Newstead. ”Parenchymal enhancement on breast MRI: Pattern, kinetics and comparison with breast density.” (submitted).

PUBLICATIONS IN PREPARATION

1. Sanaz A. Jansen, Tatjana Paunesku, Xiaobing Fan, Gayle Woloschak, Erica Markiewicz, Suzanne Conzen, Gillian Newstead and Gregory Karczmar. "X-Ray fluorescence microscopy and dynamic contrast enhanced MR Imaging of Gd-DTPA in murine ductal carcinoma *in situ*."
2. Sanaz A. Jansen, Suzanne Conzen, Xiaobing Fan, Erica Markiewicz, Thomas Krausz, Gillian Newstead and Gregory Karczmar. "A first look at the progression of ductal carcinoma *in situ* in a transgenic mouse model of breast cancer."

FIRST AUTHOR ABSTRACTS

1. Sanaz A. Jansen, Tatjana Paunesku, Gayle Woloschak, Stefan Vogt, Suzanne Conzen, Gillian M. Newstead and Gregory S. Karczmar. "Why do Ductal Carcinoma in situ Lesions Enhance on Dynamic Contrast Enhance MRI of the Breast? Using X-Ray Fluorescence and MRI to Track the Spatial Distribution of Gd-DTPA in Murine DCIS." in 16th Annual Meeting of the Society for Magnetic Resonance in Medicine, May 2008.
2. Sanaz A. Jansen, Gillian Newstead, Suzanne D. Conzen, Marta Zamora, Thomas Krausz and Gregory Karczmar. "Do all in situ cancers progress to invasive disease? A first look at progression of mammary cancer from in situ to invasive carcinoma in vivo." in 16th Annual Meeting of the Society for Magnetic Resonance in Medicine, May 2008.
3. Sanaz A. Jansen, Xiaobing Fan, Gregory Karczmar, Maryellen Giger, Hiroyuki Abe and Gillian M. Newstead. "Are Kinetic Parameters Diagnostically Useful for Breast Lesions Exhibiting Nonmass-like-Enhancement?" in 16th Annual Meeting of the Society for Magnetic Resonance in Medicine, May 2008.
4. Sanaz A. Jansen, Gregory Karczmar, Akiko Shimauchi, Hiroyuki Abe and Gillian M. Newstead. "Are Kinetic Parameters Related to Prognostic Indicators in ¡2.0 cm Invasive Ductal Carcinomas?" in 16th Annual Meeting of the Society for Magnetic Resonance in Medicine, May 2008.
5. Sanaz A. Jansen, Xiaobing Fan, Gregory S. Karczmar, Hiroyuki Abe, Akiko Shimauchi and Gillian M Newstead. "Non-mass vs. mass-like enhancement: Which kinetic parameters distinguish benign and malignant breast lesions?" in108th Annual Meeting of the American Roentgen Ray Society, April 2008.
6. Sanaz A. Jansen, Akiko Shimauchi, Hiroyuki Abe, Gregory S. Karczmar and Gillian M Newstead. "The kinetic and morphologic characteristics of mammographically occult, MR visible breast cancers: How different are the extra cancers found at MR imaging?" in 108th Annual Meeting of the American Roentgen Ray Society, April 2008.
7. Sanaz A Jansen, Suzanne Conzen, Marta Zamora, Thomas Krausz, Gillian M Newstead and Gregory S Karczmar. "A new approach to studying the progression of breast cancer in mice: High resolution MRI of early cancer and DCIS." in 30th Annual San Antonio Breast Cancer Symposium, December 2007.
8. Sanaz A Jansen, Hiroyuki Abe, Akiko Shimauchi, Gregory S Karczmar and Gillian M Newstead. "How does ER/PR and Her2/Neu status affect the MR characteristics of invasive ductal carcinoma?" in 30th Annual San Antonio Breast Cancer Symposium, December 2007.
9. Sanaz A Jansen, Hiroyuki Abe, Akiko Shimauchi, Gregory S Karczmar, Olufunmilayo Olopade, Lindsay Zak and Gillian M Newstead. "Are the MRI characteristics of malignant breast lesions different for African American women?" in 30th Annual San Antonio Breast Cancer Symposium, December 2007.
10. Sanaz A. Jansen, Xiaobing Fan, Gregory Karczmar, Hiroyuki Abe, Robert A. Schmidt and Gillian M. Newstead. "DCEMRI of Breast Lesions: Is Kinetic Analysis Equally Effective for Both Mass and Non-mass-like Enhancement?" in 93rd Scientific Assembly and Annual Meeting of the Radiological Society of North America, November 2007.
11. Sanaz A. Jansen, Cheng Yang, Hiroyuki Abe, Akiko Shimauchi, Gregory Karczmar and Gillian M. Newstead. "DCEMRI of Malignant Breast Lesions: Should a Fixed Volume of Contrast be Injected, or a Fixed Dose" in 93rd Scientific Assembly and Annual Meeting of the Radiological Society of North America, November 2007.
12. Sanaz Arkani, Hiroyuki Abe, Akiko Shimauchi, Robert A. Schmidt, Gregory Karczmar, and Gillian M. Newstead. "Dynamic MR Imaging of Invasive Ductal Carcinoma: Studying Kinetics by Estrogen Re-

ceptor, Progesterone Receptor and Her2/Neu Amplification Status Molecular Markers" in 107th Annual Meeting of the American Roentgen Ray Society, May 2007.

13. Sanaz Arkani, Xiaobing Fan, Hiroyuki Abe, Gregory Karczmar, Robert A. Schmidt, and Gillian M. Newstead. "Improving the Diagnostic Accuracy of 3D Breast DCEMRI Data Using an Empirical Mathematical Model" in 15th Annual Meeting of the Society for Magnetic Resonance in Medicine, May 2007.
14. Sanaz Arkani, Hiroyuki Abe, Akiko Shimauchi, Gregory Karczmar, and Gillian M. Newstead. "Molecular Markers and DCEMRI of Breast Cancer: Relationship with Kinetics in Invasive Ductal Carcinoma" in 15th Annual Meeting of the Society for Magnetic Resonance in Medicine, May 2007.
15. Sanaz Arkani, Suzanne Conzen, Thomas Krausz, Marta Zamora, Gillian M. Newstead, and Gregory Karczmar. "MRI of Ductal Carcinoma in situ and Other Early Mammary Cancers in Transgenic Mice" in 15th Annual Meeting of the Society for Magnetic Resonance in Medicine, May 2007.
16. Sanaz Arkani, Vicky Chen, Caroline Cranford, Lindsay Zak, Hiroyuki Abe, Gregory Karczmar, Robert A. Schmidt, Funmi Olopade and Gillian M. Newstead. "Parenchymal enhancement on breast MRI may be a marker for cancer risk: correlation of parenchymal enhancement with breast density" in 29th Annual San Antonio Breast Cancer Symposium, December 2006.
17. Sanaz Arkani, Hiroyuki Abe, Akiko Shimauchi, Gregory Karczmar, Robert A. Schmidt and Gillian M. Newstead. "MR Imaging of Pure Ductal Carcinoma in Situ: Kinetics, Morphology, and Correlation with Mammographic Presentation and Nuclear Grade" in 92nd Scientific Assembly and Annual Meeting of the Radiological Society of North America, November 2006.
18. Sanaz Arkani, Vicky Chen, Caroline Cranford, Lindsay Zak, Hiroyuki Abe, Gregory Karczmar, Robert A. Schmidt, Funmi Olopade and Gillian M. Newstead. "Women at High Risk for Breast Cancer: Classification of Parenchymal Enhancement on Breast MR Imaging and Correlation with Mammographic Density" in 106th Annual Meeting of the American Roentgen Ray Society, May 2006.
19. Sanaz Arkani, Hiroyuki Abe, Gregory Karczmar, Robert A. Schmidt and Gillian M. Newstead. "Ductal Carcinoma in Situ (DCIS): Kinetic and Morphologic Characteristics on Dynamic Contrast Enhanced Magnetic Resonance Imaging (DCEMRI)" in 105th Annual Meeting of the American Roentgen Ray Society, May 2005.
20. Sanaz Arkani, Hiroyuki Abe, Gregory Karczmar, Robert A. Schmidt and Gillian M. Newstead. "Characteristics of Ductal Carcinoma in Situ on Dynamic Contrast Enhanced Magnetic Resonance Imaging" in 13th Annual Meeting of the Society for Magnetic Resonance in Medicine, May 2005.

OTHER ABSTRACTS

1. Bradbury AR, Newstead G, Li LS, Arkani S, Abe H, Cummings S, Olopade OI. Breast MRI surveillance in women at high risk for breast cancer, in 27th Annual San Antonio Breast Cancer Symposium, December 2004.
2. Hiroyuki Abe , Gillian M. Newstead, Sanaz Arkani , Charlene Sennett, Robert A. Schmidt, Gregory Karczmar et al . Effect of Magnetic Resonance Imaging on the Clinical Management of Women with Newly Diagnosed Breast Cancer, in 90th Scientific Assembly and Annual Meeting of the Radiological Society of North America, November 2004.
3. Gillian M. Newstead, Sanaz Arkani, Hiroyuki Abe, Robert A. Schmidt, Charlene Sennett, Cheng Yang. Dynamic Breast MR Imaging: Comparison of Kinetic and Morphologic Characteristics of Malignant Lesions by Tumor Type and Grade. in 91st Scientific Assembly and Annual Meeting of the Radiological Society of North America, November 2005.
4. Akiko Shimauchi, Hiroyuki Abe, Sanaz Arkani, Charlene Sennett, Robert A. Schmidt, Gillian M. Newstead. A Practical Approach to the Differential Diagnosis of Benign Lesions Detected at Breast MR Imaging, in 92nd Scientific Assembly and Annual Meeting of the Radiological Society of North America, November 2006.
5. Gillian M. Newstead, Hiroyuki Abe, Sanaz Arkani, Akiko Shimauchi, Charlene Sennett, Robert A. Schmidt. Magnetic Resonance-guided Vacuum-assisted Breast Biopsy: Diagnostic Utility in a Clinical Breast MR

Program, in 92nd Scientific Assembly and Annual Meeting of the Radiological Society of North America, November 2006.

6. Weijie Chen, Maryellen Giger, Gillian M. Newstead, Ulrich Bick, Li Lan, Sanaz Arkani et al. Multi-category Feature Extraction in Computer-aided Diagnosis of Breast MRI, in 92nd Scientific Assembly and Annual Meeting of the Radiological Society of North America, November 2006.
7. Hui Li, Maryellen Giger, Yading Yuan, Charlene Sennett, Li Lan , Andrew Jamieson et al. Conversion of Screen Film Mammographic CADx for FFDM, in 92nd Scientific Assembly and Annual Meeting of the Radiological Society of North America, November 2006.
8. Sean Foxley Sanaz Arkani, Xiaobing Fan, Marta Zamora, Erica Markiewicz, Gregory Karczmar. Serial Imaging of Transgenic Mice Prostate Tumors Using High-Resolution EPSI, in 92nd Scientific Assembly and Annual Meeting of the Radiological Society of North America, November 2006.
9. Akiko Shimauchi, Sanaz A. Jansen, Hiroyuki Abe, Kirti Kulkarni, Robert A. Schmidt, Gillian M. Newstead et al. Cancers Not Detected at MR Imaging: Review of False-Negative Lesions, in 93rd Scientific Assembly and Annual Meeting of the Radiological Society of North America, November 2007.
10. Steven Thiel, Rajshri Shah, Sanaz A. Jansen, Hiroyuki Abe, Akiko Shimauchi, Gillian M. Newstead. Evaluating the Extent of Disease with MRI in the Setting of Breast Calcifications Suggestive of DCIS, in 93rd Scientific Assembly and Annual Meeting of the Radiological Society of North America, November 2007.
11. Weijie Chen, Maryellen Giger, Gillian M. Newstead, Sanaz A. Jansen, Ken Chiang, Li Lan et al. Breast Cancer Diagnosis Using DCE-MRI: Role of Computer in Interpretation of 4D Data, in 93rd Scientific Assembly and Annual Meeting of the Radiological Society of North America, November 2007.
12. Gillian M Newstead, Hiroyuki Abe, Sanaz A Jansen, Akiko Shimauchi, Charlene A Sennett,, Robert A Schmidt, Lindsay Zak, Olufunmilayo Olopade, Nora Jaskowiak. Effect of magnetic resonance imaging on the clinical management of women with newly diagnosed breast cancer, in 30th Annual San Antonio Breast Cancer Symposium, December 2007.
13. Kirti Kulkarni, Gillian M Newstead, Sanaz A Jansen, Hiroyuki Abe, Akiko Shimauchi, Robert A Schmidt, Nora Jaskowiak. Does MRI improve chances of obtaining negative surgical margins after localized excision? A retrospective study. in 30th Annual San Antonio Breast Cancer Symposium, December 2007.
14. Xiaobing Fan, Sanaz Arkani, Gregory S Karczmar, Hiroyuki Abe, Robert A Schmidt, Gillian M Newstead. Using three-parameter empirical mathematical model to analyze breast DCEMRI data; comparison with conventional BI-RADS classification, in 30th Annual San Antonio Breast Cancer Symposium, December 2007.